4-2018

A Mathematical Model of Late Phase Calcium Dyshomeostasis in Axon Degeneration Promoted by SARM1's NAD Cleavage Activity

Jessica Crowley

A Mathematical Model of Late Phase Calcium Dyshomeostasis in Axon Degeneration Promoted by SARM1's NAD Cleavage Activity

A thesis submitted in partial fulfillment of the requirement for the degree of Bachelor of Science

in Neuroscience from The College of William and Mary

by

Jessica Maris Crowley

Accepted for_____

Prof. Randolph Coleman, Director

_____

Prof. William Buchser, Outside Member

_____

Prof. Lizabeth Allison

_____

Prof. Lisa Landino

_____

Williamsburg, VA

April 25, 2018

Abstract

Axon (Wallerian) degeneration, an early event preceding neuronal loss in neurodegenerative disease and traumatic brain injury, is the active process of dismantling the axon. Degeneration of the cytoskeleton occurs through the protease activity of calpains, which are activated by a characteristic late rise in intra-axonal calcium following axonal injury (execution phase). The increase in calcium may be influenced by the signature disruption of energy homeostasis in Wallerian degeneration; however, defining this relationship and the progression of the execution phase remains to be established. Recently, studies demonstrated that the executioner protein SARM1 performs NADase activity resulting in the generation of cyclic ADP-ribose. This novel SARM1 enzymatic activity may bridge the gap in understanding the relationship between these two events. Here, we use a computational model to investigate the relationship between energy state and intra-axonal calcium influenced by the enzymatic activity of SARM1. We have defined a mechanistic model that incorporates the cleavage products and can predict the effects on the temporal release of calcium from intracellular stores and monitor ATP and NAD concentrations. Construction of the mathematical model is based on Biochemical Systems Theory (BST), which has been applied successfully in predicting outcomes of neurodegenerative diseases. MATLAB analyzes the biochemical reactions represented as ordinary differential equations (ODEs) and allows for perturbations of the system to mimic experimental interventions. In our model, we have gathered data demonstrating a depleted energy state and altered calcium concentration from SARM1's NADase activity promotes degeneration in axons. By comparing these data to results from axotomized primary neuronal cultures, we can assess the plausibility of the proposed mechanism occurring *in vitro*. The process of active degeneration in axons is complex and the

use of a computational model representing the degeneration pathway will help elucidate its mechanisms and possibly provide insight for development of future therapeutic targets.

1. Introduction

Axon (Wallerian) degeneration is a highly conserved, self-destruction pathway that functions to dismantle injured axons in both the central and peripheral nervous systems in a synchronous fashion. This degeneration is an early event preceding neuronal loss in neurodegenerative disease and traumatic brain injury and is the main driver of pathology in peripheral neuropathies. Therefore, understanding the mechanisms of axon degeneration is of utmost importance due to its prevalence in a wide array of neurological disorders and injuries.

The mechanisms of Wallerian degeneration remain poorly understood. However, this process can be modeled experimentally through the disruption of axonal transport (e.g. axon transection, crush, vincristine treatment) or energy deprivation. Wallerian degeneration has been characterized by the fragmentation of the distal axons to the site of injury after a characteristic lag time, termed the latent phase. This latent phase lasts for 36 to 44 hours in mouse sciatic nerve and about 3 hours in primary retinal ganglion cell culture from zebra finch embryos (Beirowski et al., 2005).

The spontaneous Wlds mutation in mice led to major insight into the degenerative process by providing a means to assess if axonal loss in various diseases is related to Wallerian degeneration. WLD^s is a chimeric protein, with the 70 amino acids of the N-terminus being the same as the N-terminus of Ube4b and the amino acids of the C-terminus containing the full length of nicotinamide mononucleotide adenylyl transferase 1 (Nmnat1). Ube4b is an ubiquitin-ligase and Nmnat1 is an enzyme that synthesizes NAD from nicotinamide mononucleotide

(NMN) and ATP. Transected axons in the sciatic nerve of mice expressing WLD^s are protected for over two weeks, whereas transected axons in wild type mice survive for about 1.5 days (Mack et al., 2001; Sasaki, 2009; Milde, Freeman, & Coleman, 2013; Yahata et al., 2009; Babetto et al., 2010). Experiments disrupting the enzymatic activity of the Nmnat1 domain in WLD^s demonstrate that Nmnat1 is crucial for the protection against axon degeneration. Axons expressing WLD^s with a loss of function mutation of the Nmnat1 domain show survival comparable to wild type axons (Conforti et al., 2009). Although the Nmnat1 isoform is localized to the nucleus, the protective action of WLD^s has been shown to be outside of the nucleus (Cohen et al., 2012; Sasaki, & Milbrandt, 2010; Conforti et al., 2009). Overexpression of other Nmnat isoforms also demonstrate protective action against axonal degeneration in non-nuclear locations (Yahata et al., 2009; Sasaki, & Milbrandt, 2010; Conforti et al., 2007). Overall, the spontaneous mutation of Wlds led to the appreciation of axon degeneration as an active, regulated process.

The proposed mechanism of axonal protection mediated by WLD^s is mimicking the function of the endogenous protein Nmnat2, which is lost in disruption of axonal transport by injury. Removal of Nmnat2 causes uninjured axons to undergo axonal degeneration, which can be rescued by WLD^s expression (Gilley et al., 2013; Gilley, & Coleman, 2010; Hicks et al., 2012). Although WLD^s expression and increased Nmnat activity prevent early declines in ATP in the distal axon, neither increase NAD in injured axons compared to healthy, wild type axons, which is counterintuitive to the enzymatic function of Nmnat (Sasaki, Araki, & Milbrandt, 2006; Wang et al., 2005; Coleman, & Conforti, 2014; Wang, & He, 2009). Furthermore, inhibiting NAD consuming enzymes, such as PARP1 and CD38, to increase intra-axonal NAD

concentrations do not confer axonal protection (Sasaki et al., 2009). Therefore, it remains unclear if NAD is the protective product generated through Nmnat enzymatic activity.

There are two phases in Wallerian degeneration referred to as the initiation phase and the execution phase. An established part of the Wallerian degeneration pathway is a disruption of calcium homeostasis in the distal axon after injury (Yang et al., 2013; George, Glass, & Griffin, 1995; Zhai et al., 2003; Adalbert et al., 2012; Ma et al., 2013). This disruption occurs during the execution phase, which is downstream of Nmnat loss, NAD depletion, and depolarization due to energy failure (Coleman, & Conforti, 2014; Yang et al., 2013; Adalbert et al., 2012; Mishra et al., 2013; Gerdts et al., 2015). Large increases in cytosolic calcium cause calcium sensitive proteases, such as calpains, to activate and degrade cytoskeletal components of the distal axon (George, Glass, & Griffin, 1995).

There are two phases of calcium rises following axonal transection termed the early and late calcium increases, respectively. The early calcium increase follows immediately after axonal injury due to the opening left from the transection. Calcium homeostasis is quickly reestablished and a lag phase follows where there is no observable evidence of axon degeneration. Previously, it was shown that the expression of WLD^s did not change this early calcium influx (Vargas et al., 2015). Additionally, inducing multiple early calcium increase events through multiple axon transections did not alter the time course of degeneration. Although there is degeneration in the early phase in both the distal and proximal axons nearest to the injury site, this early rise in calcium is not necessary for Wallerian degeneration (Vargas et al., 2015).

However, late phase calcium increase is required for Wallerian degeneration to take place in the distal axon. This late rise in calcium is seen at the end of the lag phase, immediately before degeneration (Vargas et al., 2015). Additionally, this late increase depends on extracellular

calcium since chelating extracellular calcium protected injured axons from degeneration (Mishra et al., 2013). The injury induced depolarization from energy failure in the distal axon causes L-type voltage gated calcium channels (VGCCs) to open allowing the influx of extracellular calcium (Mishra et al., 2013; Shen et al., 2013). Extracellular calcium influx through these channels is known to induce cellular pathways that trigger the release of calcium from intracellular stores, such as activation of the ryanodine and IP3 receptors. Furthermore, the removal of calcium from intracellular stores mediated a similar delay in axonal fragmentation, which confirms the involvement of intracellular release of calcium in this late rise (Villegas et al., 2014). Injured axons expressing WLD^s do not demonstrate this late rise of calcium and were protected from degeneration (Avery et al., 2012). However, the prevention of extracellular calcium influx by blocking VGCCs only delays the late calcium rise, and thus confers moderate axonal protection (Bramley et al., 2016; George, Glass, & Griffin, 1995). Such observations indicate that alternative mechanisms may be releasing calcium from intracellular stores to account for the late rise in calcium of the distal axon.

Although the initiators of this pathway remain unknown, the sterile alpha and TIR motif containing 1 (SARM1) protein is necessary in propagating axonal degeneration (Gerdts et al., 2013; Gerdts et al., 2015). Knockout animal models of SARM1 demonstrate protection of injured axons comparable to protection mediated by WLD^s (Osterloh et al., 2012). However, it is still unclear what causes the activation of SARM1 in distal axons after injury and whether SARM1 is involved in the initiation or executions phases of axon degeneration. Until recently, the enzymatic function of SARM1 also remained elusive. Work by Essuman et al. (2017) demonstrated SARM1 as a NAD consumer that generates the products cyclic ADP-ribose (cADPR), ADP-ribose (ADPR), and Nam. Here, a potential mechanism for this novel enzymatic

activity of SARM1 in Wallerian degeneration is proposed by using a testable mathematical model (see Appendix for full figure). Two hypotheses are investigated: (i) due to cytosolic calcium rises in spite of L-type VGCC blockage, ADPR and cADPR generated from SARM1 NADase activity may be sufficient in contributing to significant cytosolic calcium accumulation for degeneration to proceed following injury, and (ii) SARM1's NADase activity may contribute to the characteristic energy failure observed in Wallerian degeneration through depleting NAD and promoting cytosolic calcium accumulation. The model incorporates the generation of SARM1's cleavage products and predicts their effects on calcium and energy homeostasis in injured axons to provide insight into the progression of degeneration.

2. Methods

Here, methods for axon degeneration for zebra finch retinal ganglion cell (RGC) assays are presented and major pathways contributing to the pathology of axon degeneration are outlined. These biochemical pathways were represented visually using the program CellDesigner. In the accompanying models, arrows indicate transitions between species and states. Species with a (*) indicate the active form of the species. Modulation of reactions is represented with an open circle for catalysis and a hard edge for inhibition. Formation of complexes was considered reversible unless otherwise indicated. A full version of the model may be found in the Appendix.

2.1 Axon Degeneration Assay (Embryonic Zebra Finch RGC)

The following methods were described previously in Bramley et al. (2016), where I was cited in the Acknowledgements. Specific changes to the methods employed in my experiments on neuronal cultures are included where appropriate.

Plate coating

Neurons were cultured on 24-well plates (Falcon 353047, Fishersci, Pittsburgh, PA). The plates were coated in preparation for cell culture with 10 μg/ml poly-d-lysine (Sigma P7886, St Louis, MO), refrigerated overnight, and then rinsed with water three water washes. These plates were then coated with 10 μg/ml laminin (LifeTech 23017-015, Carlsbad, CA) and incubated overnight at 37 °C. Before explants were added, the laminin was removed and allowed to dry for five minutes.

Primary neuronal culture

All animal work was approved by the William & Mary IACUC (IACUC-2017-03-18-11976-wjBramley "Neurodegeneration in Songbirds"). Staging was determined using the established staging guide that aligns zebra finch (*Taeniopygia guttata*) development with classic chick development (Murray et al., 2013). Retinal explants containing retinal ganglion cells (RGCs) were dissected from eight day-old embryonic zebra finch eggs. Dissection methods established in chickens were applied here to zebra finches (Bronner-Fraser, 1996). Retinas were obtained by removing the eyes of the chick and peeling away the outer epithelium layers in phosphate-buffered saline (PBS). The retinas were then placed in their own separate wells of L-15 (Thermo Fischer Scientific 21083027, Waltham, MA) where the pigment layer was removed. The retina was then divided into explants using fine forceps and pipetted onto the laminin plates.

Following dissection, the plated retinal explants were incubated at 37 °C in a low volume of DMEM + 10 % FBS (Gibco Invitrogen, Carlsbad, CA) to promote adherence to the tissue culture plate. After this initial incubation, RGC explants were grown in 500 μL DMEM/FBS

supplemented with nerve growth factor (Sigma n0513, St Louis, MO) for five days *in vitro* and inspected for sufficient axon length before experimentation and imaging.

Physical axon injury

Axotomy served as the physical injury. Axotomy was administered to cultured RGCs using a stainless steel blade (Fine Science Tools, 10035-10, Foster City, CA). The cut was made in close proximity to the explant, and cells were incubated at 37 °C for 15 or 24 hours. After 15 or 24 hours, the cells were fixed in 10% PFA (Electro Microscopy Sciences 15714-S) for 10 minutes followed by two 1x PBS washes. The degeneration inhibitor Nifedipine (Sigma N7634, St Louis, MO) was used in experiments immediately following axotomy at 3 µM, 6 µM, and 18 µM treatments.

Fluorescence microscopy

Fixed neurons were stained with CellMask Orange Plasma membrane stain (Life Technologies, C10045, Carlsbad, CA). Cells were incubated with the stain for 10 min at 37 °C. Images were acquired immediately after staining using a scanning confocal microscope (Nikon Ti Microscope with A1 Confocal). Nine images of each explant were acquired (using the '3 × 3 large image' settings).

In separate experiments to uncover the time course of axon degeneration, live cells were placed in a live-cell chamber suspended in imaging media (FluoroBrite DMEM A18967, Life Technologies, Carlsbad, CA) for time-lapse imaging.

Image analysis

Fragmentation of the axons was detected and quantified Using NIH ImageJ (FIJI). The quantitative measure resulting from this analysis is the degeneration index (DI), where 1 is completely degenerated and 0 is fully intact adapted from Gerdts et al. (2011). The data set was imported into the visualization program Spotfire (Tibco, Palo Alto, CA). The acquired images were then quality controlled to determine if they were in focus and contained axons. If images did not meet these criteria, they were removed from the final statistical analysis. There were 3 replicates considered. The DI for each explant well is the average of the image tiles comprising the well. DIs of wells on the same plate receiving the same treatment were then averaged to obtain the final DI for the corresponding replicate.

2.2 Depolarization in Response to Injury

2.2.1 Inhibition of voltage gated calcium channels via nifedipine treatment

Following axonal injury, a depleted energy state leads to hindered function of the Na^+/K^+ ATPase (Stys et al., 1992; Wang et al., 2012). Without the constant separation of these ions, resting membrane potential cannot be maintained and the axon becomes depolarized through sodium and potassium currents. Depolarization through the interplay of these currents allows for opening of L-type voltage gated calcium channels (VGCCs) and a means for extracellular calcium to flood into the axon (Lipscombe, Helton, & Xu, 2004; Moldovan, Alvarez, & Krarup, 2009; Mishra et al., 2013). Furthermore, depolarization of the distal axon reverses the action of the Na^+/Ca^{2+} exchanger at the plasma membrane, which causes further intra-axonal calcium accumulation from extracellular sources (Stirling & Stys, 2010) (Figure 1).

Application of L-type VGCC inhibitors, such as dihydropyridines, delay axotomy induced axon degeneration both *in vitro* (Bramely et al., 2016; Gerdts et al., 2011) and *in vivo*

(George, Glass, & Griffin, 1995). This observation supports the important role of depolarization since dihydropyridines, such as nifedipine, block the voltage sensing of VGCCs, which is a necessary characteristic for activating channels on intra-axonal calcium stores such as the ryanodine receptor (Villegas et al., 2014).

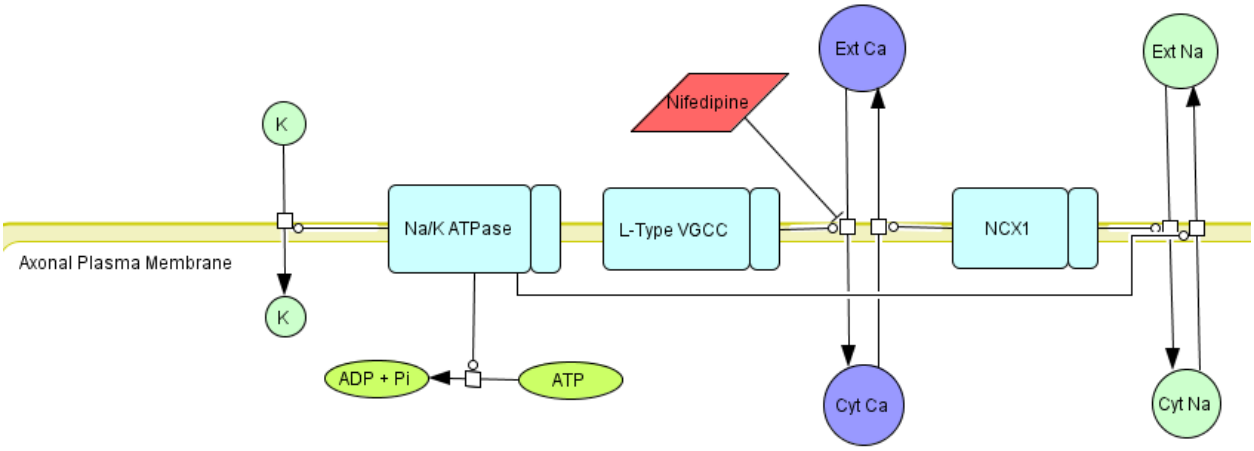

Figure 1 Calcium influx mechanisms at the plasma membrane.

2.3 Calcium Dyshomeostasis

2.3.1 Cytosolic calcium

Cytosolic calcium levels are kept very low (~100nM) during homeostasis. However, there is a substantial increase in intra-axonal calcium levels in response to injury. As mentioned previously, one proposed mechanism of this calcium rise is due to L-type voltage gated calcium channel activation. Upon VGGC activation, an influx of extracellular calcium into the axon is observed as well as activation of calcium release from intra-axonal stores, such as the axoplasmic reticulum (AR) and mitochondria (Villegas et al., 2014). Such large increases in calcium allow for calcium sensitive proteases, such as calpain, to activate and degrade axonal cytoskeletal components (Ma et al., 2013). Although there are mechanisms in place to counter small-scale increases of calcium concentration, such as calcium buffers (Schwaller, 2010), the

substantial increases observed in axon degeneration may allow for a positive feedback mechanism of release from intra-axonal compartments.

There are also transporters at the plasma membrane that function to remove calcium from the cytosol. The two transporters considered in the model are the plasma membrane calcium ATPase (PMCA) and Na^+/Ca^{2+} exchanger (NCX) (Figure 2). The PMCA hydrolyzes ATP to pump cytosolic calcium into the extracellular space. Its activity is also modulated by calmodulin. Upon calmodulin binding calcium to form the calcium-calmodulin complex (binding affinity in the low micro molar range), the complex can interact with a binding site near the PMCA's C-terminal domain to increase the ATPase's affinity for calcium and release autoinhibiton (Brini & Carafoli, 2003; Zhou et al., 2013). Furthermore, binding of calcium-calmodulin exposes sites for phosphorylation by protein kinase C (PKC) to upregulate the PMCA's removal of cytosolic calcium (Wang et al., 1991; Strehler & Zacharias, 2001). Under homeostatic conditions where the Na^+/K^+ ATPase is functioning, the NCX harnesses the sodium electrochemical gradient to remove calcium from the cytosol with a 4:1 stoichiometry (Dong, Dunn & Lytton, 2002). However, in injury conditions, there is a reversal of NCX activity at the axonal plasma membrane causing an influx of extracellular calcium (LoPachin & Lehning, 1997). Overall, these two transporters significantly contribute to the removal of calcium from the cytosol under homeostatic conditions and maintain important roles in axonal injury (Brini & Carafoli, 2011; Stirling & Stys, 2010).

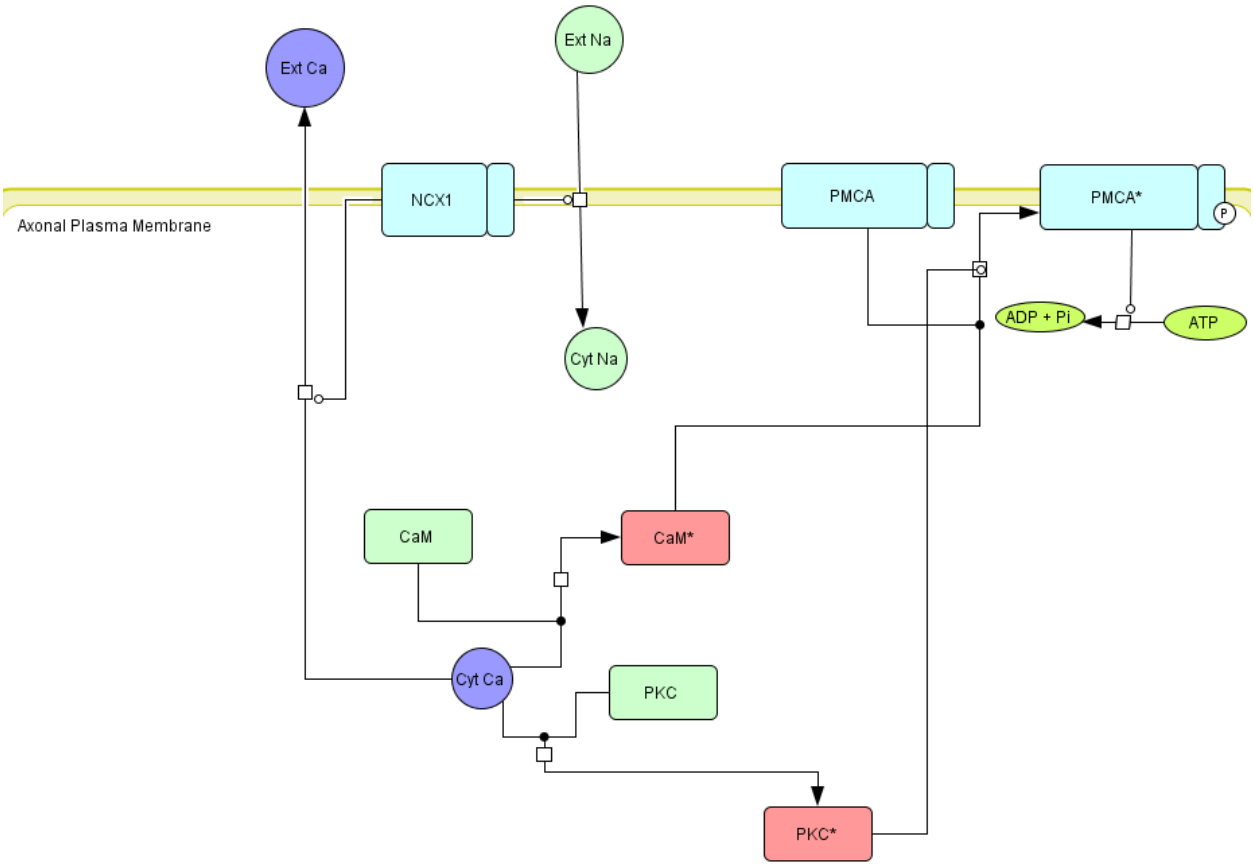

Figure 2 Mechanisms of calcium removal at the plasma membrane.

2.3.2 Role of axoplasmic reticulum in calcium dyshomeostasis

The axoplasmic reticulum (AR) is an important target of intra-axonal calcium release. Calcium release from this store is robustly mediated through the ryanodine receptor (RyR) and inositol triphosphate receptor (IP3R) (Stirling & Stys, 2010; Villegas et al., 2014). The axoplasmic reticulum also acts as a sink for excess cytosolic calcium. Through the activity of the smooth endoplasmic reticulum calcium ATPase (SERCA) pump, the AR takes up cytosolic calcium rapidly in an ATP dependent manner.

Ryanodine receptors are activated by the accumulation of intra-axonal calcium and other signaling molecules such as cyclic ADP-ribose (cADPR) (Guse, 1999). Calcium binding affinity

is enhanced for the RyR in the presence of cyclic ADP-ribose (cADPR) (Higashida et al., 2007). IP3Rs become activated when bound to inositol triphosphate (IP3). IP3 is generated by the cleavage of phosphatidylinositol 4,5-bisphosphate (PIP2) by phospholipase C (PLC). The PLCβ isoform becomes activated through G-protein coupled receptor signaling, and PLCγ is regulated through phosphorylation by tyrosine kinases (Kim et al., 1999). However, the activation of other isoforms such as PLCδ1, which is ubiquitously expressed in neuronal cells, relies on binding free calcium (Kim et al., 1999). Although all PLC isozymes are activated by Ca^{2+} *in vitro*, PLCδ seems more sensitive to Ca^{2+} than the other isozymes. Furthermore, PLC activity is attenuated through activated PKC. An increase in Ca^{2+} ion concentration within the physiological range (0.1–10 μM) is sufficient to stimulate PLCδ1 but not PLCβ1 (Kim et al., 1999). For simplicity, only the PLCδ1 isoform is considered in this model (Figure 3).

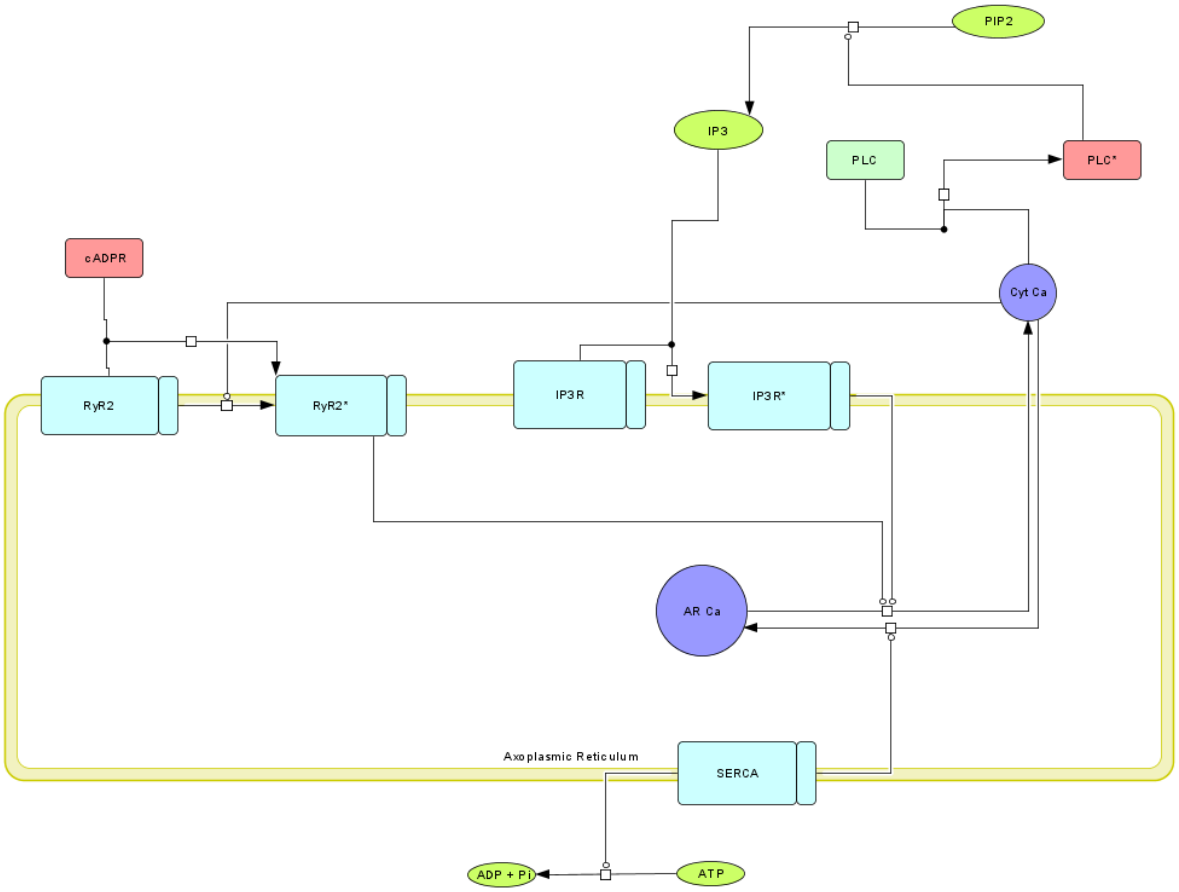

Figure 3 Calcium release and uptake at the axoplasmic reticulum.

2.3.3 Role of mitochondria in calcium dyshomeostasis

Mitochondria are also an important intracellular source of calcium. At small increases of cytosolic calcium, the mitochondria serve as a sink to buffer the fluctuation. However, larger perturbations in cytosolic calcium lead to mitochondrial dysfunction and release of its calcium (Brookes et al., 2004; Yan et al., 2006; Court, & Coleman, 2012). Following axonal injury, there is a loss of mitochondrial membrane potential and prominent mitochondrial swelling in distal axon segments before fragmentation (Park et al., 2013; Barrientos et al., 2011).

There is evidence that axoplasmic calcium release through ryanodine and IP3 receptor activity leads to the opening of the mitochondrial permeability transition pore (mPTP), which is a crucial event in axotomy induced axon degeneration (Villegas et al., 2014; Barrientos et al., 2011). Cytosolic calcium enters the mitochondria through the mitochondrial uniporter (MCU), which may lead to calcium overload and subsequent opening of the mPTP (Chappell & Crofts, 1965; Crompton & Costi, 1985; Villegas et al., 2014). Through the mPTP, calcium can exit the mitochondria and flood into the cytosol along with other mitochondrial solutes under 1.5kDa (Peng & Jou, 2010; Giacomello et al., 2007; Marchi et al., 2014). Other consequences of mPTP opening in axon degeneration include the loss of the mitochondrial membrane potential (Halestrap, 2009), decrease in ATP production (Villegas et al., 2014), and generation of reactive oxygen species (ROS) (Court & Coleman, 2012). Through loss of the membrane potential, calcium may also leave the mitochondria through the reversal of the MCU (Giacomello et al., 2007).

The model also includes antiporters present on the mitochondrial membrane including the Na^+/Ca^{2+}, H^+/Ca^{2+}, and the Na^+/H^+ exchanger (Figure 4). The Na^+/Ca^{2+} and H^+/Ca^{2+} exchangers both extrude calcium from the mitochondria with a stoichiometry of three sodium or hydrogen ions for every two calcium ions (Giacomello et al., 2007), and the Na^+/H^+ exchanger shuttles one sodium ion out of the mitochondria while one hydrogen ion is removed from the cytosol. The transport of each species in this model is electroneutral and based off respective species' concentration gradients. These antiporters maintain a substantial role in the movement of ions considered in the model due to their ubiquitous expression and are thus necessary to include in the model.

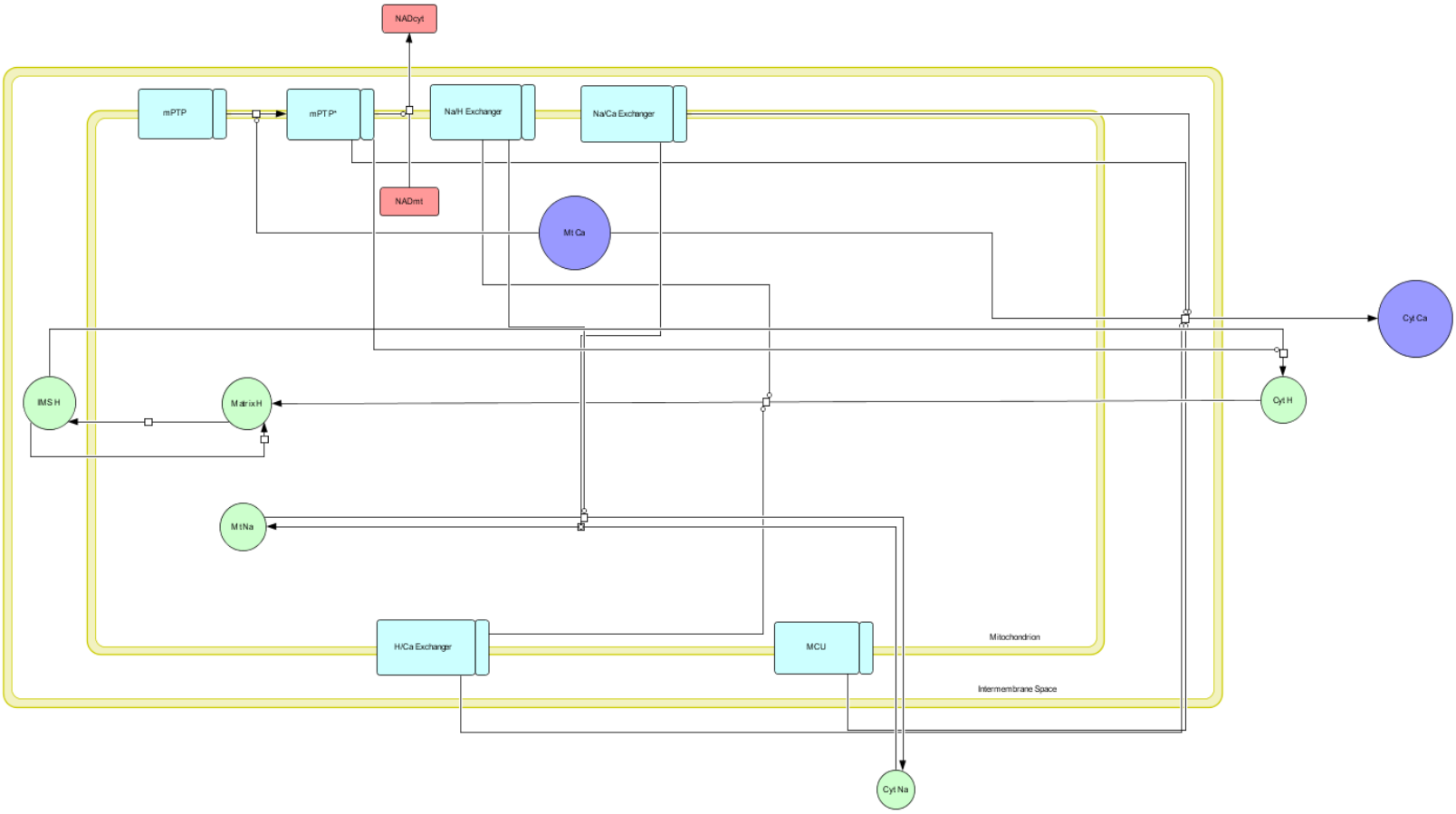

Figure 4 Calcium release and uptake at the mitochondria.

2.4 NAD Biosynthesis

Nicotinamide adenine dinucleotide (NAD) biosynthesis is represented in the model through the NAD salvage pathway. Although the *de novo* pathway utilizing tryptophan also contributes to the generation of NAD, the salvage pathway is heavily relied on for NAD synthesis and is representative of the mechanism used by neurons in primary culture (Canto et al., 2015; Nikiforov et al., 2011). NR and Nam, collectively termed niacins, are precursors used in the NAD salvage pathway (Belenky, Bogan, & Brenner, 2007; Stein & Imai, 2012). NR is converted into nicotinamide mononucleotide by NRK and Nam is converted into NMN by nicotinamide phosphoribosyl transferase (NAMPT). Nam is the precursor of the salvage pathway

considered in the model since it is the main substrate present in cell culture media (Nikiforov et al., 2011).

2.4.1 NAMPT

As mentioned above, NAMPT converts Nam into NMN, which can then contribute to the cytosolic NAD pool (Figure 5). NAMPT is also homogeneously distributed in neurons (Esposito et al., 2012), and is the rate limiting enzyme of NAD synthesis from the salvage pathway. Although it is intuitive that inhibition of NAMPT decreases NAD synthesis, and studies have demonstrated elevated levels of NAD to be protective (Bramely et al., 2016; Sasaki et al., 2009; Shen et al., 2013), NAMPT inhibition actually protects against Wallerian degeneration. Studies inhibiting NAMPT activity usually employ the compound FK866 (Bramely et al., 2016; Sasaki et al., 2009; Shen et al., 2013; Esposito et al., 2012). Inhibiting NAMPT raises the concentration of Nam and lowers NMN concentration, thus effectively lowering NAD concentration.

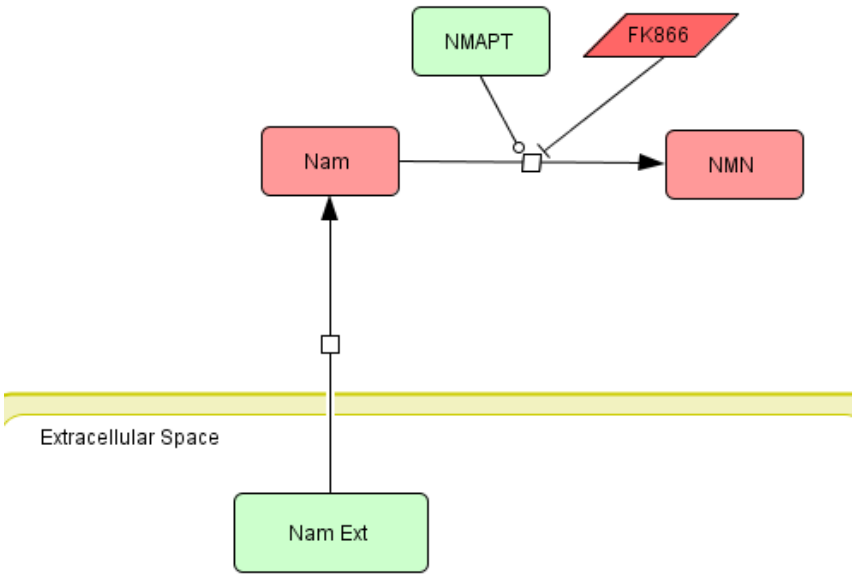

Figure 5 Enzymatic activity of NAMPT.

2.4.2 NMNAT enzymatic function and degradation by PHR1

Nicotinamide mononucleotide adenylyl transferase (Nmnat) uses ATP to convert NMN into NAD (Figure 6). There are three isoforms: Nmnat1, Nmnat2, and Nmnat3. Each isoform is localized to a different compartment in neurons (DiStefano & Conforti, 2013; Lau et al., 2009). Nmnat1 is localized to the nucleus, Nmnat2 is found in the cytosol and undergoes anterograde transport in axons, and Nmnat3 is localized to the mitochondria (Berger et al., 2005). Nmnat1 is the protective subunit of the WLD^s protein, and other studies expressing Nmnat demonstrate its protective effects against Wallerian degeneration (Araki et al., 2004; Babetto et al., 2010). Although Nmnat1 is normally expressed in the nucleus, its protective role in WLD^s displays an extranuclear mechanism of protection (Coleman & Freeman, 2010; Beirowski et al., 2009; Yahata et al., 2009; Cohen et al., 2012). Furthermore, expression of Nmnat1 outside of the nucleus confers robust axonal protection (Sasaki et al., 2009; Sasaki & Milbrandt, 2010). Due to this protective cytosolic localization, high neuronal specific expression, and the necessary expression to prevent axon degeneration, the model considers Nmnat2 and its transport (Gilley & Coleman, 2010). Importantly, Nmnat2 loss is sufficient to induce Wallerian degeneration (Gilley et al., 2013; Hicks et al., 2012). Further studies correlating Nmnat2 turnover and onset of axon degeneration lend support for considering the Nmnat2 isoform (Gilley & Coleman, 2010; Beirowski et al., 2005; Yan et al., 2010).

The model also encompasses the ability of Nmnat to catalyze the reverse direction generating NMN and ATP from NAD. The directionality of the reaction is dependent on the

relative concentrations of NAD and NMN, where the relative abundance of one will shift synthesis in favor of the other.

Nmnat maintains a short half-life, where its turnover rate is approximately 4 hours (Gilley & Coleman, 2010). This rapid turnover is due to its association to Golgi-derived vesicles through an intact palmitoylation site (Milde et al., 2013) during axonal transport and degradation by the ubiquitin-proteasome system, where degradation of Nmnat2 is directed by the E3 ubiquitin ligase PHR1 (Gilley & Coleman, 2010; Babetto et al., 2013). The model also incorporates transport of Nmnat2, and the introduction of injury blocks this transport to the distal axon. The decrease in axonal Nmnat2 in response to axotomy is inversely correlated with the active SARM1 in the model.

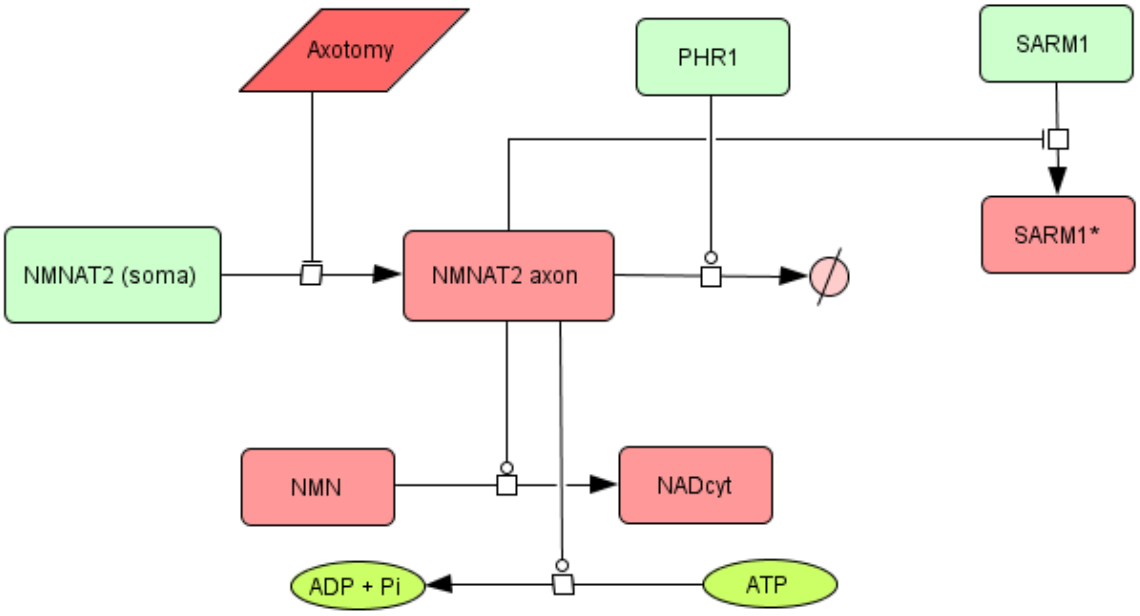

Figure 6 Enzymatic activity of Nmnat and degradation of Nmnat by PHR1.

2.4.3 NAD compartmentalization

There are distinctive pools of NAD in a cell: nuclear, cytosolic, and mitochondrial (Belenky, Bogan, & Brenner, 2007; Stein & Imai, 2012). The model considers cytosolic and mitochondrial NAD pools since after injury these are the only two pools available in the distal axon segment (Figure 7). Cytosolic NAD is synthesized from various extracellular precursors including NR, NA, NAR, and Nam. These precursors are derived from diet in living organisms. In cell culture, however, it is common for the only NAD precursor available to be Nam. Due to variability in diet and the majority of NAD being derived from Nam in physiological settings, the model only considers synthesis of cytosolic NAD from the Nam precursor (Nikiforov et al., 2011). The model also includes the cytosolic NADase SIRT2, which generates Nam through NAD cleavage, and the plasma membrane associated NADase CD38, which cleaves NAD to give Nam and ADPR or cADPR (Belenky, Bogan, & Brenner, 2007; Stein & Imai, 2012).

The mitochondria contain up to 70% of the cell's NAD and cannot traverse the mitochondrial membrane (Nikiforov et al., 2011). Since Nmnat3 is found at very low levels in neurons, this enzyme's presence in mitochondria allows for only small levels of mitochondrial NAD synthesis and is omitted from this mathematical model. The intermediate NMN in the NAD biosynthesis pathway has been shown to cross the mitochondrial inner membrane through an unidentified channel to serve as a precursor for mitochondrial NAD synthesis (Nikiforov et al., 2011). It is important to include this NAD pool in the model due to its significant size. Furthermore, opening of the mPTP in axon degeneration is a well-characterized event that allows all molecules of 1.5 kDa or less to exit the mitochondria into the cytosol including NAD. Thus, the mitochondria potentially provide a significant source of cytosolic NAD in axon degeneration.

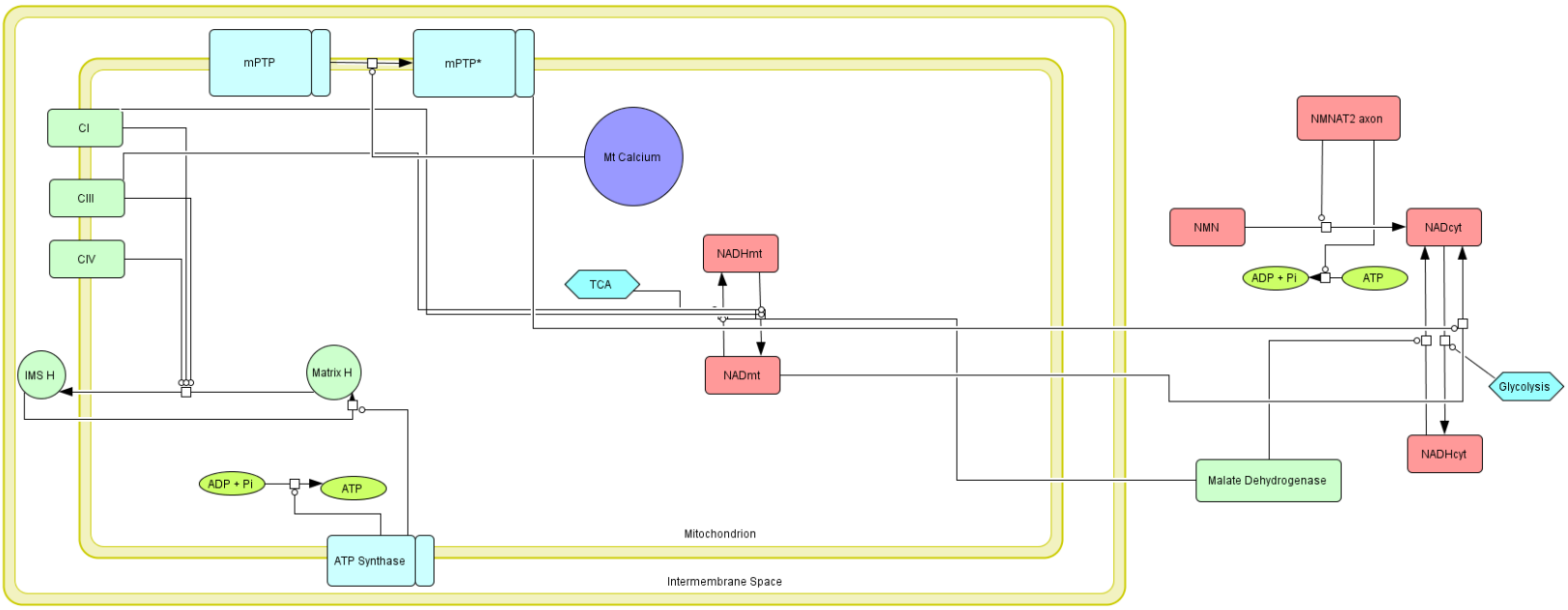

Figure 7 Cytosolic and mitochondrial NAD and contributions to ATP production.

2.5 SARM1 and NAD consumption

2.5.1 Generation of NAD cleavage products and influence on calcium release

Recently, the novel NADase activity of sterile alpha and TIR motif-containing protein 1 (SARM1) was discovered (Essuman et al., 2017). The cleavage products from SARM1's activity include ADP-ribose (ADPR), cyclic ADP-ribose (cADPR), and nicotinamide (Nam). Both ADPR and cADPR influence calcium concentration in the distal axon by regulating channels at the plasma membrane and internal membranes respectively (Perraud et al., 2001; Till and Ladurner, 2009; Guse et al., 1999). ADPR binds TRPM2 at the axonal plasma membrane (Sumoza-Toledo & Prenner, 2011; Islam, 2012), which contributes to the influx of extracellular calcium into the cytosol. TRPM2 also acts to cleave ADPR generating AMP (Sumoza-Toledo & Prenner, 2011). cADPR enhances calcium release from the axoplasmic reticulum through binding ryanodine type II receptors to increase their open probability as well as their affinity for calcium (Cancela et al., 2000; Higashida et al., 2007). cADPR can act as an agonist on ryanodine

receptors to increase cytosolic calcium levels as well as act cooperatively with calcium to induce feed forward mechanisms of calcium release at ryanodine receptors (Higashida et al., 2001). Nam was also shown to provide negative feedback to NAD cleavage by SARM1 (Essuman et al., 2017). The implications of SARM1's action are of high interest in the context of Wallerian degeneration since there are precipitous drops in NAD after a lag phase (approximately 4 hours) immediately before observable degeneration in injured axons. However, the mechanism of this drastic drop along with NAD's significance in the Wallerian degeneration remain elusive (Freeman, 2014).

In the model, SARM1 contributes to the consumption of NAD in response to axonal injury (Figure 8). A well-known class of NAD consuming enzyme includes ADP ribose cyclases, such as CD38. CD38 generates ADPR and cADPR and can hydrolyze cADPR to ADPR (Graeff et al., 2009; Belenky, Bogan, & Brenner, 2007; Higashida et al., 2007). This enzyme was included for its ubiquitous expression in neurons (Mizuguchi et al., 1995). However, CD38 knockout models of axonal injury confer no protection against axon degeneration (Sasaki et al., 2009), whereas expression of SARM1 is necessary for Wallerian degeneration to occur (Osterloh et al., 2012).

The model also investigates the temporal dependence of SARM1's activation as well as its dependence on the presence of Nmnat2 as there are no identified activators of SARM1. SARM1 activation in the model is represented as the proposed "trophic factor model" (Freeman, 2014), which states that the presence of a survival factor (Nmnat2) is needed to suppress the default axon destruction program (SARM1 activation and Wallerian degeneration). Although it remains unclear if the presence of Nmnat2 inhibits SARM1 enzymatic activity, whether through

direct or indirect mechanisms, the model inversely correlates the concentration of Nmnat2 with the concentration of active SARM1.

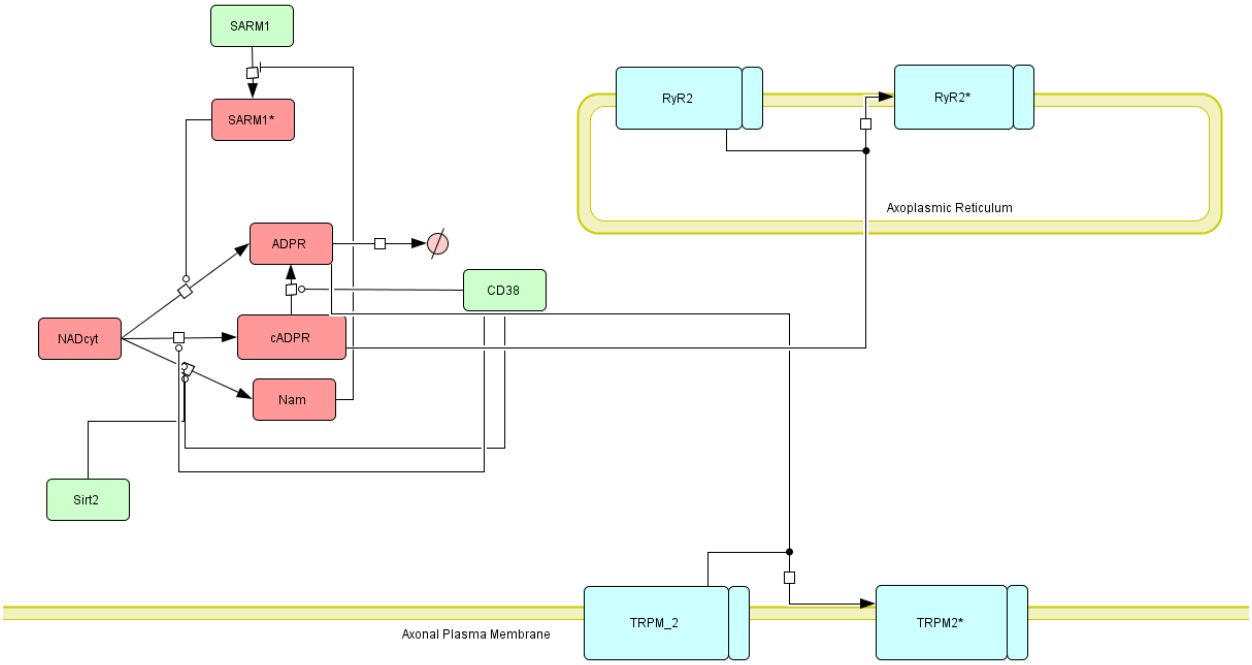

Figure 8 NAD cleavage products influence calcium mobilization.

2.6 Energy Dyshomeostasis

2.6.1 NAD depletion

In axon degeneration, precipitous drops in ATP and NAD are seen about 4 hours following axotomy. However, axons remain viable at about 30% of original ATP concentration (Shen et al., 2013). NAD is coupled to ATP production through the electron transport chain (ETC). To contribute to ATP production in the ETC, NAD must be in its reduced form, NADH (Figure 7). NADH is generated through glycolysis in the cytosol and uses the malate-aspartate shuttle to move its reductive capacity into the mitochondrial matrix. NAD that is in the

mitochondrial matrix can also become reduced to NADH through the tricarboxylic acid (TCA) cycle.

The malate-aspartate shuttle consists of cytosolic malate dehydrogenase, mitochondrial malate dehydrogenase, malate-alpha-ketoglutarate antiporter, and glutamate-aspartate antiporter (Berg, Tymoczko, & Stryer, 2006). Cytosolic malate dehydrogenase oxidizes NADH and concurrently reduces oxaloacetate to malate. Malate is then able to enter the mitochondrial matrix via the malate-alpha-ketoglutarate antiporter. In the matrix, malate dehydrogenase oxidizes malate to oxaloacetate and reduces mitochondrial NAD to NADH. Oxaloacetate is transformed into aspartate by mitochondrial aspartate aminotransferase and is moved into the cytosol by the glutamate-aspartate antiporter where it is converted back into oxaloacetate. The model has transport of NADH from the cytosol contingent upon the abundance of malate dehydrogenase present in the cytosol. It is assumed that concentrations of malate and oxaloacetate remain unchanged over the degenerative time course.

In the model, generation of NADH from cytosolic NAD via the glycolytic process is assumed to occur at a fixed rate since the concentrations of glycolytic enzymes in the context of axon degeneration have not been shown to be perturbed. A similar assumption is made for the conversion of matrix NAD being reduced to NADH via the TCA cycle.

In the presence of NADH and FADH2, the ETC oxidizes these electron carriers and is able to move matrix hydrogen ions into the inter membrane space of the mitochondria. Generation of ATP is by the ATP synthase, which moves four hydrogen ions down hydrogen's concentration gradient from the inter membrane space into the matrix and combines ADP and inorganic phosphate to form ATP. The model assumes there is an abundance of ADP and

inorganic phosphate, thus making generation of ATP by ATP Synthase dependent upon the proton gradient established by the ETC oxidizing available electron carriers (Figure 7).

2.6.2 Influence of ATP depletion on cytosolic calcium

As mentioned previously, reductions in ATP lead to failure of the Na+/K+ ATPase and subsequent depolarization of the distal axon mediating extracellular influx via L-type VGCCs. Additionally, ATP reductions may contribute significantly to calcium accumulation from intracellular stores. The SERCA pump on the AR is a crucial ATPase for the reuptake of cytosolic calcium (stoichiometry of calcium to ATP is 2:1). At significantly decreased levels of ATP, failure of this pump may have a substantial contribution to the rapid accumulation of cytosolic calcium immediately preceding axonal fragmentation. Furthermore, under low ATP concentrations, failure of the PMCA (stoichiometry of calcium to ATP is 1:1) may also contribute to cytosolic calcium accumulation.

2.7 Degeneration

Calpastatins, which inhibit calpains, effectively block the fragmentation observed in axon degeneration (Yang et al., 2013). Specifically, m-calpain is implicated in Wallerian degeneration (Ma et al., 2013). Thus, the model incorporates such calcium sensitive proteases, which become activated in the range of cytosolic calcium 100uM - 1000uM. Common cytoskeletal substrates cleaved by m-calpain and crucial to structural integrity of the axon including alpha tubulin, beta tubulin, and neurofilament heavy chain (NF-H), are represented in the model initially as intact cytoskeletal components (Figure 9).

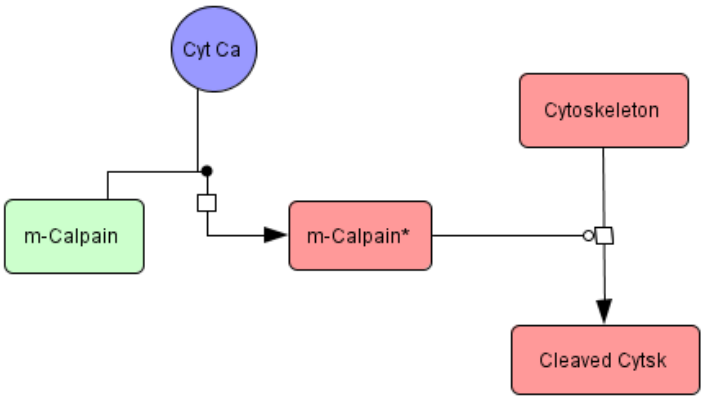

Figure 9 Calpain activation through binding cytosolic calcium.

2.8 Mathematical Modeling using Biochemical Systems Theory

The visual models shown and described above are represented mathematically according to Biochemical Systems Theory (BST). BST is a mathematical framework of ordinary differential equations (ODEs) utilizing power law expansions to represent biochemical pathways (Voit, 2000). Mathematical models using power law expansions have been used to represent and analyze various biochemical systems including metabolic and genetic networks as well as cell signaling pathways (Broome & Coleman, 2011; Braatz & Coleman, 2015).

In this work, MATLAB R2017b was used to analyze a system of nonlinear, first order, autonomous ordinary differential equations. (For full code, see Appendix). The two categories of ODEs used are termed system equations and rate equations. System equations (Equation (1)) demonstrate the change of a variables' concentration over time depending on precursors, consumers, activators, and inhibitors of the variable.

Equation (1)

$$\frac{dX(2)}{dt} = X(1) * k_{synthesis} - X(2) * k_{degradation}$$

$$X(1) \xrightarrow{k_{synthesis}} X(2) \xrightarrow{k_{degradation}} \emptyset$$

Here, the ODE shown represents the change in concentration of species $X(2)$ over time. This example reaction has no modifiers. The rates of synthesis and degradation of $X(2)$ are $k_{synthesis}$ and $k_{degradation}$ respectively.

If a reaction has modifiers, rate equations (Equation (2)) are used to describe the change in rate of catalysis or inhibition on a reaction over time corresponding to the prevalence of activators or inhibitors, respectively. The rate equation applying to a reaction consists of a constant multiplied by the sum of all activator and inhibitor species. In the sum, activators are represented as positive values and the inhibitors are negative values.

Equation (2)

$$\frac{dX(5)}{dt} = C * [X(3) - X(4)]$$

$$X(1) \xrightarrow{X(5)} X(2)$$

Here, we consider the synthesis of $X(2)$ to be dependent on the presence of catalyst $X(3)$ and inhibitor $X(4)$. Thus, the rate of synthesis is no longer represented as $k_{synthesis}$, but as a new value $X(5)$ that changes in time. C is a constant that can be empirically determined for each reaction.

Each species in the model is assigned a concentration, and each reaction has a corresponding rate. These values were derived from databases (PaxDB, PBD, and HMDB) and primary literature. For proteins, values were obtained in parts per million from the frontal cortex, and through utilization of corresponding molecular weights, were converted to micro molar

concentration. Furthermore, each species is categorized as a dependent or independent variable. Dependent variables are defined as species that will change in concentration over time. Independent variables are defined as species that are not a product of a reaction in the model, and thus will maintain constant concentration over time.

The figures generated by the model fall into three categories: control condition (baseline), injured condition (axotomy), and treatment condition. To analyze the effect of treatments, the difference between the states were taken where applicable. By taking the difference between treatment and control conditions and difference between treatment and disease conditions respectively, we can qualitatively assess the effectiveness of treatments and their targets. Any positive values for species then indicates an increase between states, and negative values indicate decreases. For each treatment, there were two categories: early treatment and late treatment. Early treatment is administered at the beginning of the injury (t=0.1).

3. Results

The results encompass qualitative predictions for potential mechanisms of Wallerian degeneration. Such mechanisms were investigated through the introduction of pharmacological treatments frequently used on primary neuronal cultures and knockout conditions for certain species in the mathematical model. All pharmacological treatments were administered early in the program run time (t=0.1). Each alteration's impact on the molecular events of the axon degeneration pathway is presented below.

3.1 Characterization of Wallerian Degeneration in Zebra Finch RGCs

Equation (3)

$$Degeneraiton\ Index = \frac{DegeneratedArea}{TotalArea}$$

Degeneration Index (DI) is the fraction of degenerated axons where 0 represents no degeneration and 1 represents complete degeneration.

Equation (4)

$$y = \frac{1}{(1+\frac{t_{50}}{t})^{Hill}}$$

Where t_{50} is time of 50% degeneration (DI = 0.5), t is total time of degeneration (DI = 1), and $Hill$ is the slope of the sigmoidal function. y represents the normalized DI value.

Retinal ganglion cells (RGCs) derived from zebra finch embryos were plated and subjected to mechanical injury to induce Wallerian degeneration (Figure 10a). Quantification of degeneration is described in Equation (3). Time-lapse imaging was used to generate a sigmoidal fit (Equation (4)) for the time course of degeneration (Figure 10b). Injured axons reached maximal degeneration by about 13 hours (Figure 10c).

Axotomized axons were subjected to various dosages of nifedipine (3 µM, 6 µM, and 18 µM) to block L-type VGCCs. Treatment of axotomized axons with 6 µM nifedipine demonstrated peak protectiveness (Figure 10d). This nifedipine treatment provided 42% protection compared to axotomized axons with no nifedipine treatment (Figure 10e). Solving for the corresponding t_{50} from Equation (4) and applying a logistical regression fitted curves for degeneration in the nifedipine treatments. Injured axons reached maximal degeneration by about 23 hours when treated with 6 µM nifedipine (Figure 10c).

3.2 Simulation of Axotomy

Controls were first established before introduction of perturbations to the degenerative pathway. In the control condition, there is no axotomy and thus no perturbation to the system

components. Axotomy (axon transection) initiating the degenerative pathway induces the halt of Nmnat2 transport from the soma down the axon (Figure 11a).

The activation of the central executioner protein, SARM1, is inversely correlated with the presence of Nmnat2 in the axotomy model (Figure 11a,b). Upon axotomy, there is a fast activation of SARM1 followed by a later decline mediated by Nam inhibition and an intrinsic inactivation rate (Figure 11b). Due to rapid SARM1 activation, there is an early decline in cytosolic NAD and corresponding early increase in ADPR and cADPR products (Fig 11c,d). The increases in these cleavage products occur in ratios of product to original NAD concentration comparable to ratios generated in studies characterizing the NADase activity of SARM1 (Summers et al., 2016; Essuman et al., 2017).

Calcium released from cADPR-activated RyR channels may be taken up by the mitochondria via the MCU causing an increase in matrix calcium (Deniaud et al., 2008; Villegas et al., 2014; Vargas et al., 2015). In the model, rises in matrix calcium are sufficient to open the mPTP. The early rise in cADPR observed in the axotomy model is sufficient to cause increases in matrix calcium for mPTP opening. Upon opening of the mPTP, mitochondrial species are lost to the cytosol, including NAD (Figure 11e). This new contribution of NAD to the cytosol provides active SARM1 a larger substrate pool to generate a larger, later increase in ADPR and cADPR. With this substantial increase in NAD cleavage products, many RyR channels become activated causing the start of substantial cytosolic calcium accumulation. Although cADPR is the minor product of NAD cleavage by SARM1, its cyclic structure makes cADPR very stable with a relatively long half-life on the time scale of days (Storey & Storey, 2002). In contrast, the presence of ADPR, a major product of SARM1 NADase activity, is transient with a half-life

commonly observed on the time scale of minutes under stress conditions (Storey & Storey, 2002; Hassa et al., 2006). Therefore, both molecules may substantially influence cytosolic calcium.

Additionally, upon opening of the mPTP, the mitochondria lose their membrane potential, and thus their full capacity to generate ATP (Figure 11f). This energy failure in the distal axon causes depolarization and opening of the L-type VGCCs allowing for a steady influx of extracellular calcium into the cytosol. This event of VGCC opening is evident in the inflection point observed in cytosolic calcium (Figure 11g). Furthermore, large cytosolic calcium accumulation is promoted by energy failure through the inactivity of calcium ATPases and feed forward calcium release mechanisms from intracellular stores.

In response to large, prolonged increases in cytosolic calcium, calcium sensitive proteases become activated. In the model, m-calpain is the calcium sensitive protease that becomes activated by 100-1000 μM cytosolic calcium concentrations observed during axotomy (Khorchid & Ikura, 2002). With calpain activation, there is an increase in degraded cytoskeletal products, which follows the characteristic sigmoidal function of degeneration (Figure 11h). In Figure 11h, the curve flattens once all cytoskeletal components are degraded at approximately t=62.

3.3 SARM1 Knockout

Representation of a knockout requires the removal of the variable from the axotomy model. Removing SARM1 from the model yielded cytosolic NAD levels in axotomy comparable to that of the control (no axotomy) (Figure 12a). With the preservation of NAD, there are high levels of ATP, which will prevent depolarization of the distal axon in the time span considered (Figure 12b). There was also no generation of an early spike in cADPR that would cause cytosolic calcium uptake by the mitochondria, and thus no mPTP opening (Figure 12c). Furthermore,

cytosolic calcium in SARM1 knockout axotomy was similar to cytosolic calcium concentration of the control (Figure 12d). Since there was no calcium accumulation, there is no synchronized degeneration observed (Figure 12e). Any degeneration that occurs does so over a significantly longer time span compared to axotomy at basal calpain activity.

3.4 Nmnat2 Knockout

Removing Nmnat2 from the control model caused an increase in the amount of active SARM1 comparable to axotomy (Figure 13a). With similar amount and duration of active SARM1, there is a corresponding decrease in cytosolic NAD and increase in cleavage products (Figure 13b,c). Additionally, there is comparable cytosolic calcium accumulation to the axotomy model (Figure 13d). This calcium accumulation facilitates the opening of the mPTP, which in turn hinders ATP production by mitochondria. Chronic activity of calcium ATPases also contributes to the ATP decline observed, which feeds forward into further cytosolic calcium accumulation (Fig 13e). With similar time courses in ATP depletion and cytosolic calcium accumulation, the degeneration time course proceeds similarly in the Nmnat2 knockout of the control model compared to the axotomy model (Figure 13f).

3.5 PHR1 Knockout

Knockout of the ubiquitin proteasome PHR1 significantly increases the half-life of Nmnat2 (Babetto et al., 2013). To test this in the model, PHR1 was removed from the axotomy condition. Removing PHR1 yielded a large increase of axonal Nmnat2 similar to levels in the control model (Figure 14a). As a result of sustained Nmnat2 levels in the time course considered, SARM1 remained inactivated (Figure 14b). Without SARM1's enzymatic activity, there was no observable NAD cleavage, energy failure, or cytosolic calcium accumulation (Figure 14c-f). In

the absence of cytosolic calcium accumulation, there was only slow degeneration generated from basal activity of calpain in the model (Figure 14g).

3.6 Nifedipine Treatment

Treatment with nifedipine blocks L-type VGCCs. In primary neuronal culture, nifedipine treatment provides a short period of protection through delaying cytosolic calcium increases (Bramley et al., 2016; George, Glass, & Griffin, 1995). Nifedipine treatment in the model is set at 6 μM, which has been shown to be an effective dosage as previously presented in assays with zebra finch RGCs (see section 3.1).

Axotomy in the nifedipine treatment condition activates SARM1 to the same levels and length of time as axotomy with no drug treatment (Figure 15a). Since nifedipine treatment also does not affect mPTP opening, comparable amounts of ADPR and cADPR are generated during nifedipine treatment axotomy condition and no treatment axotomy condition (Figure 15b). Therefore, RyR receptors on internal calcium stores are activated similarly and release comparable amounts of calcium, which is evident early on in calcium accumulation (Figure 15c,d).

Although the mPTP opening causes energy failure in no treatment axotomy as well as nifedipine treatment axotomy, nifedipine demonstrates slightly elevated ATP levels over time (Figure 15e). This elevation in ATP may be attributed to the lower level of calcium ATPase activity in response to slower cytosolic calcium accumulation in nifedipine treatment axotomy. Slow cytosolic calcium accumulation is due to the inactivity of the VGCCs in spite of energy failure, leaving the main source of calcium accumulation to be released from internal stores.

Due to a slower time course of cytosolic calcium accumulation in nifedipine treatment, it takes longer for the cytosolic concentration to reach the high micromolar range where calpains are activated. Thus, the delayed calpain activation causes a delay in the axonal degeneration time course. However, when calpains become activated degeneration proceeds at a rate comparable to no treatment-axotomy (Figure 15f).

3.7 FK866 Treatment

FK866 treatment inhibits the action of NAMPT from converting Nam to NMN. In primary neuronal culture, FK866 treatment provides modest protection, although the protective mechanism remains elusive (Conforti, Gilley, & Coleman, 2014). FK866 treatment in the model is set at 0.5 μM, which has been shown to be in the range of effective dosage from previous assays with zebra finch RGCs (Bramley et al., 2016). Differences between species were obtained through the difference of the FK866 treated-axotomy and no treatment-axotomy models.

In response to FK866 treatment there is a slight decrease in the amount of active SARM1 compared to axotomy with no treatment (Figure 16a). The model represents an inhibiting effect of Nam binding SARM1 since Nam is an inhibiting cleavage product of SARM1 (Summers et al., 2016; Essuman et al., 2017). Support for the mechanism of FK866 treatment is observed in the substantial increase of Nam (Figure 16b).

With a decreased amount of active SARM1 due to increased Nam levels, there is a net decrease in formation of NAD cleavage products (Figure 16c). In response to injury, SARM1 in FK866 treatment-axotomy has slightly lower initial activation levels, which decreases cADPR production and slightly attenuates rises in initial cytosolic calcium delaying mPTP opening. With delayed release of NAD from the mitochondria via the mPTP (Figure 16d), the time course of

ADPR and cADPR generation by SARM1 will also be delayed along with the effects of these products of cytosolic calcium accumulation.

However, in addition to forming ADPR and cADPR upon cleavage of NAD, SARM1 forms Nam (Summers et al., 2016; Essuman et al., 2017). Around the time of peak cytosolic NAD, due to release from the mitochondria, there is a rapid decline in the amount of active SARM1. With FK866 treatment-axotomy, active SARM1 decrease is more dramatic than no treatment-axotomy. This more pronounced decrease causes a net lower production of ADPR and cADPR of the second spike in Fk866 treatment (Figure 16c). With less cADPR and ADPR being formed, there are fewer active RyR and TRPM2 channels moving calcium present in the AR and extracellular space to the cytosol and thus slowing the rate of calcium accumulation (Figure 16f).

Slower cytosolic calcium accumulation over time mediated through cADPR activated RyR receptors and ADPR activated TRPM2 receptors allows for less ATP consumption by calcium ATPases. With less ATP being consumed in FK866 treatment axotomy, which still experiences energy failure, it provides an increase in ATP at each time point compared to axotomy with no treatment (Figure 16f). With a small buffer in ATP availability, it will take longer for the axon to depolarize and activate VGCCs, thus contributing to a slower cytosolic calcium accumulation time course.

As seen previously, slower cytosolic calcium accumulation in FK866 treatment due to decreased active SARM1 causes slower calpain activation and a subsequent delay in the axonal degeneration time course (Figure 16g). Thus, the protective action of FK866 treatment may be through promoting the accumulation of a SARM1 inhibitor.

3.8 mPTP Inhibition

Opening of the mPTP is an early event in axon degeneration since inhibition of the mPTP delays the onset of degeneration (Barrientos et al., 2011). To further explore the role of the mPTP in the degenerative pathway, inhibition was represented through the removal of the mPTP in the axotomy model.

Inhibition of the mPTP prevents the loss of the mitochondrial membrane potential and loss of NAD to the cytosol (Figure 17a-c). Maintaining potential allows the mitochondria to preserve their ATP producing capacity thereby providing ATP for calcium ATPase activity and preventing depolarization of the distal axon in the time course considered. Without the contribution of mitochondrial NAD, the only rises in ADPR and cADPR are from SARM1 cleaving cytosolic NAD, and no later rise in these products is observed (Figure 17c). These activities prevent large extracellular calcium influx and promote the removal of calcium from the cytosol. The early rise in calcium observed can be attributed to the activity of SARM1 (Fig 17d,e). Since Nmnat2 is lost during axotomy, SARM1 activation is still apparent. However, there is a sustained level of active SARM1 since there is less cytosolic NAD substrate available resulting in less Nam production.

Interestingly, despite a rise in cytosolic calcium, inhibition of the mPTP allows for the recovery of calcium concentration to more manageable levels in the time course considered. This recovery suggests that the release of NAD from the mitochondrial matrix provides an important substrate pool for SARM1 in the cytosol to generate the late rise in ADPR and cADPR, which enhance the movement of calcium from the extracellular space and intracellular stores respectively. This also suggests that early SARM1 activity causes a rise in mitochondrial calcium from cytosolic uptake to open the mPTP (Figure 17g). Furthermore, opening of the VGCCs and

their significant contribution to cytosolic calcium accumulation is prevented through the maintenance of energy homeostasis in mPTP inhibition during the time course.

Although inhibition of the mPTP does suggest a crucial role in degeneration, it is not completely protective. Degeneration still proceeds, albeit on a slower time course, due to moderate activation of calpain through SARM1 activity (Figure 17f).

Although the model considers a lower threshold for mitochondrial calcium concentration for mPTP opening than used in assays of mitochondrial swelling (Brustovetsky et al., 2003; Baumgartner et al., 2009; Wong, Steenbergen, & Murphy, 2013), this assumption is relevant since mitochondria take up calcium earlier in the lag phase before cytosolic calcium increases (Vargas et al., 2015), and the establishment of mPTP opening early on in the pathway may imply significant contributions to energy failure and VGCC activation. In general, oxidative stress maintains a significant role in mitochondrial dysfunction, and makes mitochondria more sensitive to calcium rises in formation of the mPTP (McStay, Clarke, & Halestrap, 2002). This is an important interaction to acknowledge since oxidative stress maintains an early role in axon degeneration (Press & Milbrandt, 2008; Fukui, 2016).

3.9 Diffusion of Axonal Calcium and Calpain Activation

Equation (5)

$$\frac{\partial A}{\partial t} = D\frac{\partial^2 A}{\partial x^2} + F(A)$$

Here, a general form of the reaction-diffusion equation is given for concentration of species A. D represents the diffusion coefficient for A, and $F(A)$ represents the relevant reactions generating and consuming the species.

A reaction-diffusion model is used here to investigate the stochastic process of calcium diffusion in axon degeneration. The two species considered are cytosolic calcium and calpain.

The space considered (axon unit) is 10 μm in length with calcium release at t=0 occurring from only intracellular stores in the center (x=5 μm) and diffusing throughout the compartment over time. Calpain is assumed to be spread homogenously throughout the space, and calcium release occurs at one site in the axon unit. No flux boundary conditions were employed for the axon unit.

The generation of active calpain occurs in the presence of cytosolic calcium concentrations greater than 100 μM. In the reaction-diffusion equations (Equation (5); see Appendix for the reaction-diffusion script), the formation of active calpain through inactive calpain binding free calcium (K_d = 25 μM) decreases the amount of free calcium and inactive calpain. The diffusion coefficient for calcium used in this stochastic model is two-orders of magnitude slower than the diffusion coefficient for freely diffusing calcium (D = 530 $\mu m^2/s$) (Donahue & Abercrombie, 1987). This assumption is made due to the small diameter of RGC axons (0.2 – 3.6 μm), which creates a significantly smaller space for calcium diffusion (Drenhaus, von Guten, & Rager, 1997; FitzGibbon & Taylor, 2012). Smaller spaces are more conducive to molecular crowding and facilitate frequent molecular interactions between calcium and other calcium binding proteins, both of which are expected to slow the apparent diffusion coefficient for calcium.

In cytoplasmic spaces of rod cells, with diameter on the same order as that of RGC axons, it has been shown that the diffusion coefficient for calcium may be 10 to 100 times slower than that of the free diffusion coefficient due to reversible binding interactions (McLaughlin & Brown, 1981). This slower diffusion coefficient is obtained from the established relationship when a species is simultaneously diffusing and partaking in reversible binding reactions. The diffusion coefficient is modified in the diffusion equation to be the apparent diffusion coefficient divided by $1 + R$, where R is the ratio of bound to free concentrations of the diffusing species

(Crank, 1956, p.347). As shown in rod cells, it is reasonable to assume there are 10 to 100 times as many calcium ions reversibly bound to other molecules as there are free calcium ions diffusing in the cytoplasm (McLaughlin & Brown, 1981). Experimental measurements of fluorescent calcium diffusion down the axons of rod cells, with comparable diameters to those of RGC axons, further support slower diffusion coefficients for calcium (Chen, Van Hook, & Thoreson, 2015). Due to molecular crowding shown in studies of fluorescent protein diffusion, these slower orders of magnitude in the diffusion coefficient of calcium have also been taken into consideration in other calcium reaction-diffusion models (Dayel, Hom, & Verkman, 1999; Means et al., 2006). Furthermore, estimations of calcium spread in dendrites have shown sensitivity to the presence of fixed calcium buffers and calcium spread of 5 μm or less from the site of release (Biess, Korkotian, & Holcman, 2011).

The initial conditions of this reaction-diffusion model define a homogenous distribution of inactive calpain in the axon and a local release of calcium following a Gaussian distribution that undergoes stochastic diffusion in the axon segments considered (Figure 18a,b). Therefore, it becomes evident that the distribution of active calpain is dependent on the location of calcium release, and degradation will occur locally (Figure 18c,d). Such behavior aligns with the characteristics of Wallerian degeneration in living systems and gives support to the trophic factor model. The trophic factor model states that the loss of a survival factor signals the start of the degeneration pathway. The reaction-diffusion model supports the trophic factor model since the loss of a survival molecule would initiate a series of events at the site of loss to cause a local release of calcium and thus local degradation (Lubinska, 1977).

The trophic factor that is lost has been speculated to be Nmnat2 since its half-life aligns with the characteristic lag phase observed in degeneration, and removal of Nmnat2 is sufficient to

induce Wallerian degeneration in uninjured axons (Gilley & Coleman, 2010). If Nmnat2 is the crucial survival factor, one protective mechanism may be to inhibit SARM1 through direct or indirect mechanisms. This mechanism is supported by the prediction from the axotomy model that enzymatic activity of SARM1 facilitates calcium release, especially from intracellular stores, to promote calpain activation and subsequent degeneration. Thus, with SARM1 activity influencing the release of calcium from local stores, calpain activation and degeneration will occur in a spatiotemporal sequence following SARM1 activation. Furthermore, 90% of calcium release at the end of the lag phase *in vivo* originates at the site of injury or distal tips, which are locations where Nmnat2 would be lost earliest (Vargas et al., 2015). These locations of calcium release along with the predictions from the axotomy and reaction-diffusion models indicate that the spatiotemporal activation of SARM1 mirrors that of Nmnat2 loss, thus supporting a potential protective role of Nmnat2 through mediating SARM1 inhibition.

Moreover, this reaction-diffusion model gives support to the initial generation of calcium mobilizing products, from cleavage of cytosolic NAD by SARM1, to be a significant contributor to mPTP opening through mitochondrial calcium overload. The axoplasmic reticulum (AR) and mitochondria are in close proximity (on the order of nm), which indicates possible calcium communication between the two stores (Villegas et al., 2014). The initial rise in cADPR generated from SARM1 activity in the axotomy model is sufficient to cause mitochondrial calcium overload and subsequent mPTP opening (Figure 11d). To further test the plausibility of this prediction, the reaction-diffusion equation for calcium encompasses an estimate of 100 μM release of calcium from the AR, due to stimulation of cADPR from initial SARM1 NADase activity, diffusing throughout the axonal unit (Fulceri et al., 2001; Chini et al., 2005; Essuman et al., 2017). Over a short period of time, relatively high levels of cytosolic calcium diffuse on the

order of 1 µm from the initial site of release (AR) (Figure 18e,f). This diffusion distance would readily encompass the close proximity of mitochondria to the AR, and expose the mitochondria to these high levels of cytosolic calcium for mPTP opening (Deniaud et al., 2008; Villegas et al., 2014). Importantly, these levels of cytosolic calcium do not meet the threshold for m-calpain activation, which further supports mitochondrial calcium overload caused by calcium release from cADPR-activated RyRs and subsequent mPTP opening occur in the lag phase immediately preceding fragmentation.

4. Discussion

4.1 Axotomy: Qualitative similarities to degeneration in primary neuron culture

The axotomy model qualitatively matches degenerative progression observed in living systems

Injury causes the loss of Nmnat2 and, in the axotomy model, subsequent activation of SARM1. Initial SARM1 activity cleaves cytosolic NAD leading to rises in ADPR and cADPR and slow accumulation of cytosolic calcium. This cytosolic calcium accumulation and its proximity to mitochondria may induce mitochondrial calcium overload to trigger the opening of the mPTP, which impairs ATP production and causes the release of matrix NAD into the cytosol for further cleavage by SARM1. This NAD release correlates with a second, larger rise in ADPR and cADPR, which would have a stronger influence on calcium influx via TRPM2 receptors and release from intracellular stores via ryanodine receptors (RyRs). Although the production of cADPR is significantly less than that of ADPR, the half-life of cADPR is much longer compared to the transient presence of ADPR. This long half-life of cADPR suggests a longer stimulation of calcium release from the AR through activation of ryanodine receptors. From these predictions,

SARM1's activity influencing cytosolic calcium accumulation should be verified in living systems.

Furthermore, mPTP opening leads to energy failure and subsequent depolarization of the distal axon, which causes the opening of VGCCs to mediate the influx of extracellular calcium into the cytosol.

The series of events from the model including early Nmnat2 loss, SARM1 activation, extracellular calcium influx through VGCCs, and degeneration following a sigmoidal function, qualitatively agree with the events of degeneration *in vitro* and *in vivo* (Barrientos et al., 2011; Park et al. 2013; Villegas et al., 2014 Vargas et al., 2015; Bramley et al., 2016). Importantly, the model suggests influential roles of SARM1's novel NADase activity and mPTP involvement in energy failure and cytosolic calcium accumulation.

4.2 Important protection mediated by Nmnat2

The model activates SARM1 based on the presence of Nmnat2. Through treatments eliminating Nmnat2 or stabilizing this protein's concentration over time, SARM1 activity is strongly modulated along with the degenerative time course in the model. Although there is no current data directly supporting this relationship, local action of proteins, such as calpain and SARM1, as well as anterograde and local axon degeneration support the need for testing this mechanism.

First, the loss of Nmnat2 occurs early in the pathway due to Nmnat2's short half-life. However, other than being active upstream of calpain activation, the role of SARM1 in the initiation or execution phases has been unestablished (Yang et al., 2013; Conforti, Gilley, & Coleman, 2014). The representation of SARM1 activation in the model, as no known activators

of SARM1 have been identified, proposes a mechanism where SARM1 is involved in the initiation phase of axon degeneration. Furthermore, over expression of SARM1 does not induce degeneration, thus indicating this protein needs an activating signal, which may be generated through Nmnat2 loss and remains to be tested in living cells and organisms (Gerdts et al., 2013). The incorporation of this correlation in the model between early Nmnat2 loss and SARM1 activation gives a qualitatively similar progression of axon degeneration to that observed *in vitro* and is the first known study investigating this possibility.

There is a hypothesis termed the trophic factor model suggesting that a continual supply of an unidentified trophic factor from the cell body suppresses the endogenously active degeneration pathway, which proceeds in the absence of this trophic factor (Lubinska 1977; Coleman & Freeman, 2010). Nmnat2 has been proposed to be this trophic factor since the lag phase observed after axonal injury would correlate with that of the half-life of the trophic factor. Indeed, the half-life of Nmnat2 is about 4 hours, which corresponds with the lag phase duration (Gilley & Coleman, 2010). Nmnat2 also relies on anterograde transport mechanisms to be transported from the cell body (site of production) to where it is needed further along the axon. Knocking down Nmnat2 is sufficient to induce Wallerian degeneration (Gilley & Coleman, 2010). Furthermore, the protective protein WLD^s has a longer Nmnat half-life compared to Nmnat2 (Gilley & Coleman, 2010). The stochastic reaction-diffusion model of calcium released from intracellular stores provides further support for the trophic factor model and implicates early SARM1 activation and mitochondrial dysfunction. With a possible early activation of SARM1 due to its novel NADase activity, Nmnat2 may be involved in mechanisms maintaining the inhibition of this enzyme.

Moreover, the enzymatic activity of proteases and SARM1 are confined locally to cause local axon degeneration (Gerdts et al., 2015). Thus, the loss of trophic factor from sites in the axon through anterograde axonal transport following injury would initiate degeneration with a corresponding anterograde directionality, which is observed in axotomized axons (Lubinska, 1977; Beirowski et al., 2005). As demonstrated through the model of stochastic diffusion of calcium and calpain activation, the site of calcium release will dictate the site of highest active calpain concentration. Locations with active calpain undergo local degeneration. Furthermore, where there is activation of SARM1, the axotomy model predicts there is a subsequent accumulation of cytosolic calcium, which implies SARM1 activation occurs earliest at locations closest to the site of injury. Thus, loss of Nmnat2 through anterograde transport fits this characteristic of local activity of SARM1 and its influence on the progression of degeneration.

Furthermore, research suggests that the NAD synthesis function of Nmnat2 is not necessary for protection against axon degeneration (Wang et al., 2005; Sasaki, Araki, & Milbrandt, 2006; Wang & He, 2009; Conforti, Gilley, & Coleman, 2014). Over expression of Nmnat2 or WLD^{s} expression does not increase NAD levels compared to controls. Therefore, other substrates and products of Nmnat need to be considered since NAD does not confer protection in degeneration (Berbusse et al., 2016). A speculated protective product of Nmnat is increasing NAD availability for conversion into NADPH to act as a cofactor for ROS scavenging enzymes (Press & Milbrandt, 2008). Increasing NADPH may be beneficial in Wallerian degeneration to ameliorate the over production of ROS and attenuate the potential signaling roles of ROS in the pathway. Further research in primary cultures and animal models should focus efforts on identifying the protective role of Nmnat2, especially if there are direct or indirect influences on SARM1 activity. Moreover, at the rate Nmnat2 produces NAD and consumes ATP, this enzyme working

in the reverse direction does not seem promising as its protective mechanism. The observation that NAD and ATP levels are very similar to that of uninjured axons in overexpression of Nmnat2 (to compensate for its short half-life) and WLD^s (stable Nmnat that functions in the cytosol) may suggest SARM1 never becomes substantially activated to progress the degenerative pathway.

4.3 Nifedipine and FK866 provide similar protection through convergence onto cytosolic calcium accumulation

The protection conferred by nifedipine treatment in the axotomy model was qualitatively similar to that observed *in vitro*: nifedipine provided modest, but not complete protection. Furthermore, both systems show the hill (slope of the sigmoidal curve) of each nifedipine treatment degenerative function to be extremely similar to the respective axotomy treatment. This similarity may be due to cytosolic calcium concentration surpassing the threshold for m-calpain activation and calpain activation occurring at the same approximate rates once the threshold is reached giving similar sigmoidal degeneration functions. Thus, the slow accumulation of cytosolic calcium initially in nifedipine treatment may be responsible for the observed delay between the two curves.

After this slow accumulation, the second ADPR and cADPR spikes generated from SARM1 activity and mPTP opening seem to be an important mechanism for mediating calcium release to reach cytosolic calcium levels that activate m-calpain. Although nifedipine treatment blocks the L-type VGCCs, it does not prevent Nmnat2 loss, subsequent SARM1 activation, mitochondrial calcium accumulation and mPTP opening. Without this second spikes in ADPR and cADPR from mPTP opening and active SARM1, there would be no activator in moving extracellular or

intracellular stores of calcium due to blockage of the L-type VGCCs, and thus no activation of m-calpains or local axon degeneration.

FK866 treatment in the axotomy model is also qualitatively similar to this treatment *in vitro* by affording modest protection against degeneration. Until now, the mechanisms of FK866 protection were unknown. Here, the protective mechanism mediated by FK866 treatment may be due to its facilitation of increasing levels of Nam, which is a negative feedback product of SARM1 activity (Essuman et al., 2017). In response to FK866 treatment, the model predicts that there is a rise in Nam, and corresponding decrease in active SARM1. However, the rise in Nam does not appear to be large enough to significantly decrease SARM1 activity to confer robust protective effects. Thus, the first spikes in ADPR and cADPR still occur, although these rises are delayed and dampened compared to those observed in the axotomy model. With these spikes still apparent, mitochondrial calcium accumulation may occur allowing for mPTP opening. Furthermore, Nam has an IC_{50} of 43.8 μM for SARM1 (Summers et al., 2016; Essuman et al., 2017), whereas in the model the increase of Nam was about 12 μM. These relative concentrations support the result that the amount of active SARM1 is reduced, but not significantly enough to prevent degeneration from proceeding, albeit at a slower time course, in the mathematical model.

Additionally, due to the delayed and slightly lower initial rises of ADPR and cADPR, the model predicts that FK866 treatment delays the second spikes of ADPR and cADPR. Since SARM1 inactivation in FK866 treatment is more pronounced than the axotomy only condition, the second spikes are also not as large, thus implicating slower cytosolic calcium accumulation and a delayed degeneration time course similar to that observed with nifedipine treatment.

4.4 SARM1's novel NADase activity may involve the mPTP leading to energy failure and cytosolic calcium accumulation

The model emphasizes the importance of SARM1's novel NADase activity in propagating the axon degeneration pathway. Specifically, the first spikes in ADPR and cADPR suggests an important role in mPTP opening, and the second spikes provide a substantial contribution to cytosolic calcium accumulation.

Due to the proximity of the mitochondria to sites of high calcium concentration near plasma membrane calcium permeable channels and the AR, mitochondria are clearly sensitive organelles to cytosolic calcium and are a sink for this calcium (Tsukita & Ishikawa, 1976; Villegas et al., 2014). Furthermore, RyR activity can trigger axonal degeneration, but with mPTP inhibition, this degeneration is prevented. This mechanism of protection emphasizes calcium release from internal stores as a critical regulator of mitochondrial dysfunction by mPTP opening and supports the findings from the mathematical model (Park et al., 2013; Summers et al., 2014; Villegas et al., 2014). Therefore, it is a possible mechanism for initial generation of ADPR and cADPR (calcium movement via TRPM2 and RyRs respectively) by SARM1 to cause rises in cytosolic calcium sufficient to cause mitochondrial calcium overload.

In the axotomy model, this mitochondrial calcium threshold is set lower than reported physiological levels that trigger mPTP opening (Halestrap, Woodfield, & Conneran, 1997; Halestrap, 2009;). However, this lowered threshold may be reasonable in the case of Wallerian degeneration since oxidative stress lowers the threshold for mitochondrial calcium in mPTP formation (McStay, Clarke, & Halestrap, 2002; Bernardi, 2013). Although the source(s) remain elusive, there is an early rise in ROS production following axonal injury (Milbrandt & Press,

2008; Fang, Bourdette, & Banker, 2012; Conforti, Gilley, & Coleman, 2014). Increases in mitochondrial calcium as well as mPTP opening may also contribute to an up regulation of ROS production leading to a positive feedback mechanism (Murphy, 2009; Peng & Jou, 2010; Court & Coleman, 2012). Therefore, mechanisms of ROS generation and relationship between ROS and the mitochondrial dysfunction via mPTP activity in Wallerian degeneration should be more thoroughly investigated.

Moreover, mPTP opening is an important event in Wallerian degeneration (Barrientos et al., 2011). Mitochondrial swelling, an indicative feature of mPTP opening, is apparent in axons up to 12 hours before axon fragmentation, suggesting early involvement and a potential convergence point in the pathway (Barrientos et al., 2011). Furthermore, in living systems (Barrientos et al., 2011) and this model, inhibition of the mPTP provides relatively robust protection against axon degeneration compared to nifedipine and FK866 treatments. mPTP activation in axons expressing WLD^s can also cause axon degeneration, which suggests the protective mechanisms of WLD^s and Nmnat lie upstream of mPTP opening and support mechanisms predicted by the axotomy model (Barrientos et al., 2011). Removal of mPTP formation confers protection observed in the model due to the preservation of energy homeostasis for the time period considered as well as the prevention of increased NAD substrate for cleavage by SARM1, which may suggest such protective mechanisms in living cells. This novel role for the mPTP predicted by the model should be verified in cell culture and animal models.

This novel role for the mPTP in Wallerian degeneration is critical support for not only loss of the mitochondrial membrane potential, which has been speculated (Milbrandt & Press, 2008; Barrientos et al., 2011), but for the release of matrix NAD into the cytosol. Release of this NAD provides more substrate for cleavage by SARM1, which corresponds to the second spikes in

ADPR and cADPR generation. These later spikes, as predicted by the model, seem to be crucial in axon degeneration following its characteristic sigmoidal progression.

Furthermore, studies on SARM1 localization support this mechanism of cytosolic NAD cleavage (Gerdts et al., 2013). SARM1 localizes to the mitochondria, but mostly resides on the cytosolic surface of the mitochondria. Moreover, deletion of SARM1's mitochondrial localization signal does not prevent degeneration (Gerdts et al., 2013), which suggests its enzymatic NADase action in response to injury takes place in the cytosol. However, the majority of the cell's NAD is stored in the mitochondria (Tischler et al., 1977; Stein & Imai, 2012). Therefore, through mPTP opening, release of matrix NAD may provide crucial substrate for the influence of SARM1 activity in Wallerian degeneration. Predictions of the model support this proposed mechanism since the prevention of mitochondrial NAD release strongly delays the degeneration time course. Therefore, this mechanism of mPTP opening and cytosolic NAD cleavage promoting a characteristic degeneration time course should be verified in living systems.

5. Conclusion

The aim of this mathematical model is to predict potential mechanisms of Wallerian degeneration to efficiently direct investigation in *in vitro* and *in vivo* systems. The results of this study predict SARM1's NADase activity to maintain significant influence in Wallerian degeneration and support the two main hypotheses of this investigation. The initial hypothesis supported is SARM1's cleavage products, namely ADPR and cADPR, may serve a significant contribution to cytosolic calcium accumulation through the movement of calcium from the extracellular space via calcium permeable membrane channels and from intracellular stores via RyRs. The second hypothesis is supported by the predicted involvement of early mPTP opening

due to SARM1's NADase activity implicating the role of SARM1 in the characteristic energy failure observed in Wallerian degeneration. Such predictions should be verified in living systems to enhance understanding of the biochemical pathways mediating Wallerian degeneration and to generate novel therapeutic targets for degenerative conditions.

Acknowledgements:

This work was supported by grants from The College of William and Mary and by The Roy R. Charles Center for Academic Excellence at The College of William and Mary.

Thank you to Lizabeth Allison and Lisa Landino for being a part of my thesis committee, and a special thank you to Randy Coleman for the support and mentorship in this project and throughout my time at William & Mary.

Thank you to Willie Buchser for guidance in this project and continual support of my endeavors.

Thank you to Morgan Shelton for the support throughout this project and engagement in many fruitful discussions.

The qualitative models used in this work were developed with the program CellDesigner version 4.2, which can be found at http://www.celldesigner.org/.

The relative protein species concentrations used in this work were obtained via the PaxDB Protein Abundance Database operated by the University of Zurich, which can be found at http://www.pax-db.org/. Physiological ion concentrations were obtained from the Human Metabolome Database (HMBD 4.0), which can be found at http://www.hmdb.ca/.

The mathematical models used in this work were developed with MATLAB R2017b, which can be found at: http://www.mathworks.com/products/matlab/.

Abbreviations:

Cyt Ca: Cytosolic Calcium
Ext Ca: Extracellular Calcium
Mt Ca: Mitochondrial Calcium
AR Ca: Axoplasmic Reticulum Calcium
Cyt Na: Cytosolic Sodium
Ext Na: Extracellular Sodium
Mt Na: Mitochondrial Sodium
K: Potassium
ATP: Adenosine Tri-Phosphate
Pi: Inorganic Phosphate
ADP: Adenosine Di-Phosphate
VGCC: Voltage Gated Calcium Channel

NCX1: Sodium Calcium Exchanger 1
CaM: Calmodulin
CaM*: Active Calmodulin
PMCA: Plasma Membrane Calcium ATPase
PMCA*: Active Plasma Membrane Calcium ATPase
PKC: Protein Kinase C
PKC*: Active Protein Kinase C
PLC: Phospholipase C
PLC*: Active Phospholipase C
PIP2: Phosphatidylinositol 4,5-bisphosphate
IP3: Inositol Tri-phosphate
IP3R: Inositol Tri-phosphate Receptor
IP3R*: Active Inositol Tri-phosphate Receptor
RyR2: Ryanodine Receptor 2
RyR2*: Active Ryanodine Receptor 2
SERCA: Smooth Endoplasmic Reticulum Calcium ATPase
AR: Axoplasmic Reticulum
cADPR: Cyclic ADP-ribose
IMS H: Intermembrane Space Hydrogen
Matrix H: Mitochondrial Matrix Hydrogen
Cyt H: Cytosolic Hydrogen
NAD: Nicotinamaide Adenine Dinucleotide
NADcyt: Cytosolic NAD
NADmt: Mitochondrial NAD
MCU: Mitochondrial Uniporter
mPTP: Mitochondrial Permeability Transition Pore
mPTP*: Active Mitochondrial Permeability Transition Pore
Nam: Nicotinamide
Nam Ext: Extracellular Nam
NAMPT: Nicotinamide Phosphoribosyltransferase
NMN: Nicotinamide Mononucleotide
NMNAT2 axon: Axonal Nicotinamide Nucleotide Adenylyltransferase 2
NMNAT2 soma: Soma Nicotinamide Nucleotide Adenylyltransferase 2
SARM1: Sterile Alpha And TIR Motif Containing 1
SARM1*: Active Sterile Alpha and TIR Motif Containing 1
PHR1: Phr1 E3 ubiquitin ligase
CI: Complex I of the electron transport chain
CIII: Complex III of the electron transport chain
CIV: Complex IV of the electron transport chain
TCA: Tricarboxylic Acid Cycle
ADPR: ADP-ribose
CD38: Cyclic ADP Ribose Hydrolase
Sirt2: Sirtuin 2
TRPM_2: Transient Receptor Potential Cation Channel Subfamily M Member 2
TRPM2*: Active Transient Receptor Potential Cation Channel Subfamily M Member 2
Cleaved Cytsk: Cleaved Cytoskeletal Components

References

Adalbert, R., Morreale, G., Paizs, M., Conforti, L., Walker, S.A., Roderick, H.L., Bootman, M.D., Siklós, L., Coleman, M.P. (2012). Intra-axonal calcium changes after axotomy in wild-type and slow Wallerian degeneration axons. *Neuroscience, 225*, 44–54.

Araki, T., Sasaki, Y., & Milbrandt, J. (2004). Increased Nuclear NAD Biosynthesis and SIRT1 Activation Prevent Axonal Degeneration. *Science, 305*, 1010-1013.

Avery, M.A., Rooney, T.M., Pandya, J.D., Wishart, T.M., Gillingwater, T.H., Geddes, J.W., Sullivan P., & Freeman, M.R. (2012). Wld^{s} prevents axon degeneration through increased mitochondrial flux and enhanced mitochondrial Ca^{2+} buffering. *Curr Biol, 22*(7), 596-600.

Babetto, E., Beirowski, B., Russler, E.V., Milbrandt, J., & DiAntonio, A. (2013). The Phr1 Ubiquitin Ligase Promotes Injury-Induced Axon Self-Destruction. *Cell Reports, 3*, 1422-1429.

Babetto, E., Beirowski, B., Janeckova, L., Brown, R., Gilley, J., Thomson, D., Ribchester, R.R., Coleman, M.P. (2010). Targeting NMNAT1 to axons and synapses transforms its neuroprotective potency *in vivo*. *J. Neurosci, 30*, 13291–13304.

Barrientos, S.A., Martinez, N.W., Yoo, S., Jara, J.S., Zamorano, S., Hetz, C., Twiss, J.L., Alvarez, J., Court. F,A. (2011). Axonal degeneration is mediated by the mitochondrial permeability transition pore. *J Neurosci, 31*(3), 966-78.

Baumgartner, H.K., Gerasimenko, J.V., Thorne, C., Ferdek, P., Pozzan, T., Tepikin, A.V., Peterson, O.H., Sutton, R., Watson, A.J., & Gerasimenko, O.V. (2009). Calcium Elevation in Mitochondria is the Main Ca2+ Requirement for Mitochondrial Permeability Transition Pore (mPTP) Opening. Journal of Biological Chemistry, 284(31), 20796-20803.

Beirowski, B., Adalbert, R., Wagner, D., Grumme, D.S., Addicks, K., Ribchester, R.R., & Coleman, M.P. (2005). The progressive nature of Wallerian degeneration in wild-type and slow Wallerian degeneration (Wlds) nerves. *BMC Neuroscience, 6*, 6.

Beirowski, B., Babetto, E., Gilley, J., Mazzola, F., Conforti, L., Janeckova, L., Magni, G., Ribchester, R.R., & Coleman, M.P. (2009). Non-Nuclear Wlds Determines Its Neuroprotective Efficacy for Axons and Synapses *In* Vivo. *Journal of Neuroscience, 29*(3), 653-664.

Belenky, P., Bogan, K.L., Brenner, C. (2007). NAD metabolism in health and disease. *Trends Biochem Sci, 32*(1), 12-19.

Berbusse, G.W., Woods, L.C., Vohra, B.P., & Naylor, K. (2016). Mitochondrial Dynamics Decrease Prior to Axon Degeneration Induced by Vincristine and are Partially Rescued by Overexpressed cytNmnat1. *Front Cell Neurosci, 10*, 179.

Berg, J.M., Tymoczko, J., & Stryer, L. (2006). *Biochemistry*. New York, NY: Freeman.

Berger, F. Lau, C., Dahlmann, M., & Ziegler, M. Subcellular Compartmentation and Differential Catalytic Properties of the Three Human NicotiNamide Mononucleotide Adenylyltransferase Isoforms. *The Journal of Biological Chemistry, 280*, 36334-36341.

Bernardi, P. (2013). The mitochondrial permeability transition pore: a mystery solved? *Front Physiol, 4*, 95.

Biess, A., Korkotian, E., & Holcman, D. (2011). Barriers to Diffusion in Dendrites and Estimation of Calcium Spread Following Synaptic Inputs. *PLOS Computational Biology, 7(10), e1002182*.

Bramley, J.C., Collins, S.A., Clark, K.B., & Bramley, W.J. (2016). Avian axons undergo Wallerian degeneration after injury and stress. *J Comp Physiol A, 202*(11), 813-822.

Brini, M., & Carafoli, E. (2011). The plasma membrane Ca^{2+} ATPase and the plasma membrane sodium calcium exchanger cooperate in the regulation of cell calcium. *Cold Spring Harb Perspect Biol, 3*(2), a004144.

Brini, M., Coletto, L., Pierobon, N., Kraev, N., Guerini, D., & Carafoli, E. (2003). A Comparative Functional Analysis of Plasma Membrane Ca^{2+} Pump Isoforms in Intact Cells. *The Journal of Biological Chemistry, 278*, 24500-24508.

Bronner-Fraser, M. (1996). *Methods in avian embryology*. San Diego, CA: Academic Press.

Brookes, P.S., Yoon, Y., Robotham, J.L., Anders, M.W., Sheu, S.S. (2004). Calcium, ATP, and ROS: a mitochondrial love-hate triangle. *Am J Physiol Cell Physiol, 287*(4), C817-33.

Brustovetsky, N., Brustovetsky, T., Purl, K.J., Capano, M., Crompton, M., & Dubinsky, J. (2003). Increased Susceptibility of Striatal Mitochondria to Calcium-Induced Permeability Transition, Journal of Neuroscience, 23(12), 4858-4867.

Cancela, J.M., Gerasimenko, O.V., Gerasimenko, J.V., Tepikin, A.V., & Petersen, O.H. (2000). Two different but converging messenger pathways to intracellular Ca^{2+} release: the roles of nicotinic acid adenine dinucleotide phosphate, cyclic ADP-ribose and inositol triphosphate. *EMBO Journal, 19*(11), 2549-2557.

Cantó, C., Menzies, K.J., & Auwerx, J. (2015). NAD metabolism and the control of energy homeostasis: a balancing act between mitochondria and the nucleus. *Cell Metab, 22*(1), 31-53.

Chappell, J.B., & Crofts, A.R. (1965). Calcium Ion Accumulation and Volume Changes of Isolated Liver Mitochondria: Calcium Induced Swelling. *Biochem J, 95*, 378-386.

Chen, M., Van Hook, M.J., & Thoreson, W.B. (2015). Ca^{2+} Diffusion through Endoplasmic Reticulum Supports Elevated Intraterminal Ca^{2+} Levels Needed to Sustain Synaptic Release from Rods in Darkness. *Journal of Neuroscience, 35*(32), 11364-11373.

Chini, E.N., Nagamune, K., Wetzel, D.M., & Sibley, L.D. (2005). Evidence that the cADPR signaling pathway controls calcium-mediated mironeme secretion in Toxoplasma gondii. *Biochem J, 389*, 269-277.

Cohen, M.S., Ghosh, A.K., Joon-Kim, H., Jeon, N., Jaffrey, S.R. (2012). Chemical Genetic-Mediated Spatial Regulation of Protein Expression in Neurons Reveals an Axonal Function for Wlds. *Chemistry & Biology, 19*, 179–187.

Coleman, M.P., Freeman M.R. (2010). Wallerian degeneration, wld(s), and Nmnat. *Annu Rev Neurosci, 33*, 245-267.

Conforti, L., Fang, G., Beirowski, B., Wang, M.S., Sorci, L., Asress, S., Adalbert, R., Silva, A., Bridge, K., Huang, X.P., Magni, G., Glass, J.D., Coleman, M.P. (2007). NAD and axon degeneration revisited: Nmnat1 cannot substitute for WldS to delay Wallerian degeneration. *Cell Death Differ, 14*, 116–127.

Conforti, L., Wilbrey, A., Morreale, G., Janeckova, L., Beirowski, B., Adalbert, R., Mazzola, F., DiStefano, M., Hartley, R., Babetto, E., Smith, T., Gilley, J., Billington, R.A., Genazzani, A.A., Ribchester, R.R., Magni, G., Coleman, M.P. (2009). WldS protein requires Nmnat activity and a short N-terminal sequence to protect axons in mice. *J. Cell Biol, 184*, 491–500 (2009).

Court, F.A., & Coleman, M.P. (2012). Mitochondria as a central sensor for axonal degenerative stimuli. *Trends Neurosci, 35*(6), 364-372.

Crank, J. (1957). *The Mathematics of Diffusion*. London, UK: Oxford University Press.

Crompton, M., & Costi, A. (1988). Kinetic evidence for a heart mitochondrial pore activated by Ca^{2+}, inorganic phosphate and oxidative stress. A potential mechanism for mitochondrial dysfunction during cellular Ca^{2+} overload. *Eur J Biochem, 178*(2), 489-501.

Dayel, M.J., Hom, E.Y., & Verkman, A.S. (1999). Diffusion of Green Fluorescent Protein in the Aqueous-Phase Lumen of Endoplasmic Reticulum. *Biophysical Journal, 76*, 2843-2851.

Deniaud, A., Sharaf el dein, O., Maillier, E., Poncet, D., Kroemer, G., Lemaire, C., & Brenner, C. (2008). Endoplasmic reticulum stress induces calcium-dependent permeability transition, mitochondrial outer membrane permeabilization and apoptosis. *Oncogene, 27*(3), 285-299.

DiStefano, M., & Conforti, L. (2013). Diversification of NAD biological role: the importance of location. *FEBS Journal, 280*(19), 4711- 4728.

Donahue, B.S., & Abercrombie, R.F. (1987). Free diffusion coefficient of ionic calcium in cytoplasm. *Cell Calcium, 8*(6), 437-448.

Dong, H., Dunn, J., & Lytton, J. (2002). Stoichiometry of the Cardiac Na+/Ca2+ exchanger NCX1.1 measured in transfected HEK cells. *Biophys J, 82*(4), 1943–1952.

Drenhaus, U., von Gunten, A., & Rager, G. (1997). Classes of axons and their distribution in the optic nerve of the tree shrew (Tupaia belangeri). *Anat. Rec, 249*(1), 103-116.

Esposito, E., Impellizzeri, D., Mazzon, E., Fakhfouri, G., Rahimian, R., Travelli, C., Tron, G.C., Genazzani, A.A., & Cuzzocrea, S. (2012). The NAMPT inhibitor FK866 reverts the damage in spinal cord injury. *Journal of Neuroinflammation,* 9, 66.

Essuman, K., Summers, D.W., Sasaki, Y., Mao, X., DiAntonio, A., & Milbrandt, J. (2017). The SARM1 Toll/Interleukin-1 Receptor Domain Possesses Intrinsic NAD Cleavage Activity that Promotes Pathological Axonal Degeneration. *Neuron, 93*(6), 1334-1343.

Fang, C., Bourdette, D., & Banker, G. (2012). Oxidative stress inhibits axonal transport: implications for neurodegenerative disease. *Mol Neurodegener, 7*, 29.

FitzGibbon, T., & Taylor, S.F. (2012). Mean retinal ganglion cell axon diameter varies with location in the human retina. *Jpn J Ophthalmol, 56*(6), 631-637.

Freeman, M.R. (2014). Signaling mechanisms regulating Wallerian degeneration. *Curr Opin Neurobiol, 27*, 224-231.

Fukui, K. (2016). Reactive oxygen species induce neurite degeneration before induction of cell death. *J Clin Biochem Nutr, 59*(3), 155-159.

Fulceri, R., Rossi, R., Bottinelli, R., Conti, A., Intrvaia, E., Galione, A., Benedetti, A., Sorrentino, V., & Reggiani, C. (2001). Ca^{2+} release induced by cyclic ADP ribose in mice lacking type 3 ryanodine receptor. *Biochem Biophys Res Commun, 288*(3), 697-702.

George, E.B., Glass, J.D., & Griffin, J.W. (1995). Axotomy-induced axonal degeneration is mediated by calcium influx through ion-specific channels. *J Neurosci, 15*(10), 644, 20025-52.

Gerdts, J., Brace, E.J., Sasaki, Y., DiAntonio, A., & Milbrandt, J. (2015). SARM1 activation triggers axon degeneration locally via NAD destruction. *Science, 348*, 453–457.

Gerdts, J., Sasaki, Y., Vohra, B., Marasa, J., & Milbrandt, J. (2011). Image-based screening identifies novel roles for IkappaB kinase and glycogen synthase kinase 3 in axonal degeneration. *J Biol Chem, 286*, 28011–28018.

Gerdts, J., Summers, D.W., Sasaki, Y., DiAntonio, A., Milbrandt, J. (2013). Sarm1-mediated axon degeneration requires both SAM and TIR interactions. *J Neurosci, 33*(33), 13569-13580.

Gerdts, J., Sasaki, Y., Vohra, B., Marasa, J. & Milbrandt, J. (2011). Image-based screening identifies novel roles for IKK and GSK3 in axonal degeneration. *J Biol Chem, 286*(32), 28011-8.

Giacomello, M., Drago, I., Pizzo, P., & Pozzan, T. (2007). Mitochondrial Ca2+ as a key regulator of cell life and death. *Cell Death Differ, 14*(7), 1267-74.

Gilley, J., & Coleman, M.P. (2010). Endogenous Nmnat2 Is an Essential Survival Factor for Maintenance of Healthy Axons. *PLoS Biol, 8*(1), e1000300.

Gilley, J., Adalbert, R., Yu, G., & Coleman, M.P. (2013). Rescue of Peripheral and CNS Axon Defects in Mice Lacking NMNAT2. *Journal of Neuroscience, 33* (33), 13410-13424.

Graeff, R., Liu, Q., Kriksunov, I.A., Kotaka, M., Oppenheimer, N., Hao, Q., & Lee, H.C. (2009). Mechanism of Cyclizing NAD to Cyclic ADP-ribose by ADP-ribosyl Cyclase and CD38. *The Journal of Biological Chemistry, 284*, 27629 –27636.

Guse, A.H. (1999). Cyclic ADP-ribose: a novel Ca2+-mobilising second messenger. *Cell Signal, 11*(5), 309-316.

Guse, A.H., da Silva, C.P., Berg, I., Skapenko, A.L., Weber, K., Heyer, P., Hohenegger, M., Ashamu, G.A., Schulze-Koops, H., Potter, B.V., & Mayr, G.W. (1999). Regulation of calcium signalling in T lymphocytes by the second messenger cyclic ADP-ribose. *Nature, 398*(672), 70-73.

Halestrap, A.P. (2009). What is the mitochondrial permeability transition pore? *J Mol Cell Cardiol, 46*(6), 821-31.

Halestrap, A.P., Woodfield, K., & Connern, C.P. (1997). Oxidative Stress, Thiol Reagents, and Membrane Potential Modulate the Mitochondrial Permeability Transition by Affecting Binding to the Adenine Nucleotide Translocase. *Journal of Biological Chemistry, 272*(6), 3346-3354.

Hassa, P.O., Haenni, S.S., Elser, M., & Hottiger, M.O. (2006). Nuclear ADP-Ribosylation Reactions in Mammalian Cells: Where Are We Today and Where Are We Going. Microbiol. Mol. Biol. Rev, 70(3), 789-829.

Hicks , A.N., Lorenzetti, D., Gilley, J., Lu, B., Andersson, K., Miligan, C., Overbeek, P.A., Oppenheim, R., & Bishop, C.E. (2012). NicotiNamide Mononucleotide Adenylyltransferase 2 (*Nmnat2*) Regulates Axon Integrity in the Mouse Embryo. *PLoS ONE, 7*(10), e47869.

Higashida, H., Salmina, A.B., Olovyannikova, R.Y., Hashii, M., Yokoyama, S., Koizumi, K., Jin, D., Liu, H., Lopatina, O., Amina, S., Islam, M.S., Huang, J., & Noda, M. (2007). Cyclic ADP-ribose as a universal calcium signal molecule in the nervous system. *Neurochemistry Int, 51*, 192-199.

Higashida, H., Hashii, M., Yokoyama, S., Hoshi, N., Asai, K., & Kato, T. (2001). Cyclic ADP-ribose as a potential second messenger for neuronal Ca2+ signaling. *J Neurochem, 76*(2), 321-331.

Islam, S. (2012). *Calcium Signaling*. Dordrecht: Springer.

Khorchid, A., & Ikura, M. (2002). How calpain is activated by calcium. *Nature Structural Biology, 9*(4), 239-241.

Kim, Y.H., Park, T.J., Lee, Y.H., Baek, K.J., Pann-Ghill Suh, P.G., Ryu, S.H., & Kim, K.T. (1999). Phospholipase C-δ1 Is Activated by Capacitative Calcium Entry That Follows Phospholipase C-β Activation upon Bradykinin Stimulation. *The Journal of Biological Chemistry, 274*, 26127-26134.

Lau, C., Niere, M., Ziegler, M. (2009). The NMN/NamN adenylyltransferase (NMNAT) protein family. *Frontiers in bioscience, 14*, 410–431.

Lipscombe, D., Helton, T.D., & Xu, W. (2004). L-type Calcium Channels: The Low Down. *J Neurophysiol, 92*, 2633-2641.

LoPachin, R.M., & Lehning, E.J. (1997). Mechanism of Calcium Entry during Axon Injury and Degeneration. *Toxicology and Applied Pharmacology, 143*(2), 233-244.

Lubinska, L. (1977). Early course of Wallerian degeneration in myelinated fibres of the rat phrenic nerve. *Brain Res, 130*(1), 47-63.

Ma, M., Ferguson, T.A., Schoch, K.M., Li, J., Qian, Y., Shofer, F.S., Saatman, K.E., & Neumar, R.W. (2013). Calpains mediate axonal cytoskeleton disintegration during Wallerian degeneration. *Neurobiol Dis. 56*, 34-46.

Mack, T. G., Reiner, M., Beirowski, B., Mi, W., Emanuelli, M., Wagner, D., Thomson, D., Gillingwater, T., Court, F., Conforti, L., Fernando, F.S., Tarlton, A., Andressen, C., Addicks, K., Magni, G., Ribchester, R.R., Perry, V.H., & Coleman, M.P. (2001). Wallerian degeneration of injured axons and synapses is delayed by a *Ube4b/Nmnat* chimeric gene. *Nature Neurosci, 4*, 1199–1206.

Marchi, E.D., Massimo, B., Giorgi, C., & Pinton, P. (2014). The mitochondrial permeability transition pore is a dispensable element for mitochondrial calcium efflux. *Cell Calcium, 56*(1), 1-13.

McLaughlin, S. & Brown, J. (1981). Diffusion of Calcium Ions in Retinal Rods: A Theoretical Calculation. *J. Gen. Phyiol, 77*, 475-487.

McStay, G.P., Clarke, S.J., & Halestrap, A.J. (2002). Role of critical thiol groups on the matrix surface of the adenine nucleotide translocase in the mechanism of the mitochondrial permeability transition pore. Biochem J, 367, 541-548.

Means, S., Smith, A.J., Shepher, J., Shadid, J., Fowler, J., Wojcikiewicz, R.H., Mazel, T., Smith, G.D., & Wilson, B.S. (2006). Reaction Diffusion Modeling of Calcium Dynamics with Realistic ER Geometry. *Biophysical Journal, 91*(2), 537-557.

Milde, S., Fox, A.N., Freeman, M.R., & Coleman, M.P. (2013). Deletions within its subcellular targeting domain enhance the axon protective capacity of Nmnat2 *in vivo*. *Scientific Reports, 3*.

Mishra, B., Carson, R., Hume, R.I., & Collins, C.A. (2013). Sodium and potassium currents influence Wallerian degeneration of injured Drosophila axons. *J Neurosci, 33*(48),18728-18739. doi: 10.1523/JNEUROSCI.1007-13.

Mizuguchi, M., Otsuka, N., Sato, M., Ishii, Y., Kon, S., Yamada, M., Nishina, H., Katada T., & Ikeda, K. (1995). Neuronal localization of CD38 antigen in the human brain. *Brain Research, 697*(1), 235-240.

Moldovan, M., Alvarez, S., & Krarup, C. (2009). Motor axon excitability during Wallerian degeneration. *Brain, 132*(2), 511-523.

Murray, J.R., Varian-Ramos, C.W., Welch, Z.S., & Saha, M.S. (2013). Embryological staging of the zebra finch, *Taeniopygia guttata*. *J Morphol, 274*, 1090–1110.

Nikiforov, A., Dölle, C., Niere, M., & Ziegler, M. (2011). Pathways and subcellular compartmentation of NAD biosynthesis in human cells: from entry of extracellular precursors to mitochondrial NAD generation. *J Biol Chem, 286*(24), 21767-21778.

Osterloh, J.M., Yang, J., Rooney, T.M., Fox, A.N., Adalbert, R., Powell, E.H., Sheehan, A.E., Avery, M.A., Hackett, R., Logan, M.A., MacDonald, J.M., Ziegenfuss, J.S., Milde, S., Hou, Y.J., Nathan, C., Ding, A., Brown, R.H., Conforti, L., Coleman, M., Tessier-Lavigne, M., Züchner, S., Freeman, M.R. (2012). dSarm/Sarm1 is required for activation of an injury-induced axon death pathway. *Science, 337*, 481–484.

Park, J.Y., Jang, S.Y., Shin, Y.K., Koh, H., Suh, D.J., Shinji, T., Araki, T., & Park H.T. (2013). Mitochondrial swelling and microtubule depolymerization are associated with energy depletion in axon degeneration. *Neuroscience, 15*, 238:258-69.

Peng, T.I., & Jou M.J. (2010). Oxidative stress caused by mitochondrial calcium overload. *Ann N Y Acad Sci, 1201*, 183-188.

Perraud, A.L., Fleig, A., Dunn, C.A., Bagley, L.A., Launay, P., Schmitz, C., Stokes, A.J., Zhu, Q., Bessman, M.J., Penner, R., Kinet, J.P., & Scharenberg, A.M. (2001). ADP-ribose gating of the calcium-permeable LTRPC2 channel revealed by Nudix motif homology. *Nature, 411*(44):595-599.

Sasaki, Y. & Milbrandt, J. (2010). Axonal Degeneration Is Blocked by NicotiNamide Mononucleotide Adenylyltransferase (Nmnat) Protein Transduction into Transected Axons. *The Journal of Biological Chemistry, 285*, 41211-41215.

Sasaki, Y., Araki, T., & Milbrandt, J. (2006) Stimulation of NicotiNamide Adenine Dinucleotide Biosynthetic Pathways Delays Axonal Degeneration after Axotomy. *Journal of Neuroscience, 26*(33), 8484-8491.

Sasaki, Y., Vohra, B., Baloh, R. & Milbrandt, J. (2009). Transgenic mice expressing the Nmnat1 protein manifest robust delay in axonal degeneration *in vivo*. *J. Neurosci, 29*, 6526–6534.

Sasaki, Y., Vohra, B.S., Lund, F.E., & Milbrandt, J. (2009). NicotiNamide Mononucleotide Adenylyl Transferase-Mediated Axonal Protection Requires Enzymatic Activity But Not Increased Levels of Neuronal NicotiNamide Adenine Dinucleotide. *J Neurosci, 29*(17), 5525–5535.

Schwaller, B. (2010). Cytosolic Ca2+ buffers. *Cold Spring Harb Perspect Biol, 2*(11), a004051.

Shen, H., Hyrc, K.L., & Goldberg, M.P. (2013). Maintaining energy homeostasis is an essential component of WldS-mediated axon protection. *Neurobiol Dis, 59*, 69–79.

Stein, L.R., & Imai, S. (2012). The dynamic regulation of NAD metabolism in mitochondria. *Trends Endocrinol Metab, 23*(9), 420-428.

Stirling, D.P., & Stys, P.K. (2010). Mechanisms of axonal injury: internodal nanocomplexes and calcium deregulation. *Trends Mol Med, 16*(4), 160–170. doi:10.1016/j.molmed.2010.02.002.

Storey, K.B., & Storey, J.M. (2002). Sensing, Signaling, and Cell Adaptation. Amsterdam, Netherlands: Elsevier Science.

Strehler, E.E., & Zacharias, D.A. (2001). Role of alternative splicing in generating isoform diversity among plasma membrane calcium pumps. *Physiol Rev, 81*(1), 21-50.

Stys, P.K., Stephen G. Waxman, S.G., & Ransom, B.R. (1992). Ionic Mechanisms of Anoxic Injury in Mammalian CNS White Matter: Role of Na+ Channels and Na+-Ca*+ Exchanger. *Journal of Neuroscience, 12*(2), 430-439.

Summers, D.W., DiAntonio, A., & Milbrandt, J. (2014). Mitochondrial Dysfunction Induces Sarm1-Dependent Cell Death in Sensory Neurons. *Journal of Neuroscience, 34*(28), 9338-9350.

Summers, D.W., Gibson, D.A., DiAntonio, A., & Milbrandt, J. (2016). SARM1-specific motifs in the TIR domain enable NAD^+ loss and regulate injury-induced SARM1 activation. *PNAS, 113*(41), E6271-E6280.

Sumoza-Toledo, A., & Penner, R. (2011). TRPM2: a multifunctional ion channel for calcium signalling. *J Physiol, 589*, 1515-1525.

Till, S., & Ladurner, A.G. (2009). Sensing NAD metabolites through macro domains. *Front Biosci (Landmark Ed), 14*, 3246-32458.

Tischler, M.E., Friedrichs, D., Coll, K., & Williamson, J.R. (1977). Pyridine nucleotide distributions and enzyme mass action ratios in hepatocytes from fed and starved rats. *Archives of Biochemistry and Biophysics, 184*(1), 222-236.

Tsukita, S., & Ishikawa, H. (1976). Three-dimensional distribution of smooth endoplasmic reticulum in myelinated axons. *J Electron Microsc (Tokyo), 25*(3), 141-149.

Vargas, M.E., Yamagishi, Y., Tessier-Lavigne, M., & Sagasti, A. (2015). Live Imaging of Calcium Dynamics during Axon Degeneration Reveals Two Functionally Distinct Phases of Calcium Influx. *Journal of Neuroscience, 35*(45), 15026-15038.

Villegas, R., Martinez, N.W., Lillo, J., Pihan, P., Hernandez, D., Twiss, J.L., & Court, F.A. (2014). Calcium Release from Intra-Axonal Endoplasmic Reticulum Leads to Axon Degeneration through Mitochondrial Dysfunction. *J Neurosci, 34*(21), 7179 –7189.

Voit, E.O. (2000). *Computational Analysis of Biochemical Systems: A Practical Guide for Biochemists and Molecular Biologists*. Cambridge, UK: Cambridge University Press.

Wang, J., & He, Z. (2009). NAD and axon degeneration. *Cell Adhesion & Migration, 3*, 77-87.

Wang, J., Zhai, Q., Chen, Y., Lin, E., Gu, W., McBurney, M., & He, Z. (2005). A local mechanism mediates NAD-dependent protection of axon degeneration. *Journal of Cell Biology, 170*(3), 349-355.

Wang, K., Wright, L.C., Machan, C.L., Allen, B.G., Conigrave, A.D., & Roufogalis, B.D. (1991). Protein Kinase C Phosphorylates the Carboxyl Terminus of the Plasma Membrane Ca^{2+} ATPase from Human Erythrocytes. Journal of Biological Chemistry, 266(14), 9078-9085.

Wang, J.T., Medress, Z.A., & Barres, B.A. (2012). Axon degeneration: Molecular mechanisms of a self-destruction pathway. *Journal of Cell Biology, 196*(1), 7-18.

Wong, R., Steenbergen, C., & Murphy, E. (2013). Mitochondrial permeability transition pore and calcium handling. *Methods Mol Biol, 810*, 235-242.

Yahata, N., Yuasa, S., & Araki, T. (2009). NicotiNamide Mononucleotide Adenylyltransferase Expression in Mitochondrial Matrix Delays Wallerian Degeneration. *Journal of Neuroscience, 29*(19) 6276-6284.

Yan, T., Feng, Y., Zheng, J., Ge, X., Zhang, Y., Wu, D., Zhao, J., & Zhai, Q. (2010). Nmnat2 delays axon degeneration in superior cervical ganglia dependent on its NAD synthesis activity. *Neurochemistry International, 56*, 101-106.

Yan, Y., Wei, C.L., Zhang, W.R., Cheng, H.P., & Liu, J. (2006) Cross-talk between calcium and reactive oxygen species signaling. *Acta Pharmacol. Sin, 27*, 821–826.

Yang, J.J., Weimer, R.M., Kallop, D., Olsen, O., Wu, Z., Renier, N., Uryu, K., Tessier-Lavigne, M. (2013). Regulation of axon degeneration after injury and in development by the endogenous calpain inhibitor calpastatin. *Neuron, 80*, 1175–1189.

Zhai, Q., Wang, J., Kim, A., Liu, Q., Watts, R., Hoopfer, E., Mitchison, T., Luo, L., He, Z. (2003). Involvement of the ubiquitin-proteasome system in the early stages of Wallerian degeneration. *Neuron, 39*, 217–225.

Zhou, Y., Xuec, S., & Yang, J.J. (2013). Calciomics: integrative studies of Ca2+-binding proteins and their interactomes in biological systems. *Metabolomics, 5*(1), 29–42.

Figures

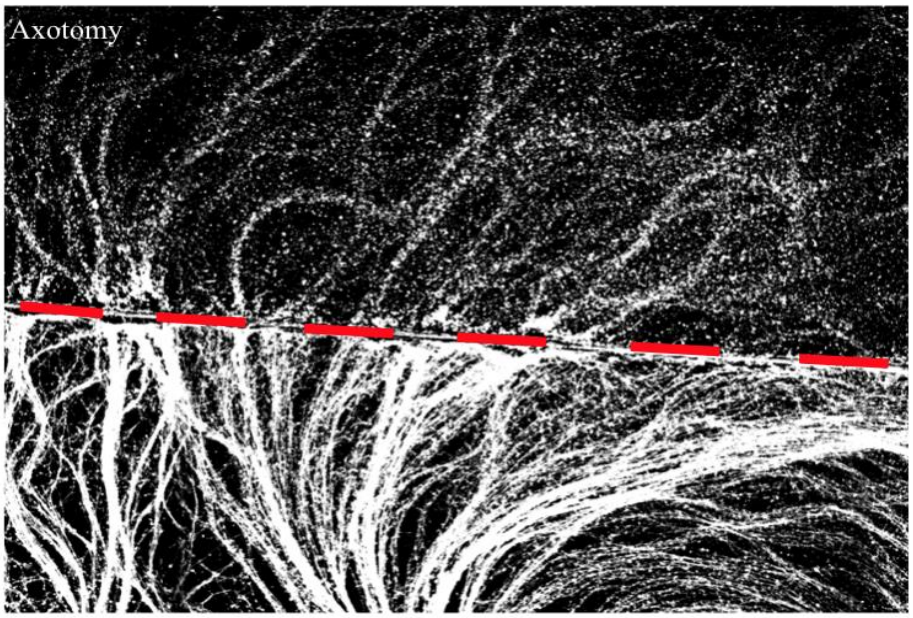

Figure 10a Axons 15 hours post-axotomy of a RGC explant. Red dashes indicate the site of injury.

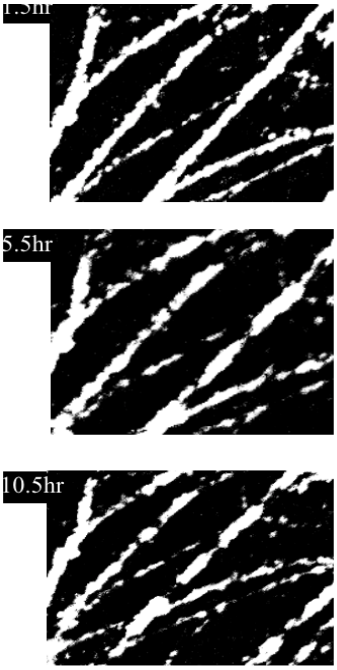

Figure 10b Time lapse of degeneration showing zoomed section of distal axons to injury site at 1.5 hours, 5.5 hours, and 10.5 hours.

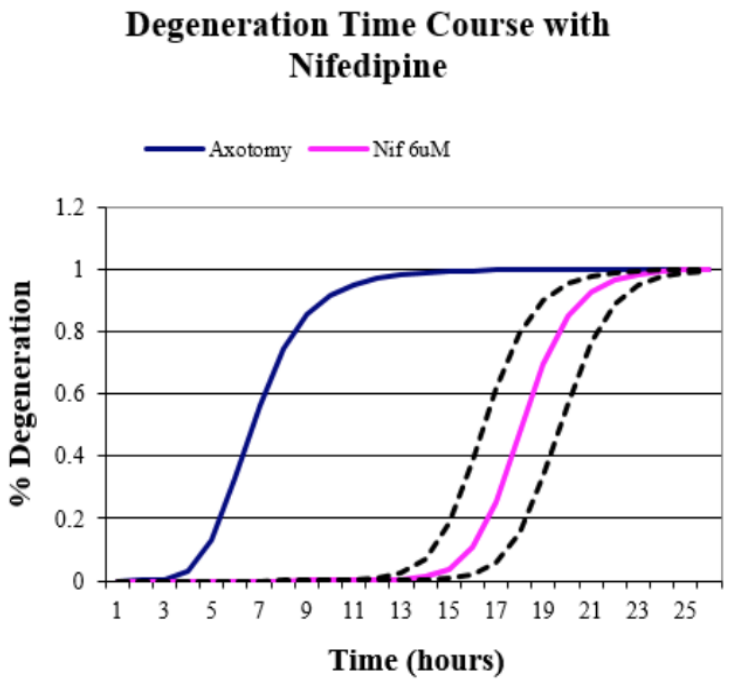

Figure 10c Degeneration time course of distal axons following axotomy with and without nifedipine treatment. Dashed lines represent $\pm$ SEM of t_{50} (SEM~5.4%); Nifedipine (Nif).

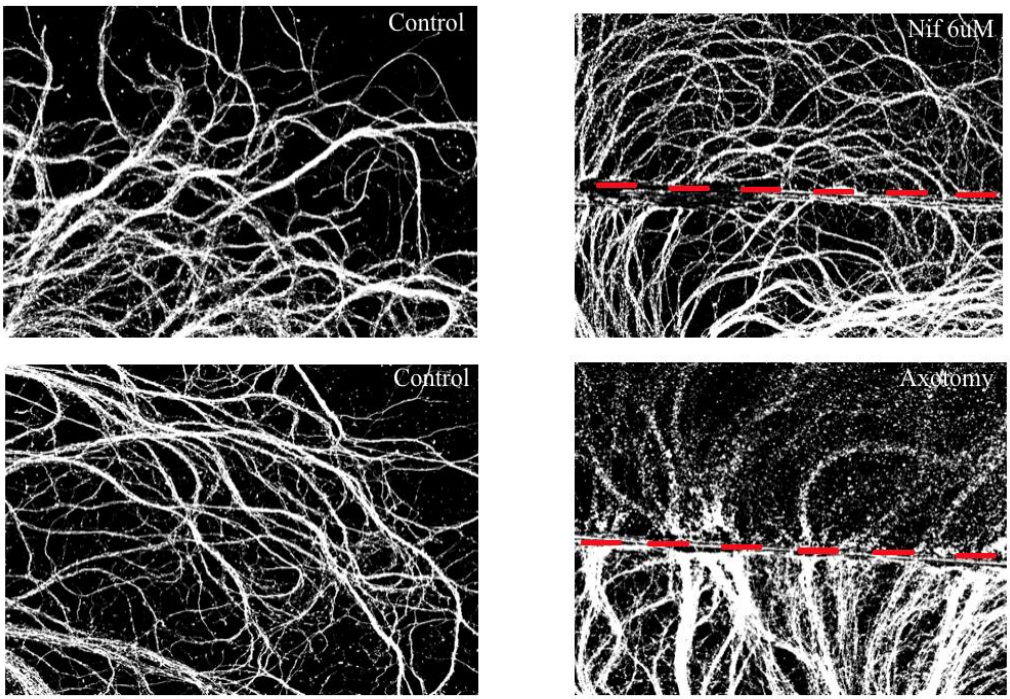

Figure 10d Morphology of distal axons with various treatments to RGC explants at 15 hours post-treatment.

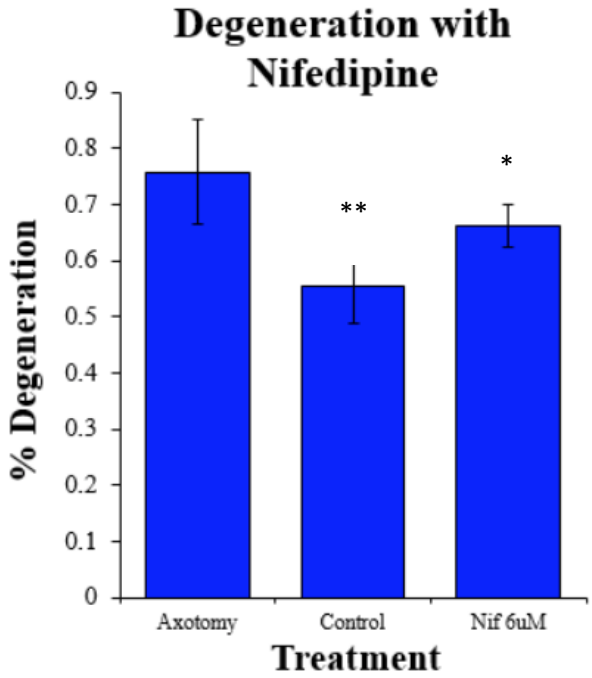

Figure 10e Percent degeneration of distal axons following axotomy at 15 hours. * Indicates $p<0.05$, ** $p<0.01$

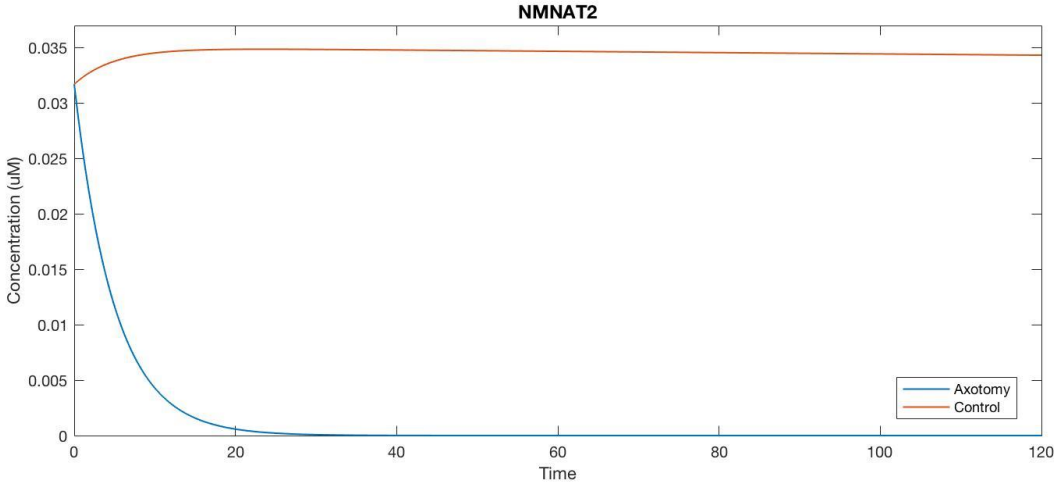

Figure 11a Presence of Nmnat2 in control and axotomy models. Nmnat2 rapidly declines following axotomy.

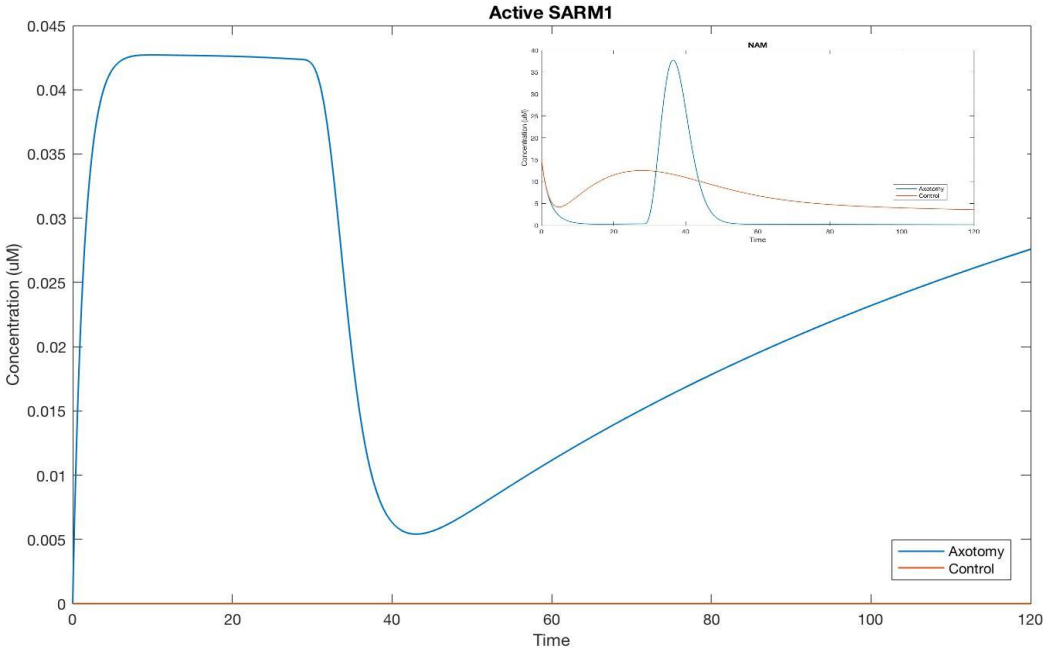

Figure 11b Presence of Active SARM1 in axotomy and control models. In the axotomy model, SARM1 rapidly activates and inactivates primarily due to Nam accumulation.

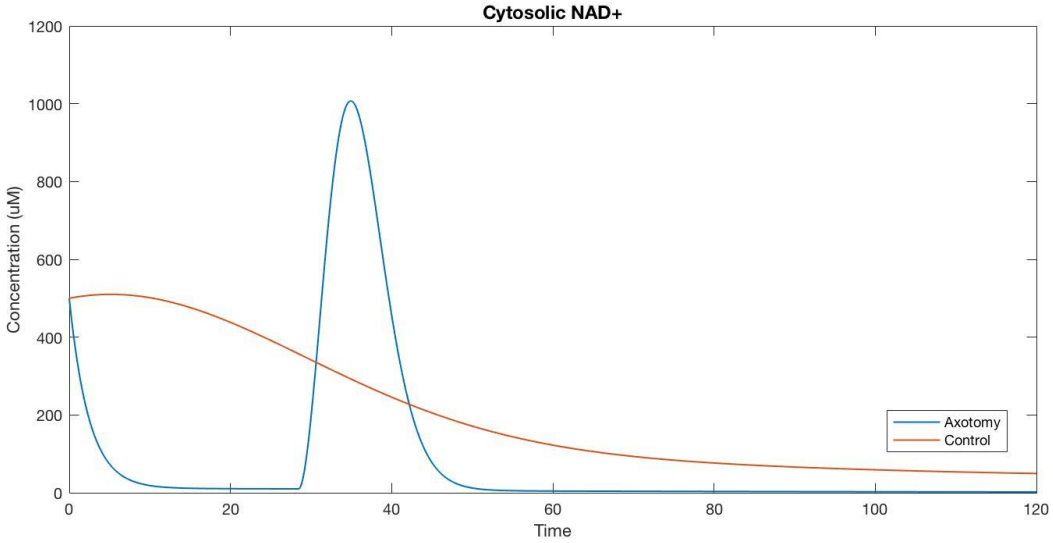

Figure 11c Cytosolic NAD consumption in axotomy and control models. In the axotomy model, there are two major NAD consumption phases. The control demonstrates stable cytosolic NAD over time as the model solves for a steady state with given initial conditions.

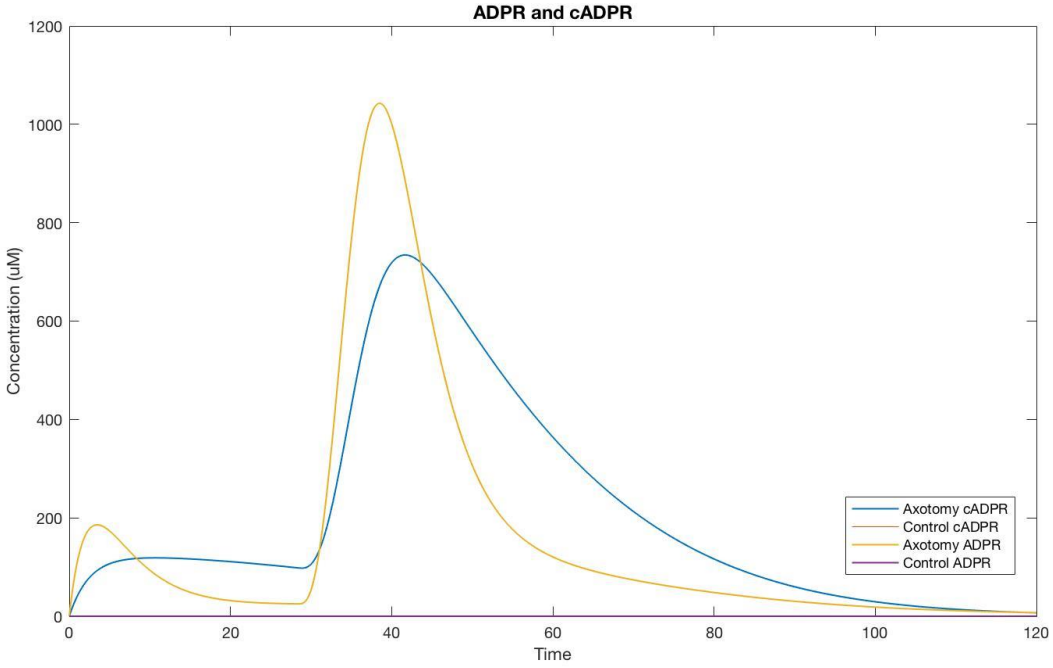

Figure 11d Presence of ADPR and cADPR in axotomy and control models. The axotomy model demonstrates two rises in ADPR and cADPR concentrations, whereas there are no rises observed in the control model. cADPR levels are also maintained longer than ADPR levels due to the more stable nature of the molecule.

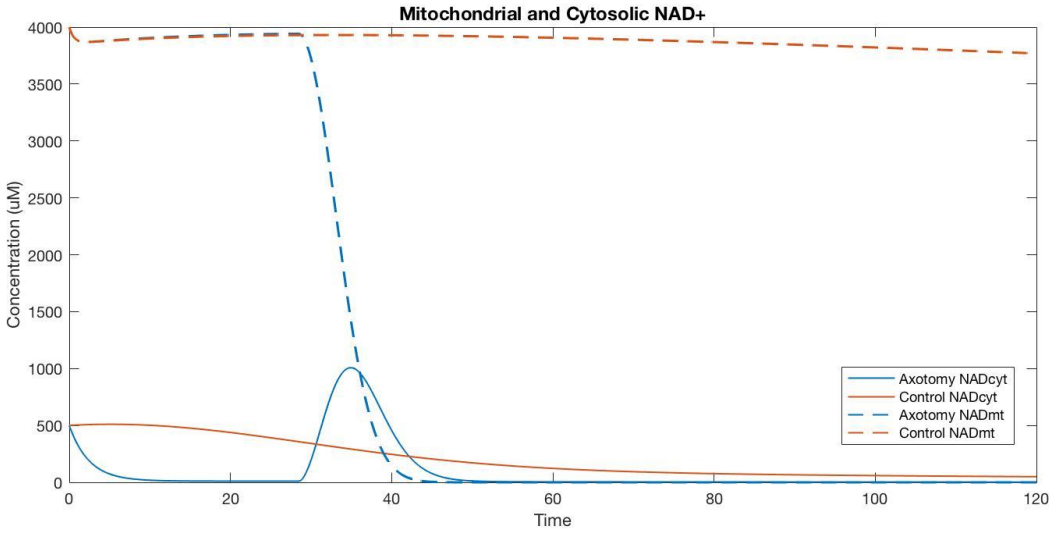

Figure 11e NAD presence in the mitochondria and cytosol in axotomy and control models. The axotomy model demonstrates the release of mitochondrial NAD into the cytosol via mPTP opening causing a late rise in cytosolic NAD. The control model shows steady levels of both cytosolic and mitochondrial NAD.

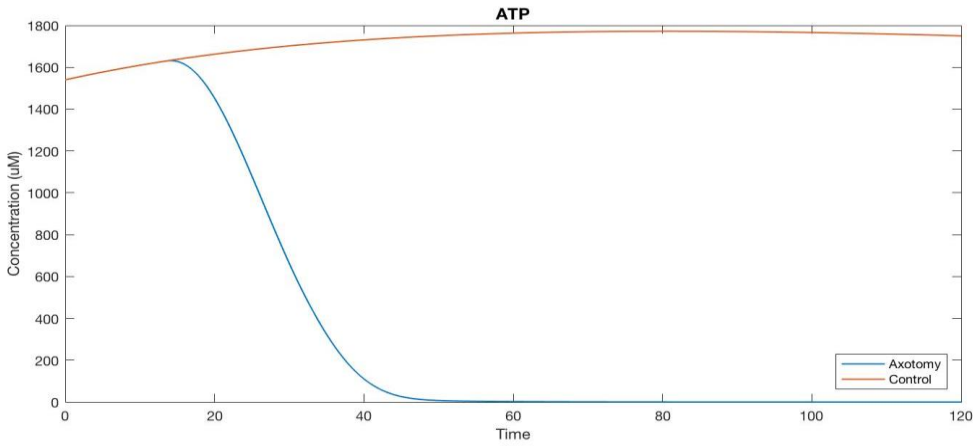

Figure 11f Decline in ATP levels observed following axotomy. The control demonstrates stable ATP levels over time as the model solves for a steady state with given initial conditions.

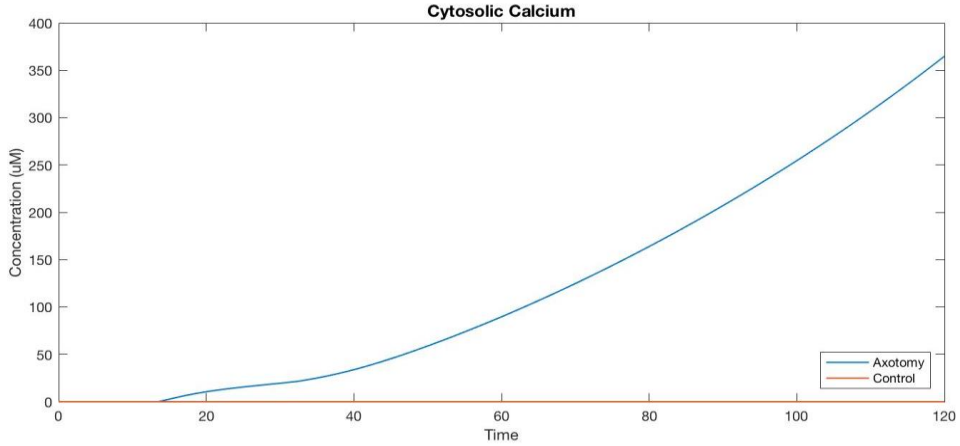

Figure 11g Increase in cytosolic calcium levels following axotomy. The inflection point of the cytosolic calcium curve for the axotomy model indicates opening of the L-type VGCCs.

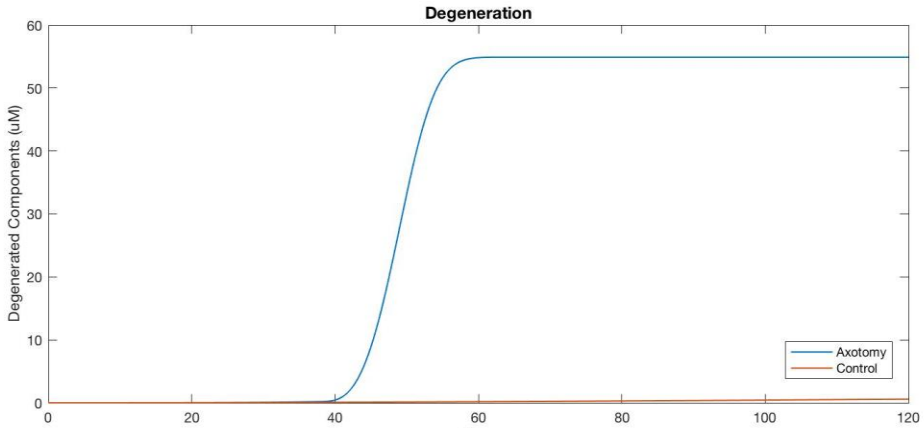

Figure 11h Degeneration time course of axotomy model. Degeneration is completed at approximately t=60. No significant degeneration is observed in the control model.

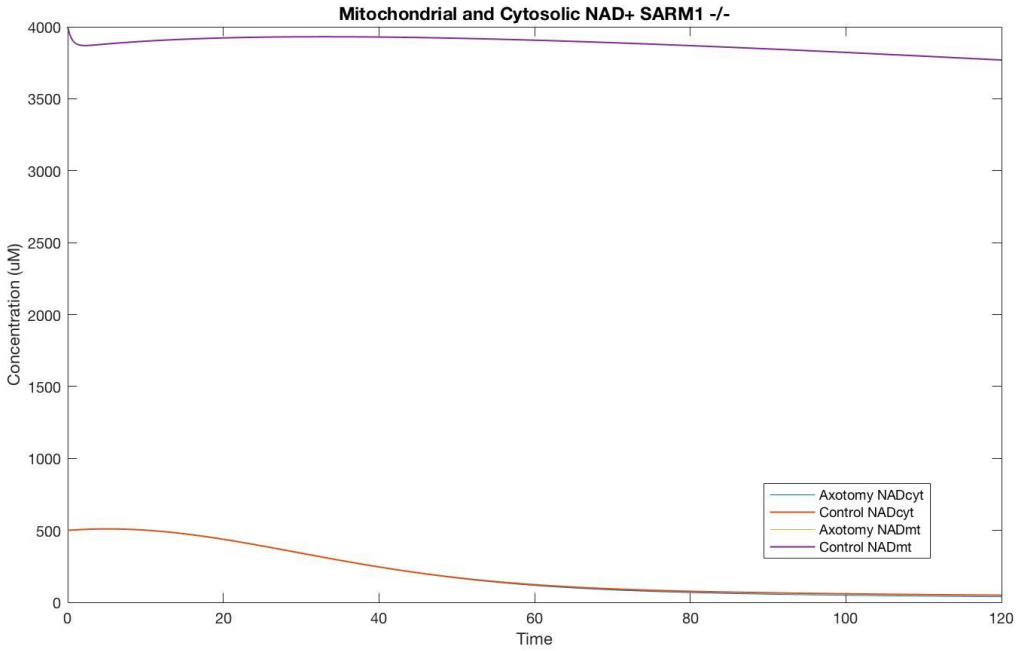

Figure 12a Mitochondrial and cytosolic calcium in the SARM1 knockout of the axotomy model are comparable to the control model.

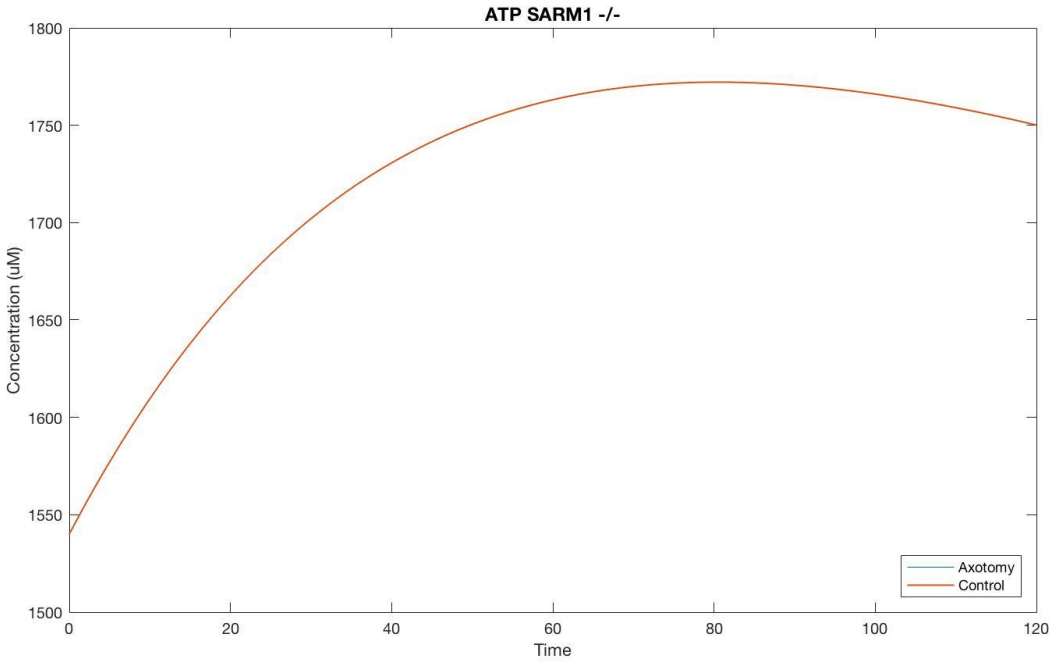

Figure 12b ATP levels in the SARM1 knockout of axotomy are comparable to the control model.

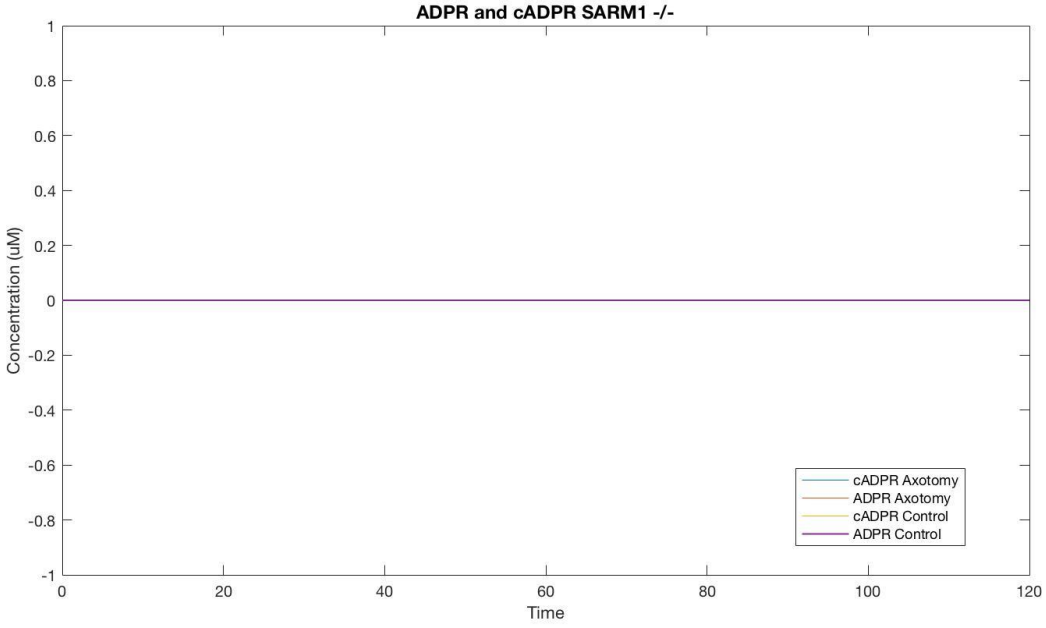

Figure 12c No generation of ADPR and cADPR in the SARM1 knockout of the axotomy model.

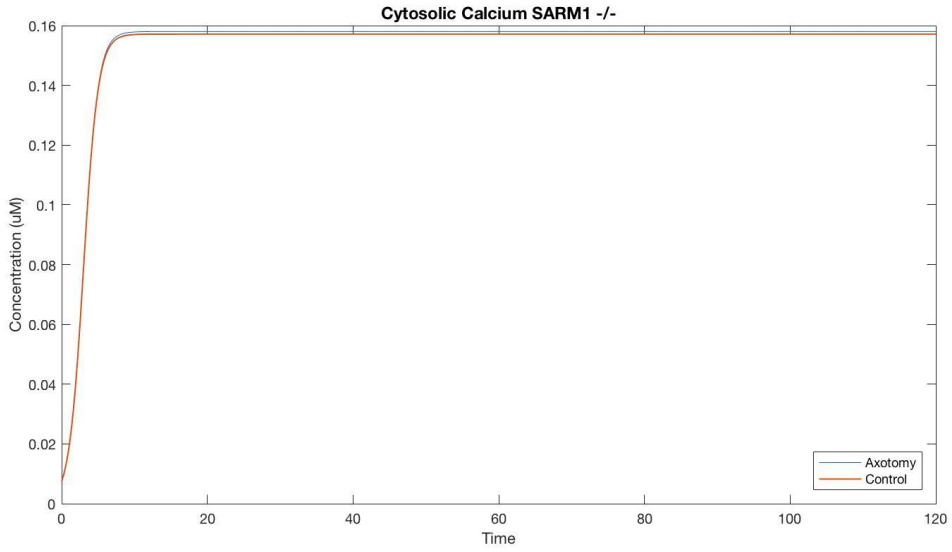

Figure 12d Cytosolic calcium in the SARM1 knockout of the axotomy model is comparable to the control model.

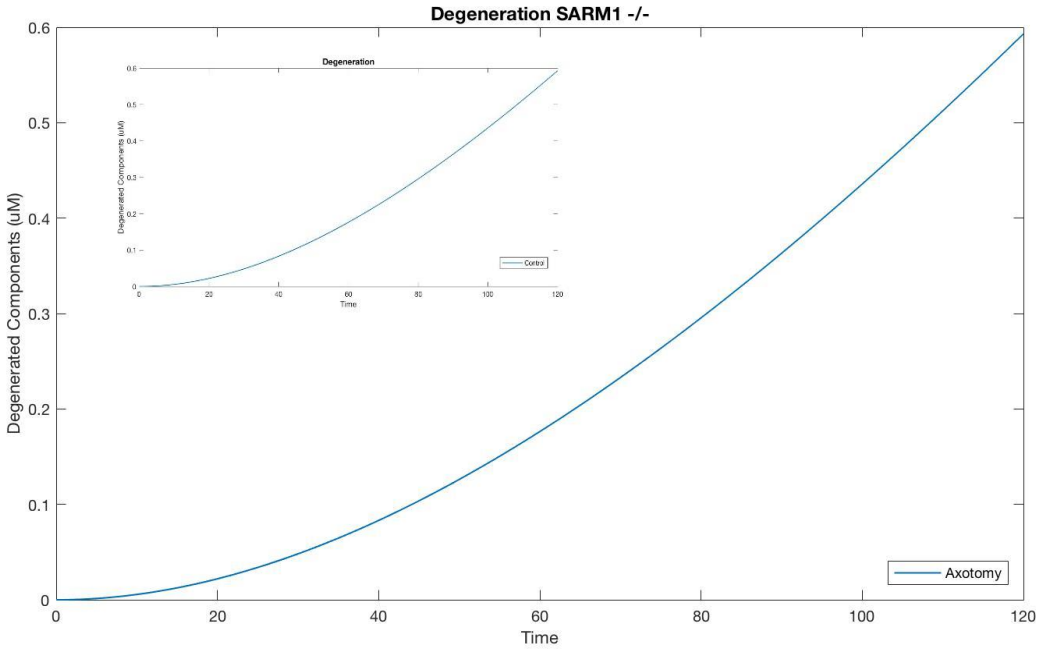

Figure 12e Main figure shows degeneration in the SARM1 knockout of the axotomy model is comparable to the control model. Inset shows degeneration of the control model due to initial conditions.

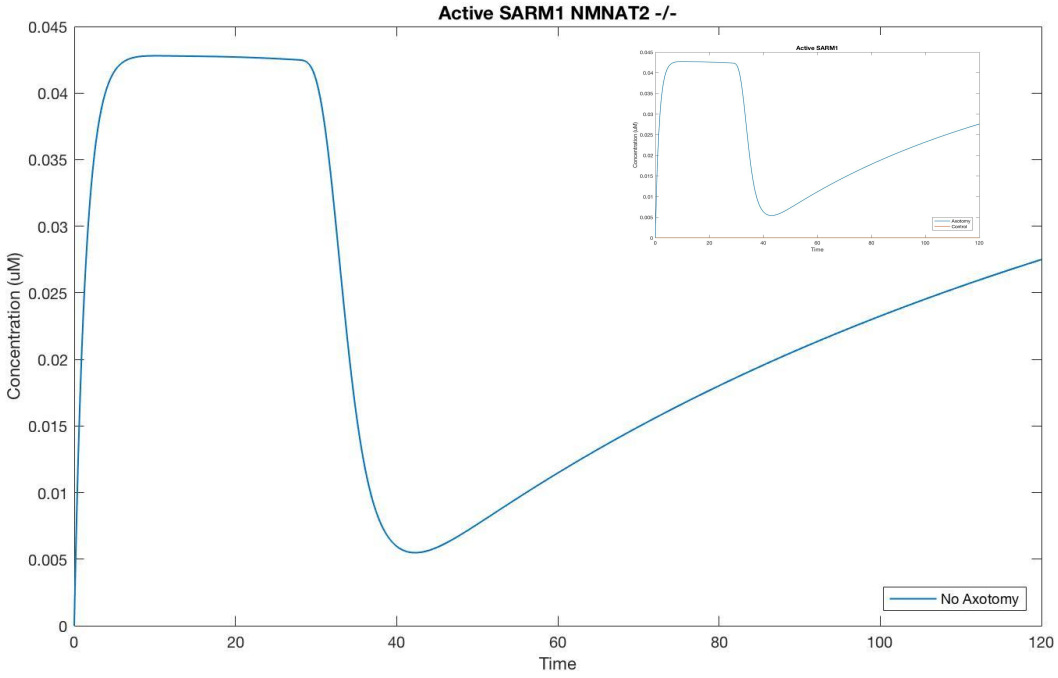

Figure 13a Main figure shows presence of SARM1 in the Nmnat2 knockout of the control model (no axotomy) is comparable to the axotomy model. Inset shows presence of active SARM1 in the initial axotomy and control models.

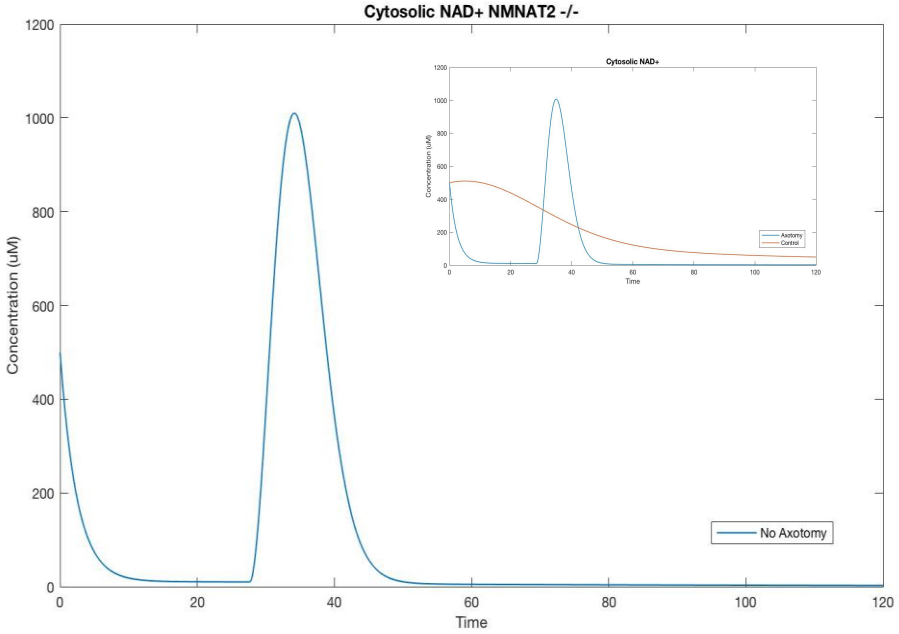

Figure 13b Main figure shows decrease in NAD in the Nmnat2 knockout of the control model (no axotomy) is comparable to the axotomy model. Inset shows cytosolic NAD of the initial axotomy and control models.

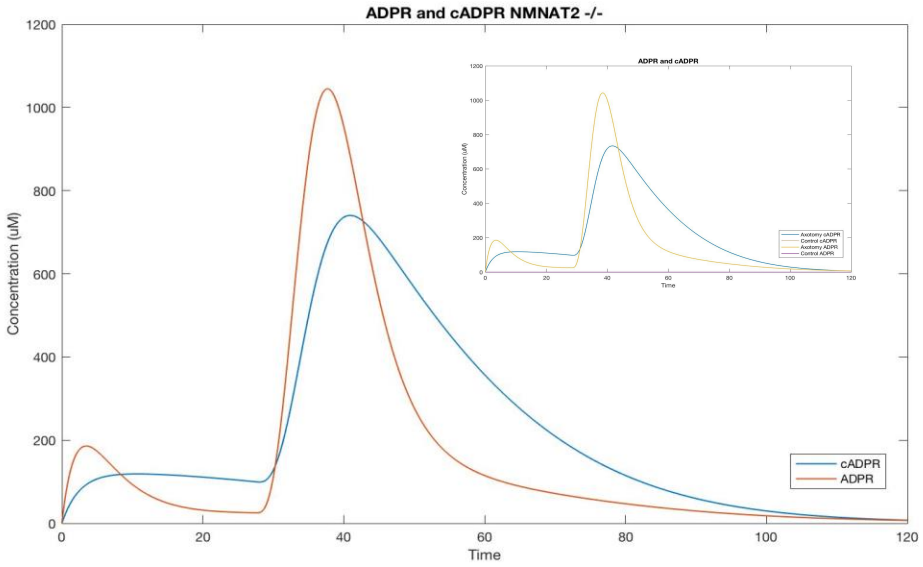

Figure 13c Main figure shows generation of ADPR and cADPR in the Nmnat2 knockout of the control model (no axotomy) is comparable to the axotomy model. Inset shows generation of ADPR and cADPR in the initial axotomy and control models.

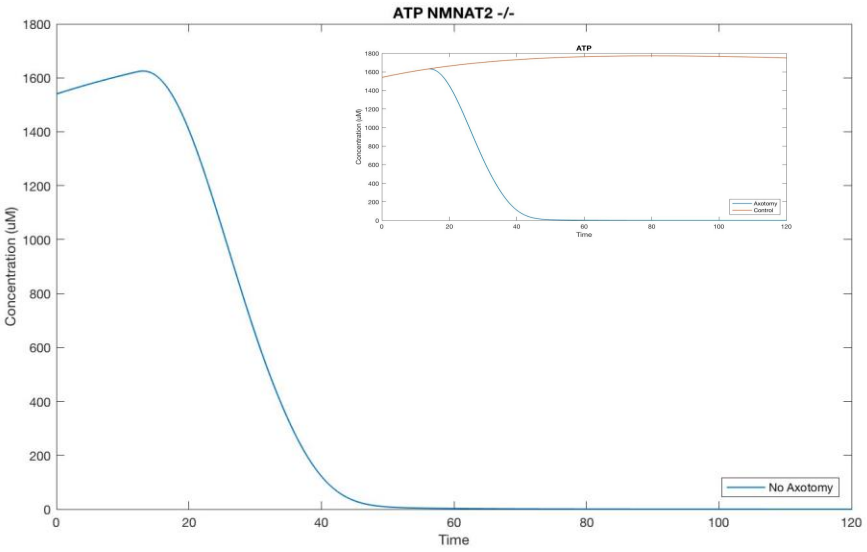

Figure 13d Main figure shows ATP levels decline in the Nmnat2 knockout of the control model (no axotomy) comparable to the axotomy model. Inset shows ATP levels in the initial axotomy and control models.

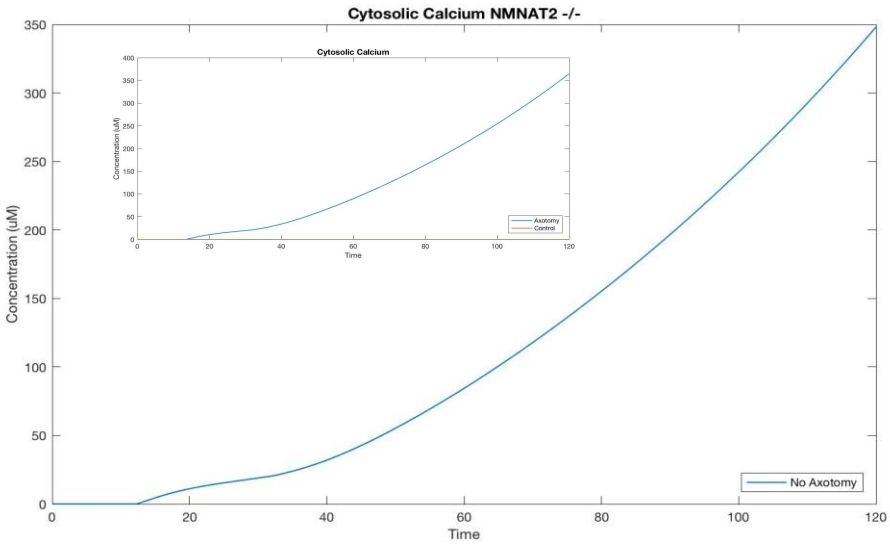

Figure 13e Main figure shows cytosolic calcium in the Nmnat2 knockout of the control model (no axotomy) is comparable to the axotomy model. Inset shows cytosolic calcium in the initial axotomy and control models.

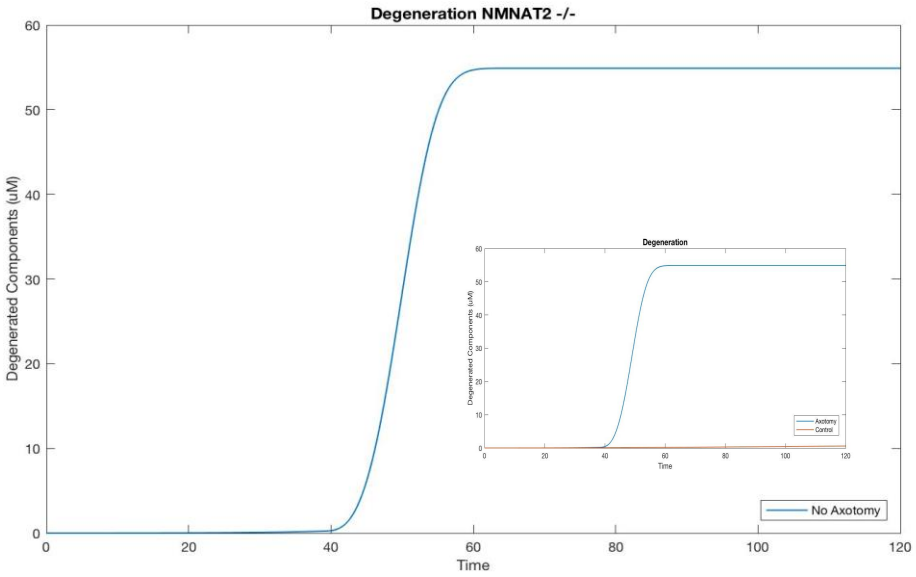

Figure 13f Main figure shows degeneration time course in the Nmnat2 knockout of the control model (no axotomy) is comparable to the axotomy model. Onset shows the degeneration time course of the initial axotomy and control models.

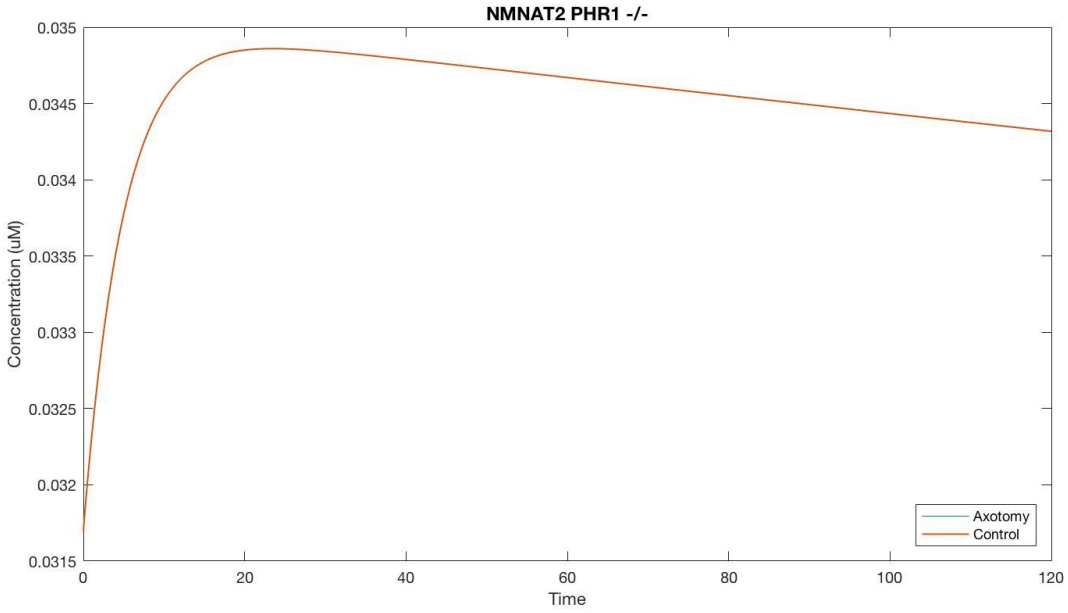

Figure 14a Presence of Nmnat in the PHR1 knockout of the axotomy model is comparable to Nmnat levels in the control model.

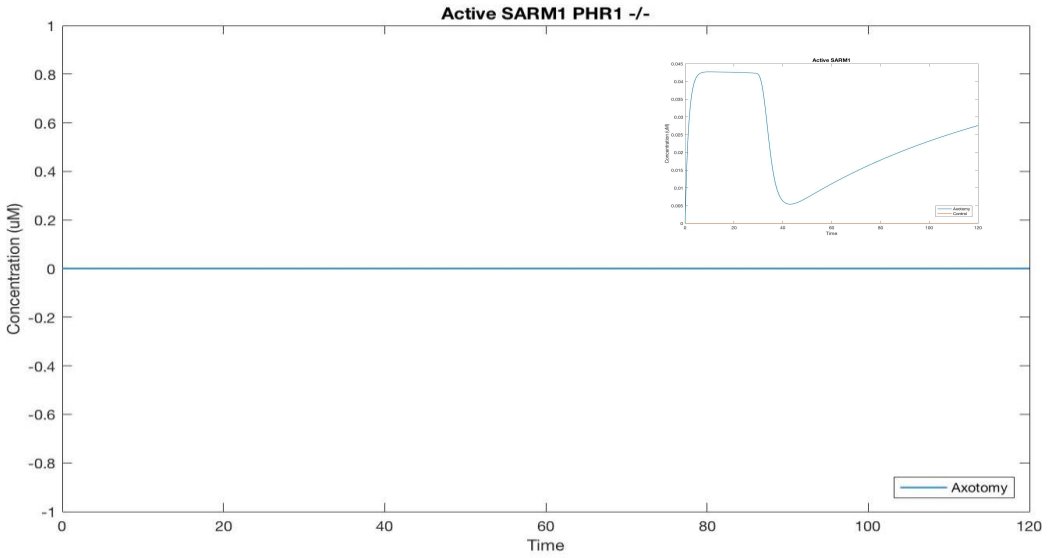

Figure 14b Main figure shows presence of active SARM1 in the PHR1 knockout of the axotomy model is comparable to the control model. Inset shows presence of active SARM1 in the initial axotomy and control models.

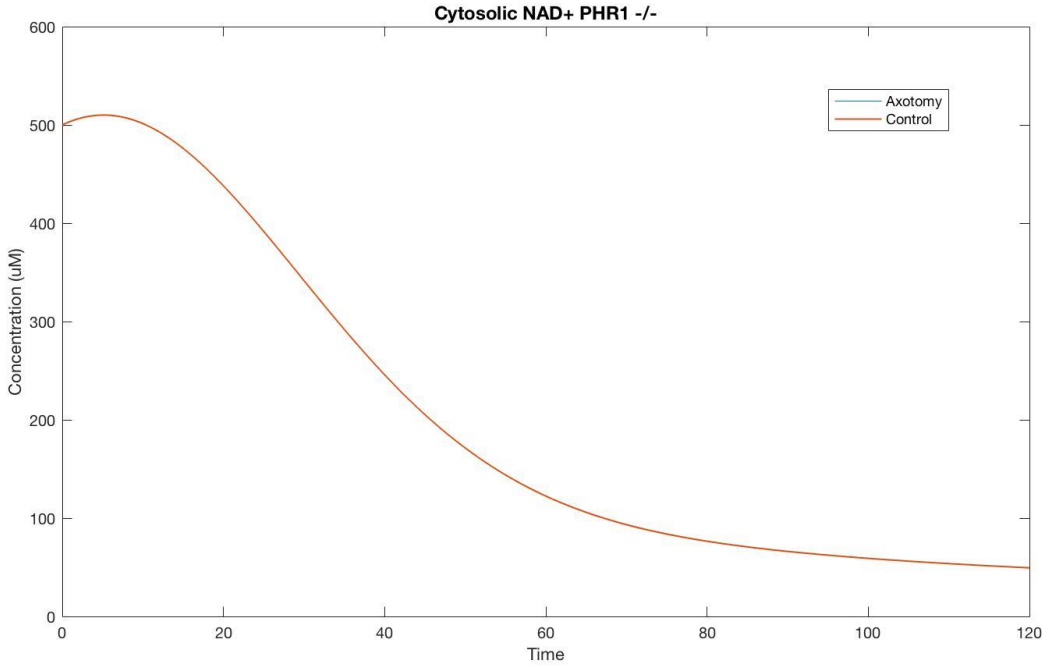

Figure 14c Cytosolic NAD in PHR1 knockout of the axotomy model is comparable to the control model.

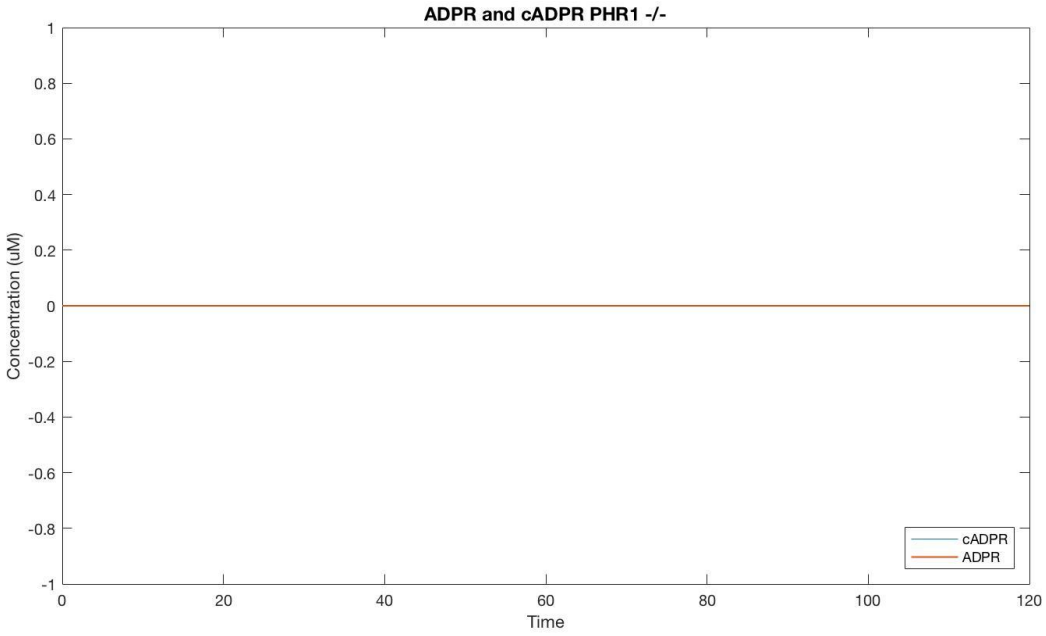

Figure 14d No generation of cADPR and ADPR in PHR1 knockout of the axotomy model.

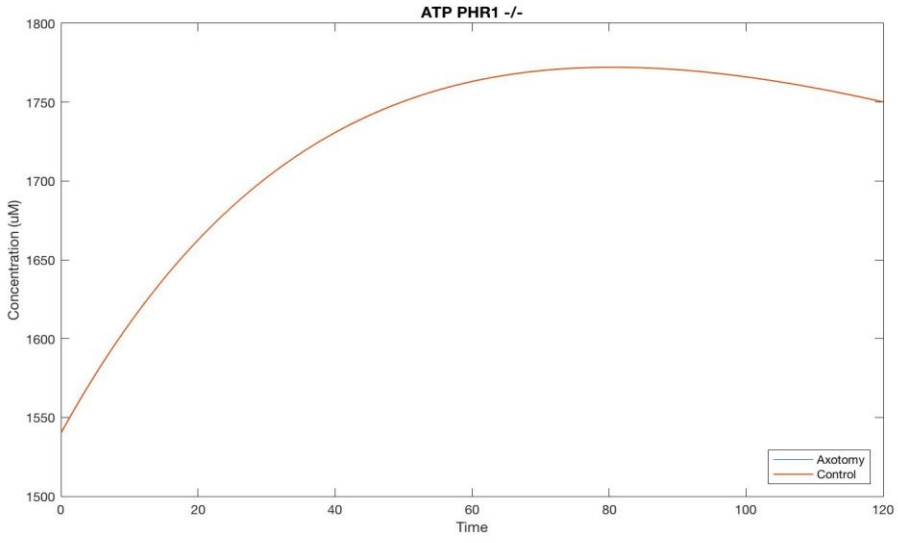

Figure 14e ATP levels in the PHR1 knockout of the axotomy model are comparable to the control model.

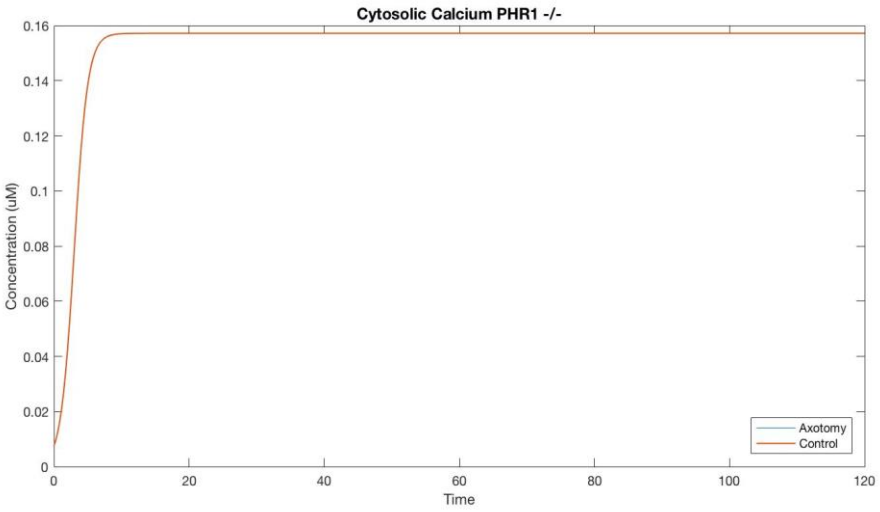

Figure 14f Cytosolic calcium in the PHR1 knockout of the axotomy model are comparable to the control model.

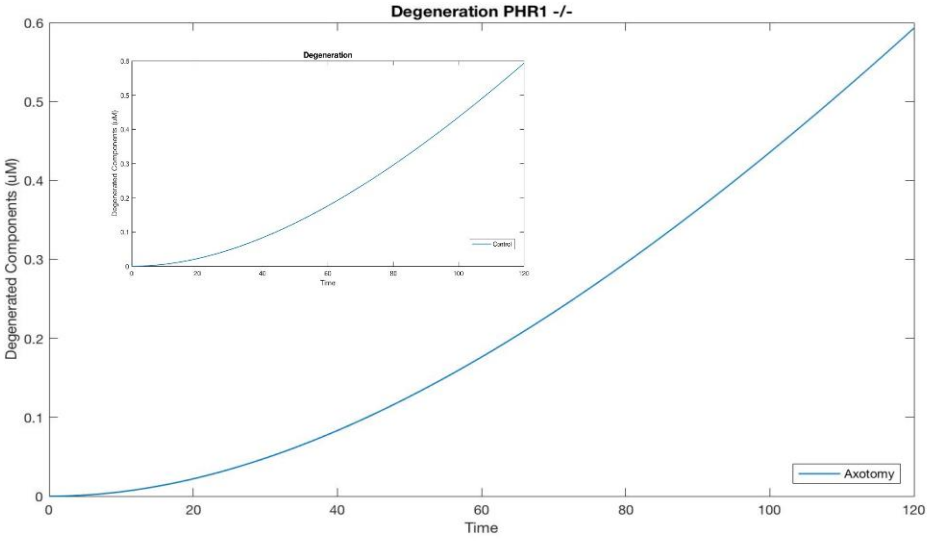

Figure 14g Main figure shows degeneration time course in the PHR1 knockout of the axotomy model is comparable to the control model. Inset shows degeneration time course for control model.

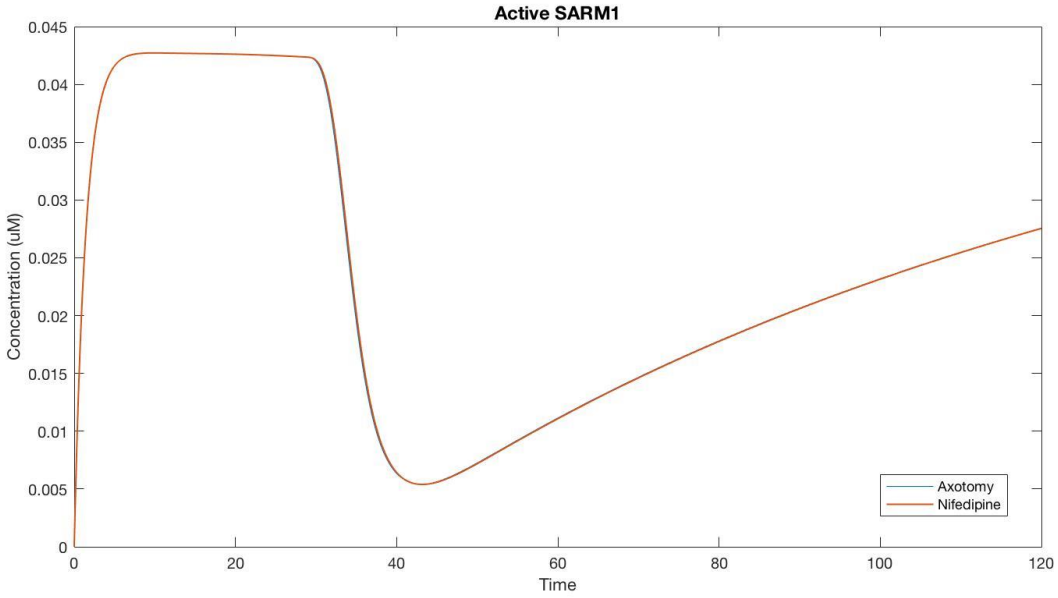

Figure 15a Active SARM1 in nifedipine treatment is comparable to the initial axotomy model.

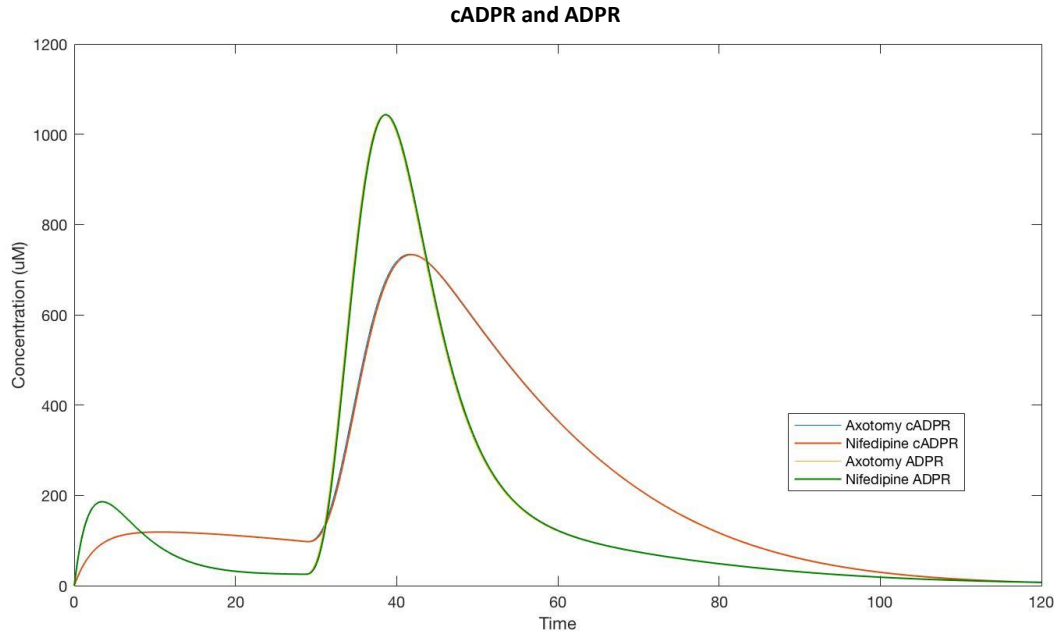

Figure 15b Generation of cADPR and ADPR in nifedipine treatment is comparable to the initial axotomy model. These species are the primary drivers behind mobilization of calcium to the cytosol in nifedipine treatment.

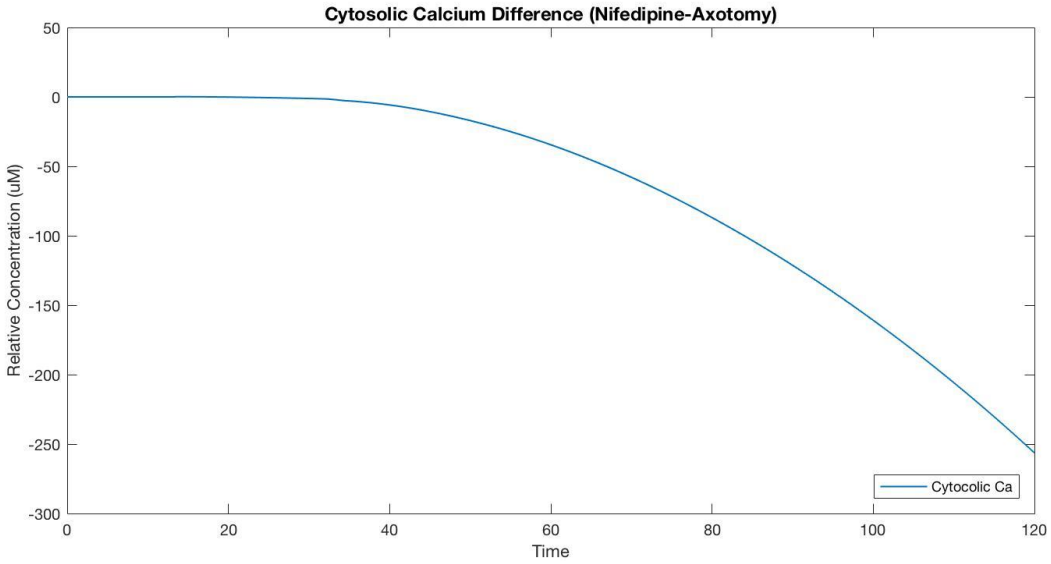

Figure 15c Difference in cytosolic calcium levels between nifedpipine treatment and the initial axotomy model. There is a less pronounced rise in cytosolic calcium in the nifedipine treated axotomy model.

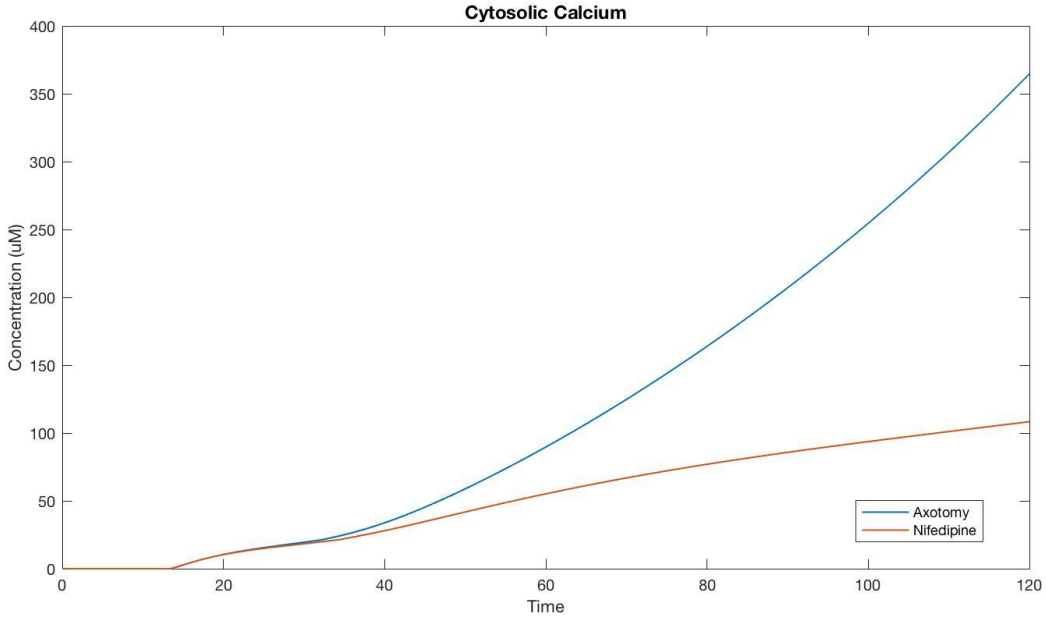

Figure 15d Increases in cytosolic calcium are less pronounced in nifedipine treatment compared to the initial axotomy model since there is no contribution to cytosolic calcium from VGCC activity.

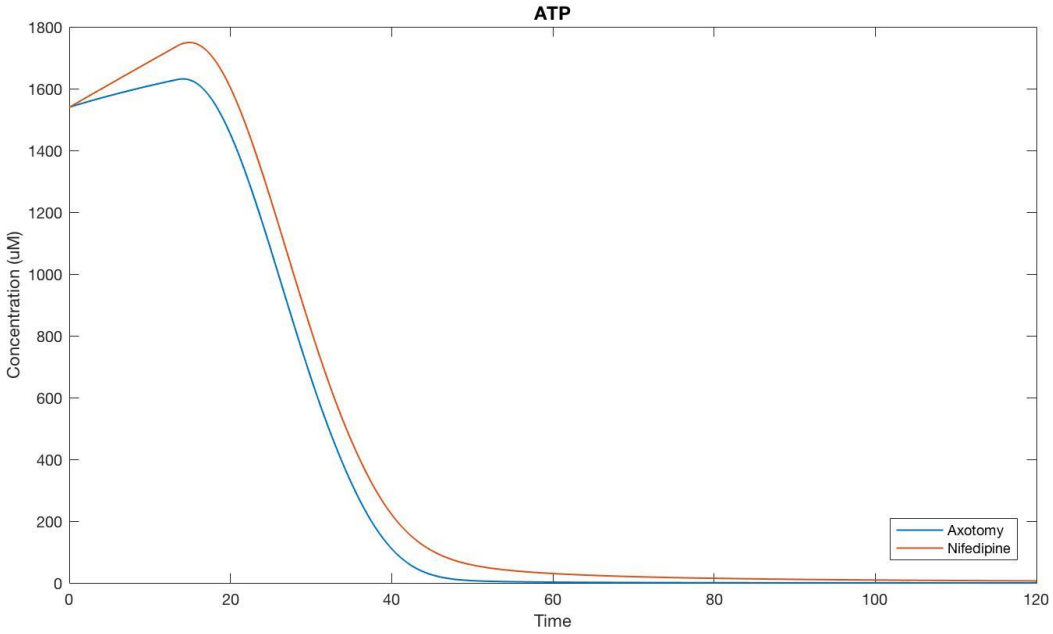

Figure 15e ATP decline in nifedipine treatment is delayed compared to the initial axotomy model. This delay is in part due to the lower levels of cytosolic calcium and slower consumption of ATP by calcium ATPases.

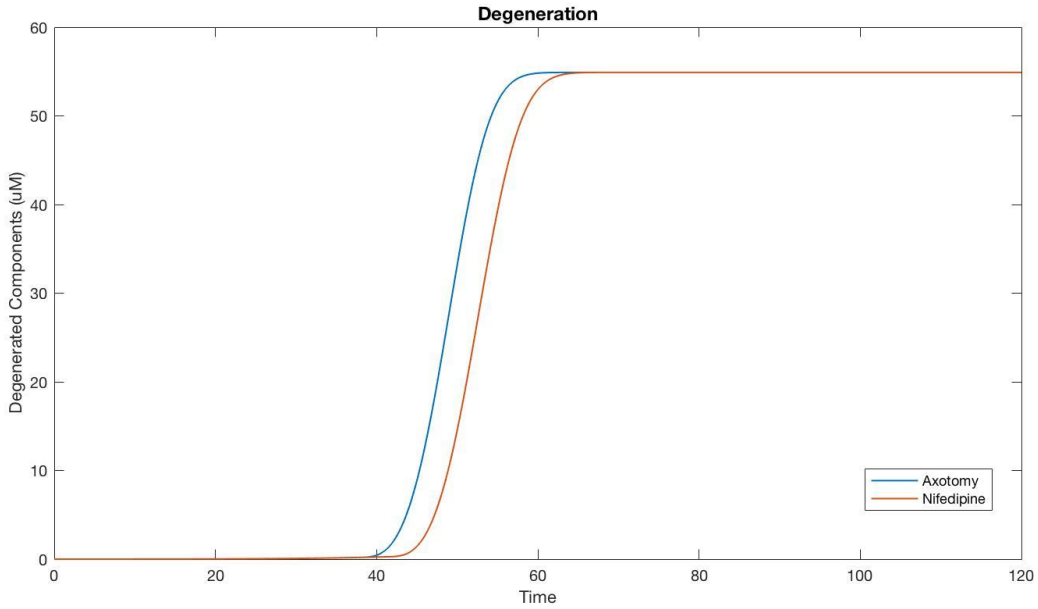

Figure 15f Delayed degeneration time course in nifedipine treatment is observed compared to the initial axotomy model due to slower cytosolic calcium accumulation.

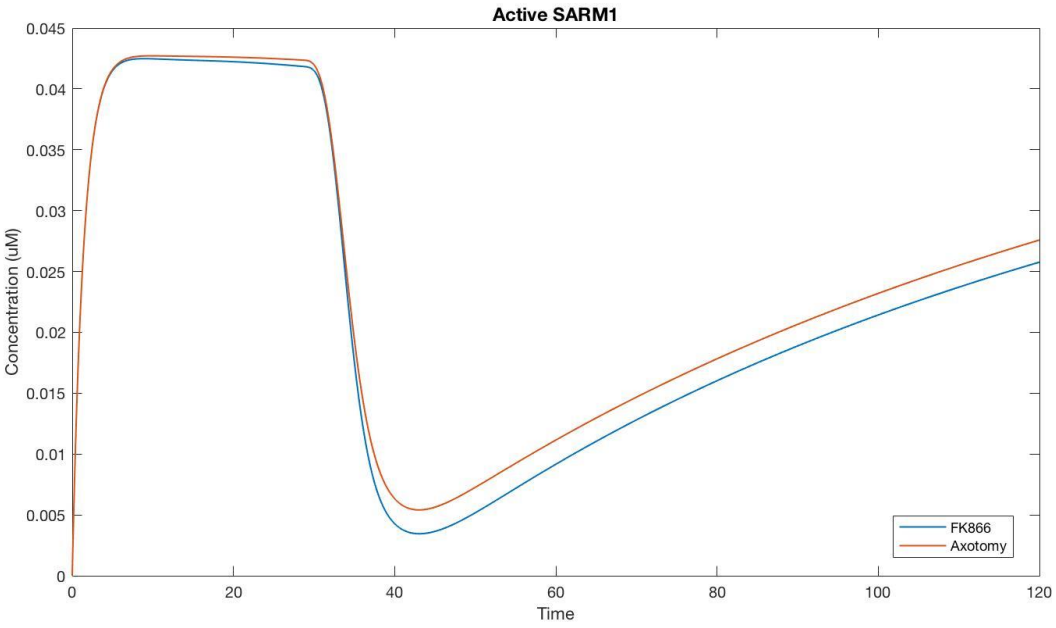

Figure 16a Active SARM1 levels in FK866 treatment are slightly less than levels in the initial axotomy model. There is a more pronounced decrease of active SARM1 in FK866 treatment around t=40 due to increased levels of Nam.

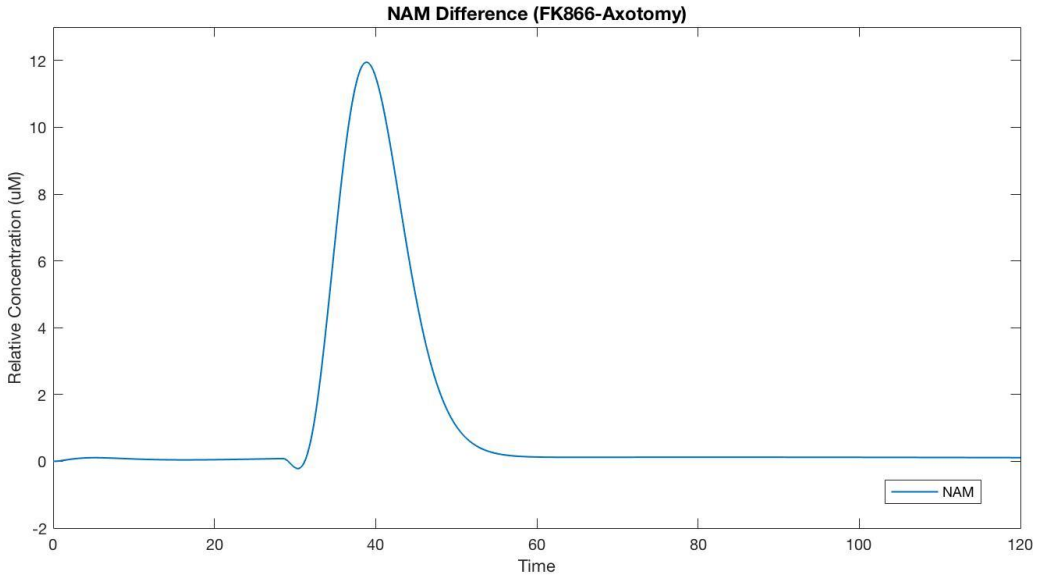

Figure 16b Difference in levels of Nam between FK866 treatment and initial axotomy model. There is greater Nam presence in the FK866 treated axotomy model.

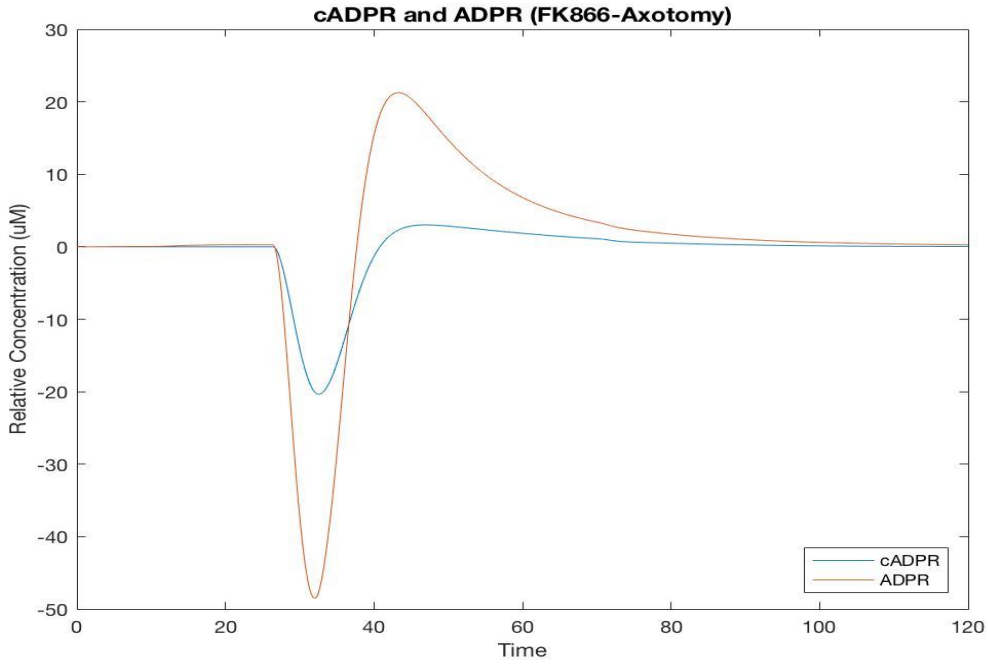

Figure 16c Difference in cADPR and ADPR levels between FK866 treatment and the initial axotomy model. There is a net decrease in both species in the FK866 treated axotomy model.

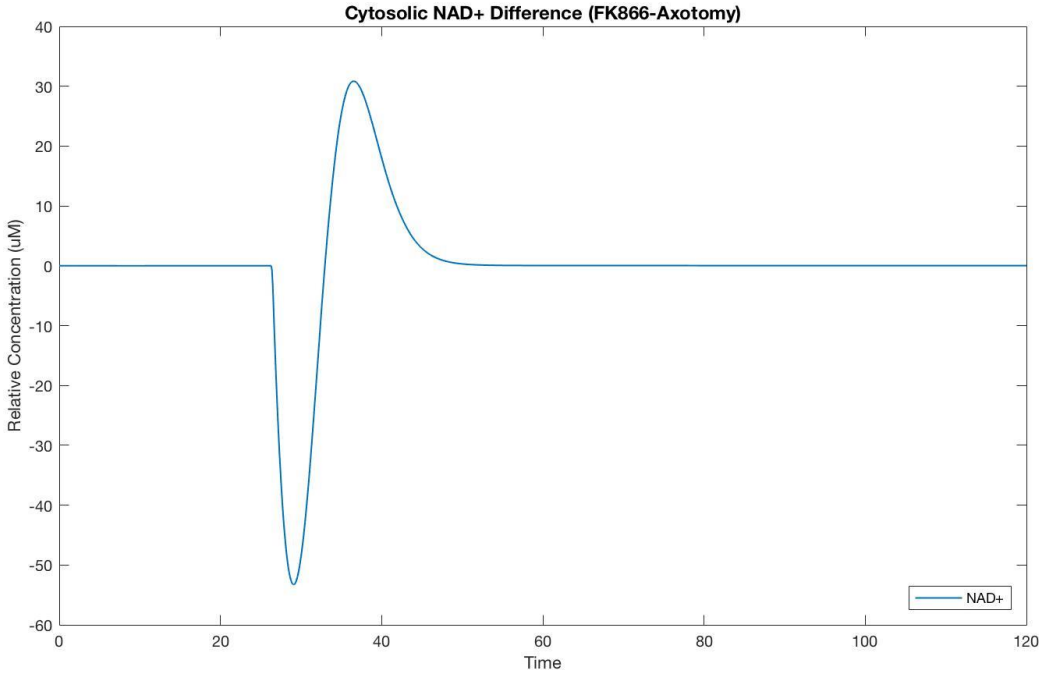

Figure 16d Difference in cytosolic NAD levels between FK866 and the initial axotomy model. There is a delayed release of mitochondrial NAD into the cytosol in the FK866 treated axotomy model.

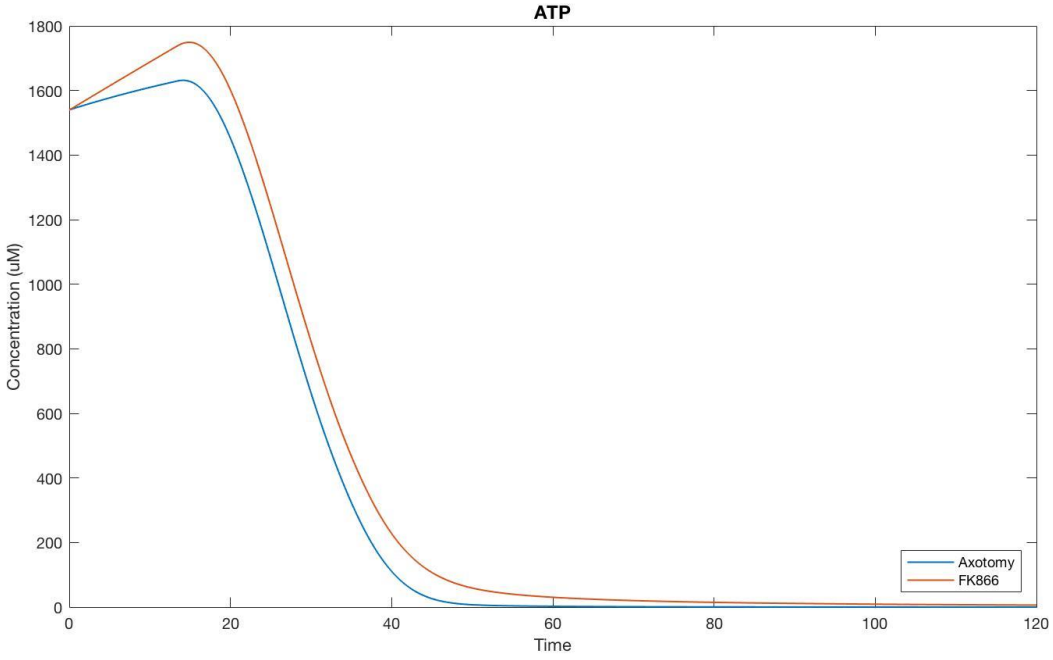

Figure 16e ATP decline in FK866 treatment is delayed compared to the initial axotomy model. This delay is in part due to the lower levels of cytosolic calcium and slower consumption of ATP by calcium ATPases.

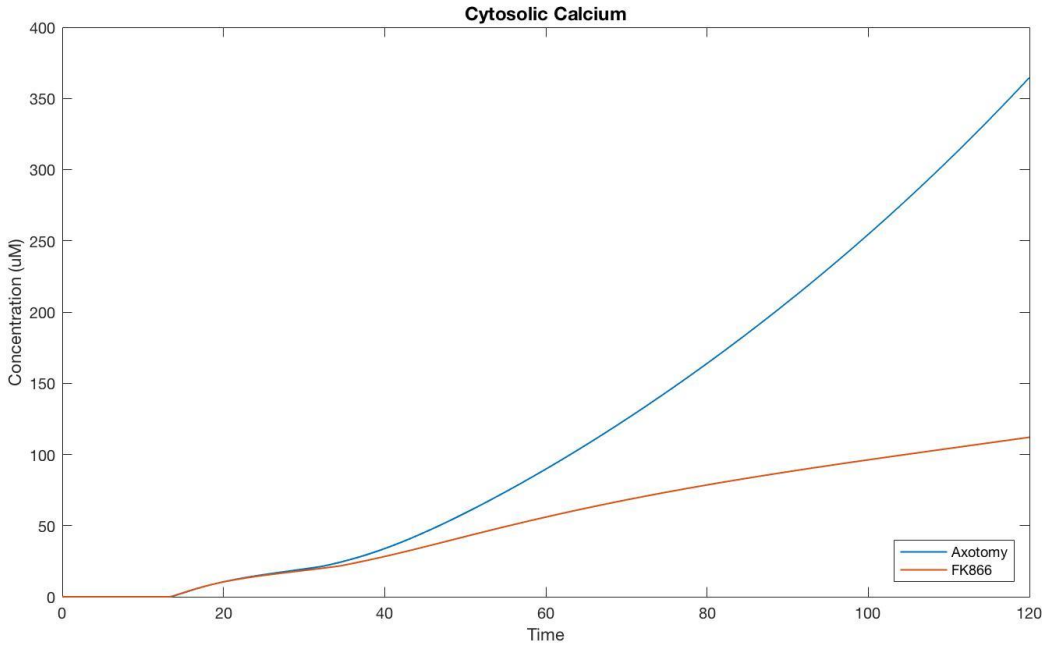

Figure 16f Increases in cytosolic calcium are less pronounced in FK866 treatment compared to the initial axotomy model since there is a decrease in SARM1 activity via inhibition by Nam.

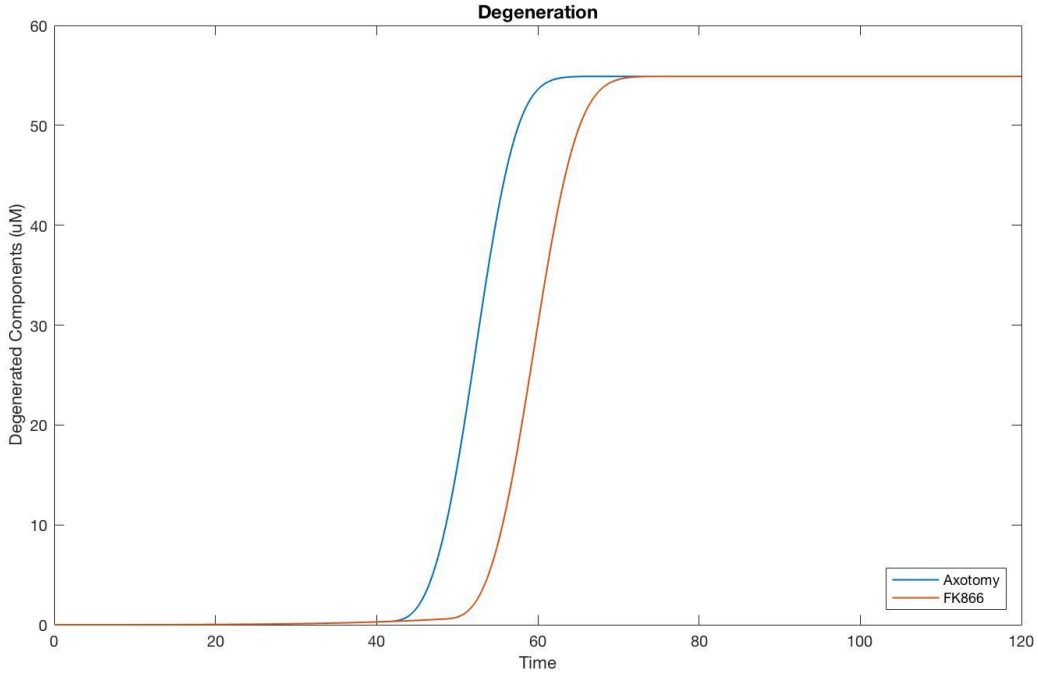

Figure 16g Delayed degeneration time course in FK866 treatment is observed compared to the initial axotomy model due to slower cytosolic calcium accumulation.

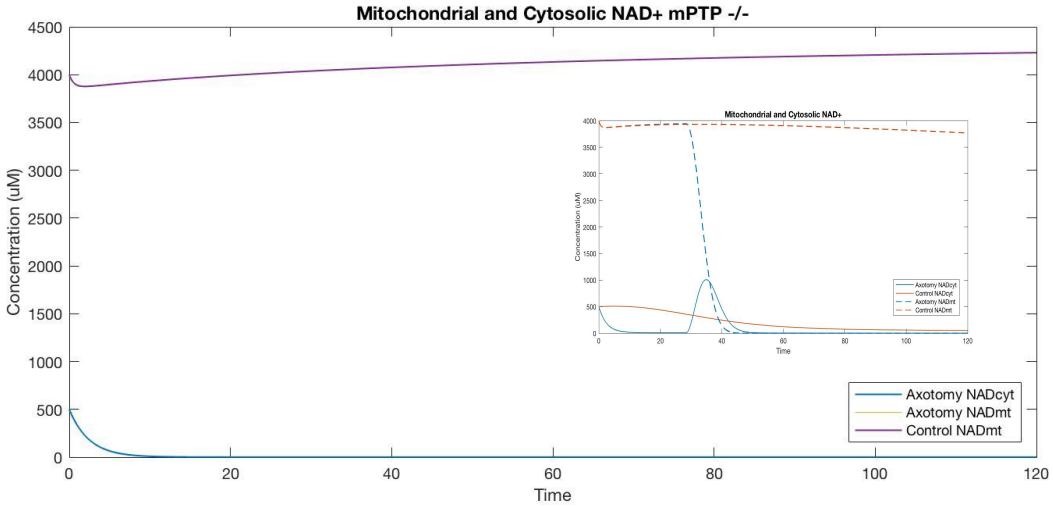

Figure 17a Main figure shows mitochondrial and cytosolic NAD levels in mPTP inhibition of the axotomy model. There is an early decline in cytosolic NAD, but there is no release of mitochondrial NAD to contribute to the cytosolic NAD pool. Inset shows mitochondrial and cytosolic NAD levels in the initial axotomy and

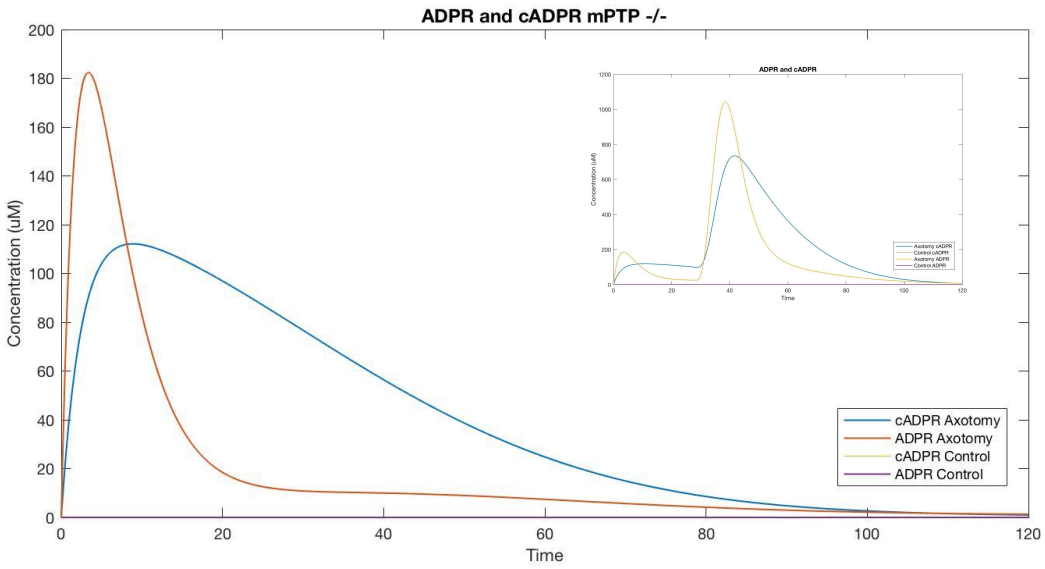

Figure 17b Main figure shows presence of ADPR and cADPR in mPTP inhibition of the axotomy model. There is a conserved early generation of these cleavage products, but no later rise as observed in the initial axotomy model (see inset).

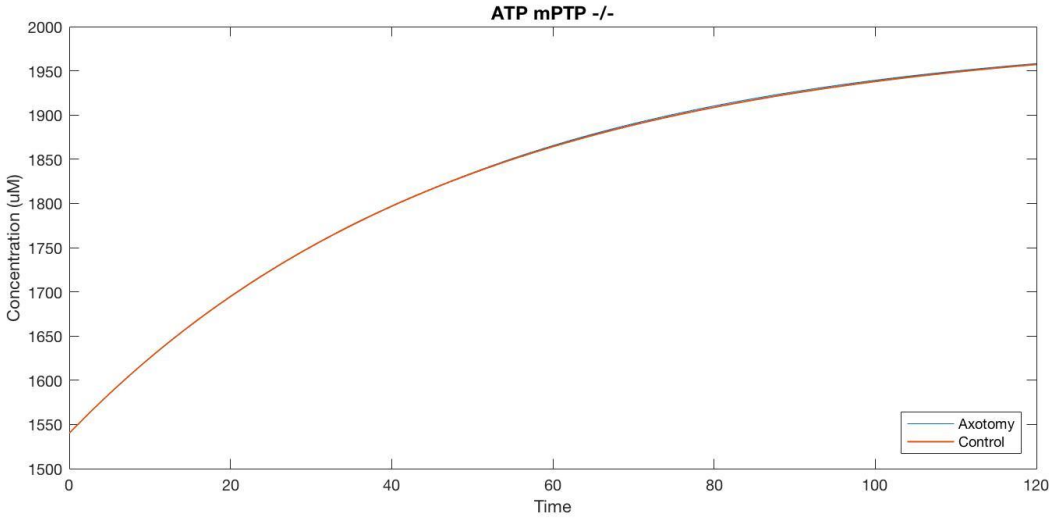

Figure 17c ATP levels are maintained in mPTP inhibition of the axotomy model comparable to the control model.

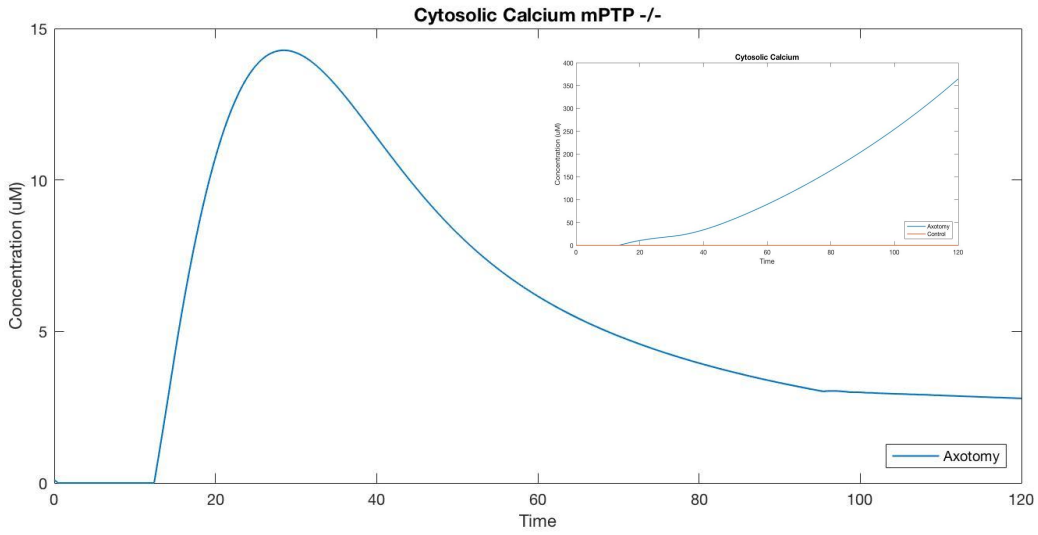

Figure 17d Main figure shows cytosolic calcium rises and recovers in mPTP inhibition of the axotomy model. Inset shows cytosolic calcium levels in the initial axotomy and control models.

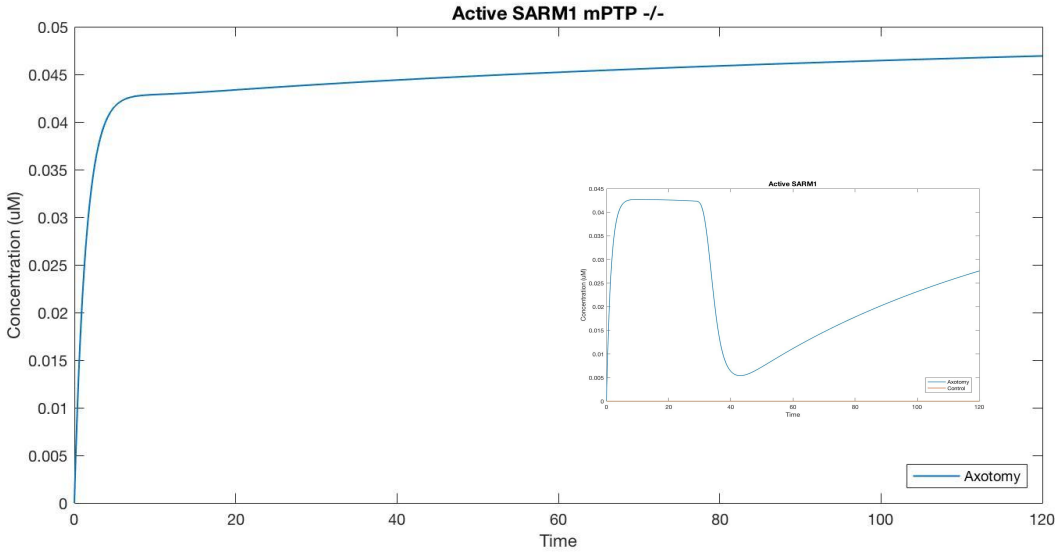

Figure 17e Main figure shows persistent levels of active SARM1 in mPTP inhibition of the axotomy model. Inset shows active SARM1 levels in the initial axotomy and control models.

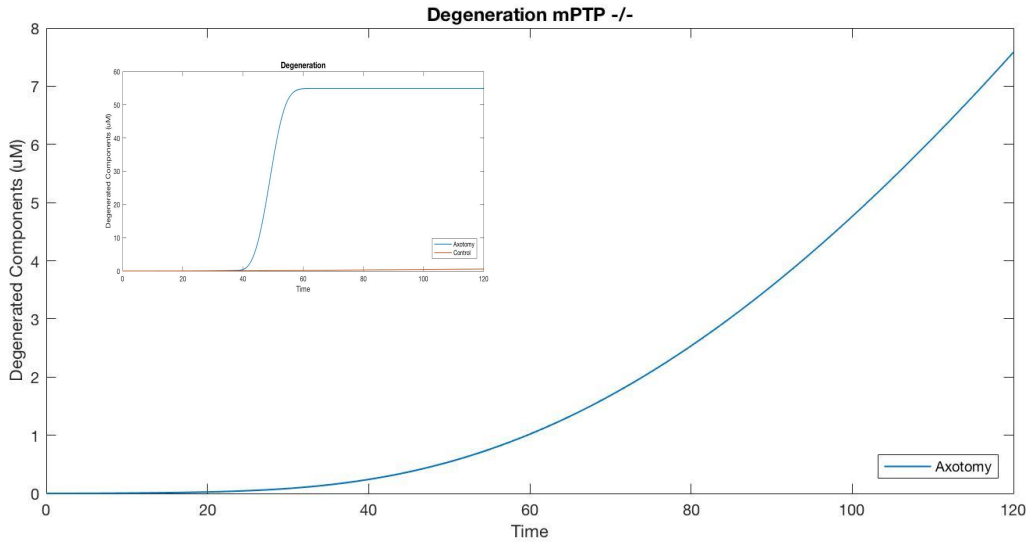

Figure 17f Main figure shows degeneration time course in mPTP inhibition of the axotomy model is substantially slower compared to the initial axotomy model. However, mPTP inhibition is less protective than SARM1 or PHR1 knockouts due to the early generation of NAD cleavage products by active SARM1. Inset shows degeneration time course of axotomy and control models.

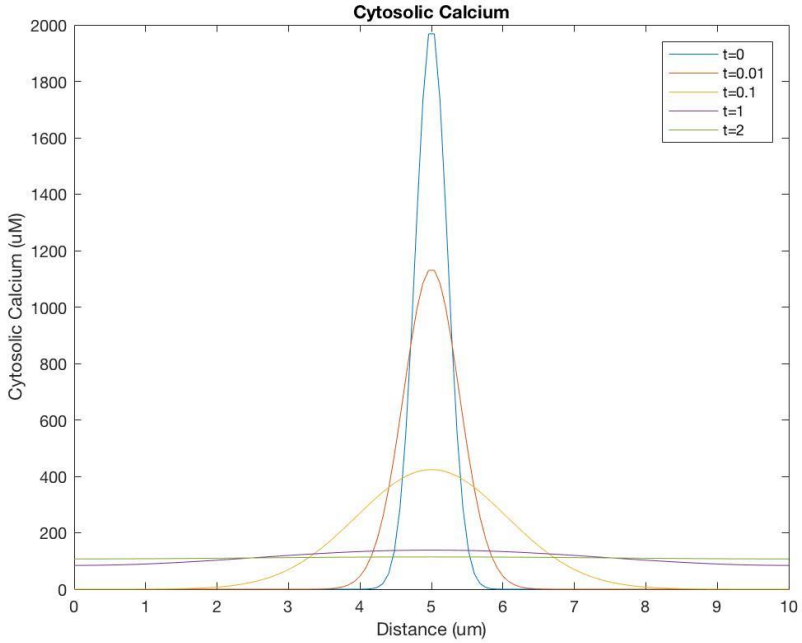

Figure 18a Cytosolic calcium diffuses quickly from an initial release source over time (s). The release of calcium is assumed to be on the order of total release from intracellular stores.

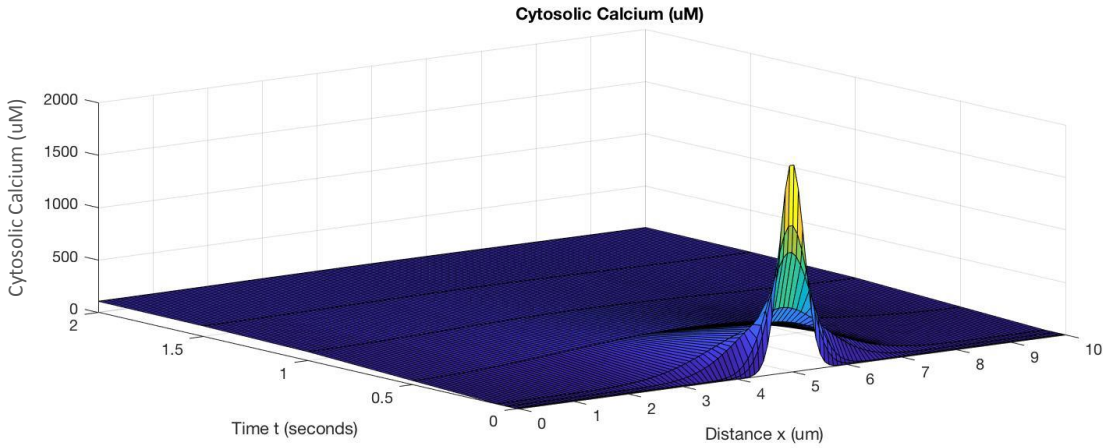

Figure 18b Diffusion of calcium from an initial release source over space and time. The release of calcium is assumed to be on the order of total release from intracellular stores.

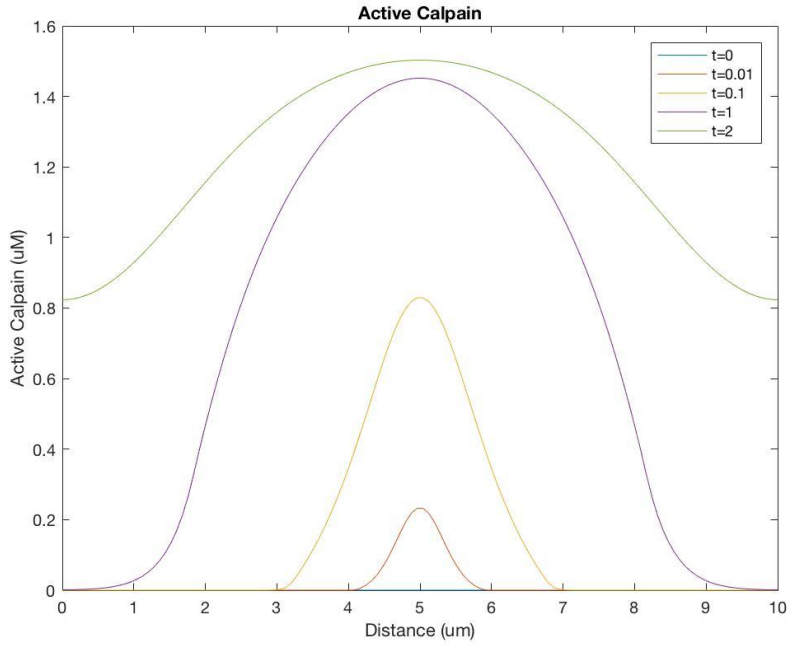

Figure 18c Spread of active calpain increases over time (s) and is dependent on the initial source of calcium release.

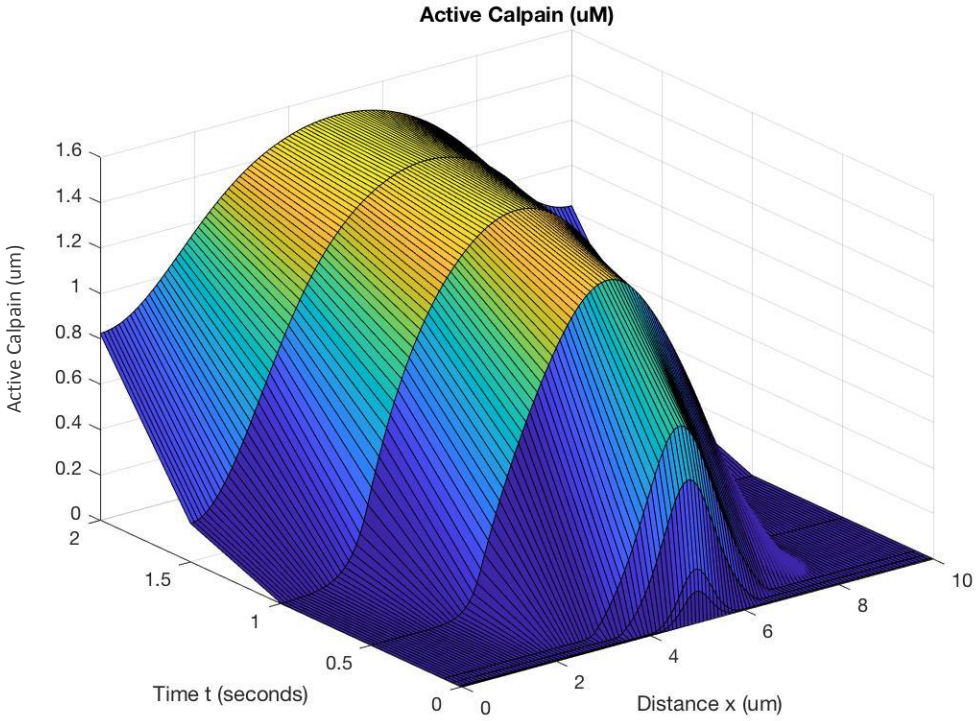

Figure 18d Spread of active calpain over space and time in the axon unit considered. This pattern of spread can be extrapolated to repeating axon units along the length of the axon corresponding to initiation of calcium release.

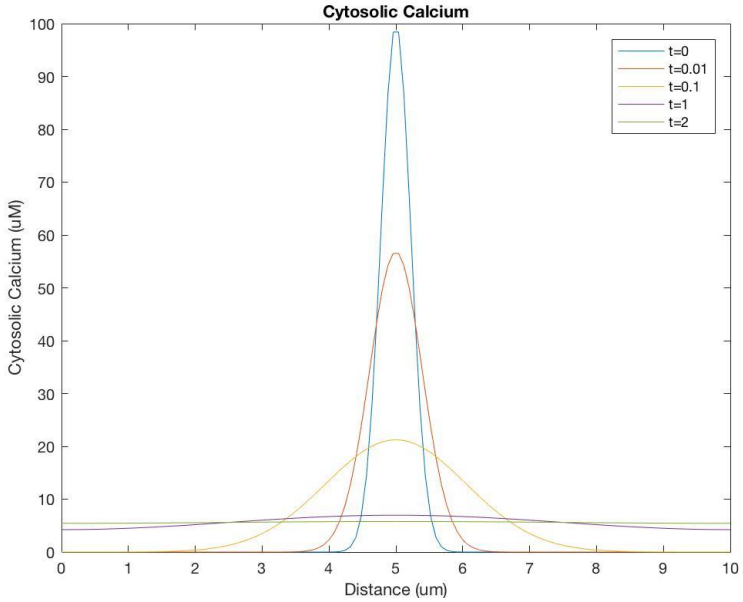

Figure 18e Cytosolic calcium diffuses rapidly from single release site (AR) and maintains high concentrations between 0.1-1 μm in diffusion distance. 100 μM of calcium release is considered due to only cADPR-activated RyRs from cleavage of cytosolic NAD by SARM1.

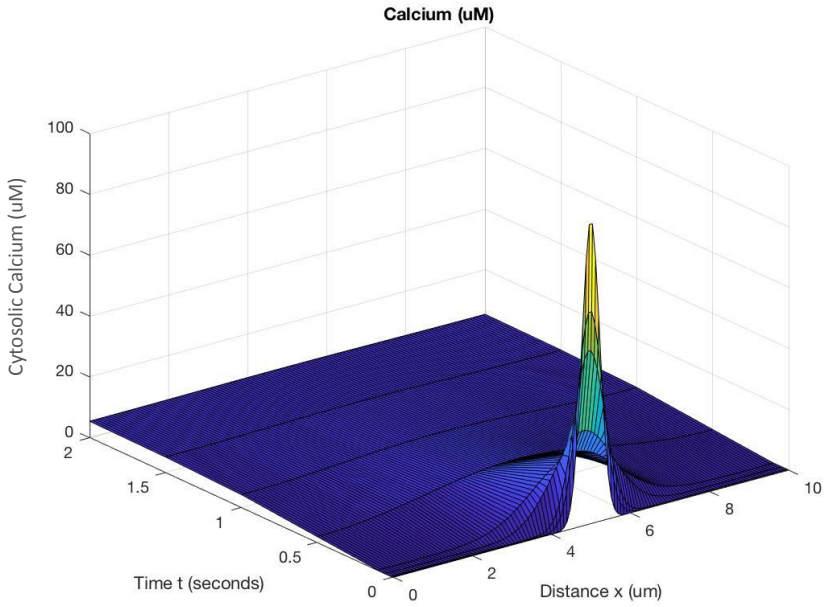

Figure 18f Diffusion of cytosolic calcium from a single release site (AR) over space and time. 100 µM of calcium release is considered due to only cADPR-activated RyRs from cleavage of cytosolic NAD by SARM1.

Appendix—MATLAB Script and Full CellDesigner Model

Equation Script

```
function [dX] = JMC_WD_HalfTreateq2( t,X )

global k Xind B C

dX = zeros(111,1);
tTreat = 0.1;

if t < tTreat
    Xind(13) = 0;
    Xind(30)=0;
else
      Xind(13) = 6*B;
      Xind(30)=0.5*C;

End

if X(11)>500
     dX(32)=0;
 else
     dX(32)=0.001*Xind(20)*(X(11)-1540);
 end

%Cytosolic Calcium
if X(32)<0.000001%need if-else because reversal not included in NCX PM loop
dX(1) = (X(15)*X(2)*k(2) + X(30)*X(2)*k(2) + X(3)*X(21)*k(2) +
X(3)*X(25)*X(4)*k(2)*k(34) ...
       + X(3)*X(33)*X(24)*k(2)*k(35)+X(27)*X(1)*X(101)*k(2)*k(37)+...

X(17)*Xind(1)*k(2)+X(13)*k(6)*0.1+Xind(1)*X(76)*k(2)+Xind(1)*X(75)*k(2))...
        - (X(9) *k(15)*X(1)*X(11)*k(36)+ X(10)*k(16)*X(1)*X(11)*k(36)...
        +X(94)*X(1)*X(11)*k(36)*k(16)+X(1)*X(26)*k(2)+1);
else
    dX(1) = (X(15)*X(2)*k(2) + X(30)*X(2)*k(2) + X(3)*X(21)*k(2) +
X(3)*X(25)*X(4)*k(2)*k(34) ...
       + X(3)*X(33)*X(24)*k(2)*k(35)+
X(17)*Xind(1)*k(2)+X(13)*k(6)*0.1+Xind(1)*X(76)*k(2)...
       +Xind(1)*X(75)*k(2)) - (X(9) *k(15)*X(1)*X(11)*k(36)+
X(10)*k(16)*X(1)*X(11)*k(36)...

+X(94)*X(1)*X(11)*k(36)*k(16)+X(1)*X(26)*k(2)+X(27)*X(1)*X(101)*k(2)*k(37)+1)
;
end

% Regulation of PMCA by Calmodulin and PKC activation
dX(53)=X(1)*X(62)*k(26)-X(53)*k(26); %CaM bind Ca
dX(62)=X(53)*k(26)-X(1)*X(62)*k(26); %Inactive CaM
dX(51)=X(1)*X(97)*k(29)-X(51)*k(32); %PKC bind Ca
dX(97)=X(51)*k(32)-X(1)*X(97)*k(29); %Inactive PKC
if X(1)<1
    k(26)=0;
    k(29)=0;
```

```
else
    k(26)=0.01;
    k(29)=0.01;
end
dX(28)=X(93)*k(27)*X(53)-X(28)*(k(30)+X(95)); %active CaM bind PMCA to give
active PMCA
dX(93)=X(28)*k(30)-X(93)*k(30)*X(53); %Inactive PMCA
dX(96)=X(28)*X(95)-X(96)*k(31); %Phosphorylated active PMCA

%NCX (Plasma Membrane)
if (Xind(1)/X(1)) >= 12000
    dX(27) = 0.00001 * Xind(2); %rate NCX Ca
    dX(23) = 0.00004 * Xind(2); %rate NCX Na
else
    if  (Xind(1)/X(1)) < 12000 && (Xind(1)/X(1)) > 100
        dX(27) = 0.0000001 * Xind(2);
        dX(23) = 0.0000004 * Xind(2);
    else
        dX(27) = 0.00000001 * Xind(2);
        dX(23) = 0.00000004 * Xind(2);
    end
end

%MCU
if X(1)<=0.7
    dX(26)=0;
    elseif X(1)>0.7
    dX(26)=0.1*Xind(18);
elseif log(X(3)/X(1))<0
    dX(26)=-0.01*Xind(18);
end

%mPTP
if X(3)<= 0.5
    dX(21) = -0.00001*X(3);
    dX(87)=-0.000001*X(3);
    dX(100)=-0.000001*X(3);
elseif X(3)>0.5
    dX(21) = 0.01 * Xind(17);
    dX(87) =0.01*Xind(17);
    dX(100)=0.1*Xind(17);
end

%NCLX (Mitochondria)
dX(6) = X(4)*k(34)*X(22)*X(3)*k(2) -
(X(6)*X(34)*X(33)*k(35)*k(34)+X(6)*X(21)*k(34));

if X(3)/X(1) < 5 && X(3)/X(1) >=2.1
    dX(22) = 0.000015 * Xind(19); %NCLX Na
    dX(25) = 0.00001 * Xind(19); %NCLX Ca
else
    if X(3)/ X(1) >= 1 && X(3) / X(1) < 2.1
        dX(22) = 0.0000015 * X(19);
        dX(25) = 0.000001 * Xind(19);
    else
        if X(3)/X(1) < 1
```

```
        dX(22) = -0.00015 * Xind(19);
        dX(25) = -0.0001 * Xind(19);
        else
            dX(22) = 0.00015 * Xind(19);
            dX(25) = 0.0001 * Xind(19);
        end
    end
end

%Na extracellular
dX(101)=X(4)*X(32)*k(34)-
(X(101)*k(37)*X(99)*X(33)*k(35)+X(101)*k(37)*X(27)*X(1)*k(2));

%Mitochondrial Hydrogen
dX(8) = (X(33)*k(35)*X(34)*X(6)*k(34)+X(37)*k(35)*Xind(24)*k(38)*X(36)...
    +X(3)*k(2)*X(33)*k(35)*X(24))...
    -
(X(8)*k(35)*X(56)*X(90)+X(8)*k(35)*X(56)*X(38)*(X(91)+X(92))+X(8)*k(10)+X(33)
*X(21)*k(35));

%Cytosolic Hydrogen
dX(33) = (X(37)*X(100)+X(98)*k(9))-(X(33)*k(35)*X(34)...
    +X(3)*k(2)*X(33)*k(35)*X(24)+X(33)*k(35)*X(99)*X(101)*k(37));
if X(8)/X(33) < 0.5 && X(3)/ X(1) >= 0.7
    dX(34) =  0.0001 * Xind(21); %Rate NCXmt (Na/H)
else
    if X(8) /X(33) > 0.7 && X(3)/ X(1) < 1
        dX(34) = 0.00001 * Xind(21);
    else
        if X(8) /X(33) >= 1
        dX(34) = -0.001 * Xind(21);
        else
            dX(34) =  0.001 * Xind(21);
        end
    end
end

%Intermembrane Space Hydrogen
if X(1)<0.5
dX(37)=(X(8)*k(44)*X(56)*(X(90)+X(91)+X(92)))-
(X(37)*k(35)*X(36)*Xind(24)*k(38));
else
    dX(37)=(X(8)*k(44)*X(56)*(X(90)+X(91)+X(92)))-
(X(37)*k(35)*X(36)*Xind(24)*k(38));...
end
%FADH and FADH2
dX(38) = X(39) * k(12) - X(38) * k(11);
dX(39) = X(38) * k(11) - X(39) * k(12);

%NAD and NADH
dX(40) = X(41) * k(14) - (X(40) * k(47)+X(56)*X(87)); %NADHcyt

%LETM1
if X(33)/ X(8) <= 2 && X(33)/ X(8) >= 1.5
    dX(24) = 0.0001 * Xind(16);
    dX(29) = 0.0001 * Xind(16);
```

```
else
    if X(33)/ X(8) < 1.5 && X(33)/ X(8) >= 1
       dX(24) = 0.00001 * Xind(16);
       dX(29) = 0.00001 * Xind(16);
    else
        if X(33)/ X(8) < 1
           dX(24) = -0.001 * Xind(16);
           dX(29) = -0.001 * Xind(16);
        else
            dX(24) = 0.001 * Xind(16);
            dX(29) = 0.001 * Xind(16);
        end
    end
end

%Mitochondrial Calcium
dX(3) = (X(1)*k(2)* X(26)) - (X(3)*k(2)*X(21) + ...
    X(3)*k(2)*X(25)*X(4)*k(34)+X(3)*k(2)*X(33)*k(35)*X(24));

%RyR2
if X(1) <= 5 %RyR2 active via CaM-Ca
    dX(7) = X(52) * X(1) * 0.0000000000000000001 - (X(7)*k(2
    dX(52)=(X(7)*k(2)+X(31)*k(23))-
(X(52)*k(23)*X(47)+X(52)*X(1)*0.0000000000000000001); %inactive RR2
else
dX(7) = X(52) * X(1) * k(2)-(X(7)*k(2));
dX(52)=(X(7)*k(2)+X(31)*k(23))-(X(52)*k(23)*X(47)+X(52)*X(1)*k(2)); %inactive
RyR2
end
    %%RyR2 binding Ca and/or cADPR
    dX(88)=X(7)*X(47)*k(23)-X(88)*k(23); %active RyR2 with cADPR and Ca
    dX(31)=X(52)*X(47)*k(23)-X(31)*k(48); %RyR2 active by cADPR
if (X(1) /X(2)) <= 0.008 && (X(1) /X(2)) >= 0
    dX(15) = 0.1 * (X(7)+X(88)+X(31));
else
    if (X(1) / X(2)) > 0.008
        dX(15) = 0.0001 * (X(7)+X(88)+X(31));
    else
        dX(15) = 0.0000001 * (X(7)+X(88)+X(31));
    end
end

%IP3R
dX(61)=X(5)*k(19)-X(61) * X(12) * k(1); %inactive IP3Rs
dX(5) = X(61) * X(12) * k(1)-X(5)*k(19); % creating active channels

if X(1) /X(2) <= 0.008 && (X(1) /X(2)) >= 0
    dX(30) = 0.01 * X(5);
else
    if (X(1) / X(2)) > 0.008
        dX(30) = 0.0001 * X(5);
    else
        dX(30) = 0.0000000001 * X(5);
    end
end
```

```
%IP3
dX(12) = Xind(11) * X(14) - k(4) * X(12);

%PLC activation and PLC inactive
if X(1) <= 6
    dX(13) = X(1) * X(105) * 0.00000000000000000001-X(13)*k(18);
    dX(105)=X(13)*k(18)-X(1) *0.0000000000000000001 * X(105);
else
        dX(13) = X(1) * k(6) * X(105)-X(13)*k(18);
        dX(105)=X(13)*k(18)-X(1) * k(6) * X(105);
end

%Axoplasmic Reticulum Calcium
dX(2) = (X(1)*X(11)*k(36)*X(9)*k(15)) - (X(15)*X(2)*k(2)+X(30)*X(2)*k(2));

dX(11) = (X(37) * Xind(24) * X(35))- (X(11) * X(9)*k(15) * X(1) + ...
     X(11) * X(10)*k(16) * X(1)+ X(11) * X(32);

%Cytosolic Sodium
if X(32)<0.000001 %dependent on depolarization
dX(4) =
(X(6)*k(34)*X(34)*X(33)*k(35)+X(6)*k(34)*X(21)+X(101)*k(37)*X(99)*X(33)*k(35)
)... -
(X(32)*X(4)*k(34)*X(11)*k(36)+X(4)*k(34)*X(23)*X(1)*k(2)+X(4)*k(34)*X(22)*X(3
)*k(2));
else
    dX(4) =
(X(23)*X(101)*k(37)*X(1)*k(2)+X(6)*k(34)*X(34)*X(33)*k(35)+X(101)*k(37)*X(99)
*X(33)*k(35)...
        +X(6)*k(34)*X(21)) -
(X(32)*X(4)*k(34)*X(11)*k(36)+X(4)*k(34)*X(22)*X(3)*k(2));
end

%Na+/H+ transporter at PM
if X(33)/X(98) < 0.6
    dX(99) =  0.0001 * Xind(21);
else
    if X(33) /X(98) > 0.6 && X(33) /X(98)<1
        dX(99) = 0.00001 * Xind(21);
    else
        if X(33) /X(98) >= 1
        dX(99) = -0.001 * Xind(21);
        else
            dX(99) =  0.001 * Xind(21);
        end
    end
end

%Extracellular hydrogen
dX(98)=X(33)*k(35)*X(99)*X(101)*k(37)-k(9)*X(98);

if X(1) >= 0.2 && X(1) <= 2
dX(18) = Xind(14) * X(1) * 0.000000000000000000000001 - k(20) * X(18);
else
    if X(1) >2 && X(1) <= 30
```

```
        dX(18) = Xind(14) * X(1) * 0.000001 - k(20) * X(18);
    else
    dX(18) = Xind(14) * X(1) * k(5) - k(20) *X(18);
    end
end

%Degradation by calpain
if X(18)<0.00001
    dX(20)=-0.1*X(18);
else
dX(20) = 0.05 * X(18); %Rate degradation by calpains
end
dX(16) = -X(20) * X(16); %Intact structural remaining
dX(19) = X(20)* X(16); %Conversion of intact to degraded

%Cv1.2
if X(32)<0.000001 %Depolarization activating Cv1.2
   dX(17) = 0.001 * (Xind(3) - Xind(13));
else
      dX(17) = -k(17)*Xind(3);
end

%NMNAT transport from soma down axon and its turnover
if Xind(7)>0 %injury stops NMNAT2 transport
    dX(43)=-X(77)*X(43);
    dX(66)=0.001*(X(43)-0.0317);
else
dX(43)=Xind(25)*k(24)-X(77)*X(43);
if X(41)<X(45) %reversal of NMNAT2 actvity depending on NAD and NMN
    dX(66)=0.001*X(43);
elseif X(45)>X(41)
    dX(66)=-0.001*X(43);
end
end

%NAD Biosynthesis (salvage pathway) and consumption
if X(46)<0.00001
dX(44)=(X(41)*k(45)*(X(69)+X(106))+Xind(4)*k(28))-X(44)*X(64); %Nam cyt
else
    dX(44)=(X(41)*k(45)*(X(69)+X(70)+X(106))+Xind(4)*k(28))-X(44)*X(64);
end
dX(45)=(X(44)*X(64))-(X(45)*X(66)+X(45)*k(25)); %NMNcyt
dX(55)=X(45)*k(25)-X(55)*X(107); %NMNmt
if X(46)<0.00001
dX(41)=(X(45)*X(66)+X(40)*k(47)+X(54)*X(87))-(X(41)*(X(69)...
    +X(71))+X(41)*k(14));
else
    dX(41)=(X(45)*X(66)+X(40)*k(47)+X(54)*X(87))-(X(41)*(X(69)...
    +X(70)+X(71)+X(78)+X(79))+X(41)*k(14));%NADcyt
end

dX(56)=(X(54)*k(22)+X(54)*k(47)*X(40))-
(X(56)*(X(90)+X(91)+X(92))+X(56)*X(87)); %NADHmt
dX(54)=(X(56)*(X(90)+X(91)+X(92)))-
(X(54)*k(22)+X(54)*k(47)*X(40)+X(54)*X(87)); %NADmt
```

```
%ADPR and cyclic ADPR synthesis and degradation
if X(46)<0.0001 %Dependent on active SARM1
    dX(47)=-(X(47)*X(72)+X(47)*k(7)); %cADPR
    dX(48)=X(47)*X(72)-(X(48)*X(74)+X(48)*k(42)); %ADPR
else
    dX(47)=X(41)*X(79)-(X(47)*X(72)+X(47)*k(7));
    dX(48)=(X(47)*X(72)+X(41)*X(78))-(X(48)*X(74)+X(48)*k(42));
end

%Calicym mobilization altered by ADPR and cADPR
dX(49)=X(50)*X(1)*k(2)-X(49)*k(2); %TRPM2 by activated by Ca
dX(65)=X(48)*k(21)*X(50)-X(65)*k(21)*0.01; %TRPM2 activated by ADPR
dX(59)=X(50)*X(48)*k(21)*X(1)*k(2)-X(59)*k(21)*k(2); %TRPM2 activated by both
ADPR and Ca
dX(50)=(X(50)*X(1)*k(2)+X(50)*X(48)*k(21))-X(48)*k(21); %rate for TRPM2 with
both Ca and ADPR
if (X(2) /X(1)) <= 100000 && (X(2) /X(1)) >= 100
    dX(74) = 0.01*(X(49)+X(65)+X(59);
else
    if (X(2) / X(1)) < 100
        dX(74) = 0.0001*(X(49)+X(65)+X(59));
    else
        dX(74) = 0.000000001*(X(49)+X(65)+X(59));
    end
end

%%SARM1 activity inhibited in the presence of NMNAT
if X(43)<0.0317 %NMNAT2 falls below its initial value
dX(46)=(X(89)*k(40)+X(111)*k(39))-
(X(46)*k(40)*X(44)+X(46)*k(41)+X(46)*X(102)); %generate active SARM1
else
    dX(46)=-(X(46)*k(40)*X(44)+X(46)*k(41)+X(46)*X(102));
end
dX(89)=X(46)*k(40)*X(44)-X(89)*k(40); %inactivation of SARM1 by NAM
dX(111)=(X(46)*k(41)+X(46)*X(102))-X(111)*k(39); %inactive SARM1

%Rate equations
dX(9) =0.1 * Xind(15);              %Rate SERCA
dX(10) =0.001 * X(28);              %Rate PMCA bound by CaM
dX(14) = 0.00001 * (X(13)-X(51)); %Rate PIP2 to IP3 catalyzed by activated
PLC and inhibited by active PKC
dX(20) = 0.05 * X(18);              %Rate degradation by calpains
dX(35) = 0.00001 * Xind(22);        %Rate ATP Synthase for ADP and Pi
dX(36) = 0.00004 * Xind(22);        %Rate ATP Synthase for H+
dX(42) = 0.00001 *Xind(22);         %Rate ATP synthase for ADP injured
dX(64)=0.01*(Xind(29)-Xind(30));  %Rate NAM to NMN with FK866 Tx
dX(69) =0.001*Xind(27);             %Rate NAD to Nam by CD38
dX(70) =0.001*X(46);                %Rate NAD to Nam by active SARM1
dX(71) =0.001*Xind(27);             %Rate NAD to cADPR by CD38
dX(72) =0.001*Xind(27);             %Rate cADPR to ADPR by CD38
dX(75) =0.001*X(50);                %Rate extracell Ca to cyt Ca by LTPRC2
active
dX(76) =0.001*X(49);                %Rate extracell Ca to cyt Ca by TRPM2
active
dX(77) =0.001*X(43);                %Rate NMNATaxon consumption by PHR1
dX(78) =0.001*X(46);                %Rate NAD to ADPR by active SARM
```

```
dX(79) =0.001*X(46);              %Rate NAD to cADPR by active SARM
dX(90)=0.001*Xind(39);            %Rate Complex I Hm to Hims
dX(91)=0.001*Xind(40);            %Rate Complex III Hm to Hims
dX(92)=0.001*Xind(41);            %Rate Complex IV Hm to Hims
dX(94)=0.01*X(96);                %Rate phosphorylated active PMCA
dX(102)=0.01*(X(43));             %Rate NMNAT inhibit SARM...-X(43) or
X(43)??
dX(106)=0.01*Xind(10);            %Rate SIRT2
dX(107)=0.01*Xind(9);             %Rate NMNAT3
dX(110)=0.01*Xind(33);            %Rate SIRT5
end
```

Initial Conditions (Run) Script

```
global k Xind X0 t
X0 = zeros(111,1);
Xind = zeros(43,1);

%Initial values for dependent values (all units: uM)
X0(1) = 0.1;                %Cyt Ca
X0(2) = 500;                %AR Ca
X0(3) = 0.2;                %MT Ca
X0(4) = 8000;               %Cyt Na
X0(5) = 0.00001;            %Active IP3R
X0(6) = 6000;               %Na MT
X0(7) = 0.00001;            %Active RyR2
X0(8) = 0.3;                %H MT
X0(11) = 1540;              %ATP
X0(12) = 0.000001;          %IP3
X0(13) = 0.000001;          %PLC bound Ca
X0(16) = 54.9;              %Intact cytoskeleton
X0(18) = 0;                 %Active calpain
X0(19) = 0;                 %Degraded cytoskeleton
X0(31) = 0;                 %Inactive RyR2 (unbind cADPR)
X0(33) = 0.06;              %H cyt
X0(37) = 0.16;              %H ims
X0(38) = 30;                % FADH2*  unsure
X0(39) = 15;                % FADH* unsure
X0(40) = 300;               % NADHcyt as seen on wiki
X0(41) = 500;               % NAD cyt as seen in lit canto 2015
X0(43) = 0.0317;            %Nmnat2 in the axon (Not KO =0.0317; KO=0)
X0(44) = 15;                %NAM cyt--estimate (reasonable between  15 and 60)
X0(45) = 30;                %NMN cyt
X0(46) = 0;                 %SARM active
X0(47) = 0;                 %cADPR
X0(48) = 0;                 %ADPR--estimate very small initial
X0(49) = 0;                 %TRPM2 active
X0(50) =0.00010;            %TRPM2 inactive
X0(51) =0;                  %PKC active
X0(52) =0.5;                %Ryr2 inactive (was 0.024)
X0(53) =0;                  %CaM active
X0(54) =4000;               %NADmt pool
X0(55) =50;                 %NMNmt
X0(56) =400;                %NADHmt
X0(88) =0;                  %active RR2 with cADPR
X0(89) =0;                  %inactive SARM by NAM (SARM-NAM)
```

```
X0(61) =0.051;              %IP3R inactive
X0(62) =24.706;             %inactive CaM
X0(68)=0;                  %NAM mt--DNE! (is now DI!)
X0(28)=0;                  %PMCA bound by CaM
X0(93)=5.234;              %PMCA nothing bound (inactive)
X0(96)=0;                  %active PMCA phosphorylated
X0(97)=0.165;              %PKC inactive
X0(98)=0.1;                %extracellular hydrogen
X0(101)=145000;            %extracellular sodium
X0(105)=1.214;             %PLC without Ca--can go up to 1.5 - 2**
X0(111)=0.06100;           %inactive SARM1 (initial)

%Initial rates for modifiers
X0(9) = 0.01;              %rate SERCA
X0(10) = 0.0001;           %rate PMCA bound
X0(14) = 0.000001;         %rate PIP2 to IP3
X0(15) = 0.1;              %rate active RR3
X0(17) = 0.001;            %rate Cv 1.2
X0(20) = 0;                %rate degradation by calpains
X0(21) = 0.001;            %rate mPTP for Ca2+
X0(22) = 0.0001;           %rate NCLX for Na (NCXmt)
X0(23) = 0.0003;           %rate NCX for Na
X0(24) = 0.0001;           %rate LETM1 for Ca
X0(25) = 0.0001;           %rate NCLX for Ca (NCXmt)
X0(26) = 0.001;            %rate MCU
X0(27) = 0.0001;           %rate NCX for Ca
X0(29) = 0.0001;           %rate LETM1 for Ca and H
X0(30) = 0.1;              %rate active IP3R
X0(32) = 0.001;            %rate Na/K pump for Na only
X0(34) = 0.0001;           %rate NCXmt for Na/H
X0(35) = 0.2;              %rate ATP Synthase for ADP and Pi
X0(36) = 0.8;              %rate ATP Synthase for H+
X0(59) =0.010;             %rate TRPM2 activated by both ADPR and Ca
X0(63) =0.010;             %rate CaM active enhances SERCA acivity
X0(64) =0.45;              %rate NAM to NMN by NAMPT
X0(65) =0.00010;           %rate TRPM2 activated by ADPR only
X0(66) =0.010;             %rate NMN to NAD by NMNAT2
X0(67) =0.010;             %rate ATP to ADP by NMNAT
X0(69) =0.000010;          %rate NAD to Nam by CD38
X0(70) =0.0050;            %rate NAD to Nam by active SARM1
X0(71) =0.00010;           %rate NAD to cADPR by CD38
X0(72) =0.000010;          %rate cADPR to ADPR by CD38
X0(74) =0.010;             %rate ADPR consumed by TRPM2 active
X0(76) =0.010;             %rate extracell Ca to cyt Ca by TRPM2 active
X0(77) =0.20;              %rate NMNAT consumption by PHR1
X0(78) =0.3;               %rate NAD to ADPR by active SARM
X0(79) =0.1;               %rate NAD to cADPR by active SARM
X0(80) =0.010;             %rate Nam inhibit active SARM
X0(87) =0.0010;            %rate mPTP for NADmt to NAD cyt
X0(90)=0.50;               %rate Complex I Hm to Hims
X0(91)=0.50;               %rate Complex III Hm to Hims
X0(92)=0.50;               %rate Complex IV Hm to Hims
X0(94)=0.10;               %rate active+phosphorylated PMCA
X0(95)=0.010;              %rate phosphorylation of active PMCA by PKC
X0(99)=0.01;               %rate Na+/H+ PM
X0(100)=0.01;              %rate mPTP Hims and Hmt to Hcyt
X0(102)=0.1;               %rate NMNAT inhibit SARM
```

```
X0(103)=0.01;              %rate malate dehydrogenase
X0(106)=0.00001;           %rate SIRT2
X0(110)=0.00001;          %rate SIRT5

% Initial values for independent variables
Xind(1) = 1200;           %extracellular calcium
Xind(2) = 5.086;          %NCX
Xind(3) = 0.08;           %Cv 1.2
Xind(4) = 30;             %NAM extracell
Xind(5) = 30.134;         %malate dehydrogenase
Xind(7) = A;              %axon cut
Xind(8) = 3.217;          %LETM1
Xind(10) = 8.2;           %SIRT2
Xind(11) = 10000;         %PIP2
Xind(14) = 1.816;         %Inactive m-Calpain
Xind(15) = 0.416;         %SERCA
Xind(16) = 0.0571;        %HCX
Xind(17) = 5;             %mPTP
Xind(18) = 0.291;         %MCU
Xind(19) = 0.143;         %NCLX
Xind(20) = 8.754;         %Na/K Pump
Xind(21) = 5.086;         %NA/H exhanger
Xind(22) = 1.466;         %ATP Synthase
Xind(24) = 270;           %ADP
Xind(25) = 7;             %NMNAT2 soma
Xind(27) = 0.756;         %CD38
Xind(29) = 0.786;         %NAMPT
Xind(31) = 0.0892;        %PHR1
Xind(33) = 1.664;         %SIRT5
Xind(39) = 10;            %Complex I ETC
Xind(40) = 10;            %Complex III ETC
Xind(41) = 10;            %Complex IV ETC
Xind(43) = 2.857;         %Na+/H+ exchanger at PM

%Initial rates (no modifiers)
k(1) = 0.001;             %rate IP3R bind IP3
k(2) = 0.007;             %rate RR3 bind Ca
k(3) = 0.001;             %rate turnover of H MT
k(4) = 0.01;              %rate degredation of IP3
k(5) = 0.001;             %rate CAPN2 bind Ca
k(6) = 0.001;             %rate PLC bind Ca
k(7) = 0.006;             %intrinsic degredation rate of cADPR
k(8) = 0.0000001;         %rate ATP depletion after axon cut
k(9) = 1e-5;              %passive diffusion of H+ extracellular into cyt
k(12) = 0.1;              %rate reduction of FADH2
k(14) = 0.001;            %rate reduciton of NADH (glycolysis)
k(15) = 0.005;            %rate SERCA bind Ca
k(16) = 0.005;            %rate PMCA bind Ca
k(17) = 0.0000000001;     %rate deactivation of Cv1.2
k(18) = 0.01;             %rate dissociation PLC and Ca
k(19) = 0.01;             %rate dissociation of IP3 and IP3R
k(20) = 0.01;             %rate calcium dissociate from CAPN
k(21) = 0.001;            %rate ADPR complex with TRPM2
k(22) = 0.0001;           %rate TCA reduce NAD to NADH
k(23) = 0.01;             %rate cADPR complex with RyR2
k(24) = 0.001;            %axonal transport of NMNAT soma to NMNAT axon
```

```
k(25)=0.0001;            %rate NMNcyt to NMNmt
k(26)=0.01;              %rate Ca bind/unbind CaM
k(27)=0.01;              %rate active CaM binds PMCA
k(28)=0.00001;           %rate NAM ext to NAM cyt
k(29)=0.01;              %rate PKC bind ca
k(30)=0.01;              %rate dissociation CaM-Ca from PMCA
k(31)=0.03;              %rate dephosphorylation of PMCA k=30 s-1
k(32)=0.01;              %rate calcium dissociate from PKC
k(33)=0.01;              %rate association of calcium with MCU
k(34)=0.01;              %rate association of Nacyt with NCLX
k(35)=0.001;             %rate association of Hcyt with LETM1
k(36)=0.01;              %rate association of ATP with SERCA and PMCA
k(37)=0.01;              %rate association of Na extra with NCX PM
k(38)=0.01;              %rate association of ADPR
k(39)=0.5;               %rate sarm become active
k(40)=0.01;              %rate NAM bind active SARM
k(41)=0.00001;           %intrinsic rate of inactivation by active SARM1
k(42)=0.2;               %intrinsic degradation rate of ADPR
k(43)=0.0001;            %rate NADmt synthesis
k(44)=0.01;              %rate Hmt associate with complexes of ETC
k(45)=0.01;              %NAD association rate
k(47)=0.0007;            %coupled rate of malate dehydrogenase
k(48)=0.001;             %rate cADPR dissociate from RyR2
```

ODE Solver

```
options = odeset('NonNegative',1:111);
disp('in run')
[t,X] = ode15s(@JMC_WD_HalfTreateq2, tspan, X0, options);
disp('finish')
```

Analysis Script

```
global dataDisease dataBaseline TCaBL TBLdiff t B C dataTreatFK866 TFK866diff
TNifdiff dataTreatNif
t=0:0.1:120;
tspan=t;

%Defining reatment states

%Axotomy
A =1; %Axotomy
B =0; %Nifedipine
C =0; %FK866
JMC_WD_run2
dataDisease = X;

%Control
A =0;
B =0;
C =0;
JMC_WD_run2
dataBaseline = X;

%Nifedipine
```

```
A= 1;
B= 1;
C= 0;
JMC_WD_HalfTreatrun2
dataTreatNif = X;

%FK866
A= 1;
B= 0;
C= 1;
JMC_WD_HalfTreatrun2
dataTreatFK866 = X;

% Differences between two models
TBLdiff = dataDisease - dataBaseline; %axotomy-control
TFK866diff= dataTreatFK866-dataDisease; %FK866-axotomy
TNifdiff=dataTreatNif-dataDisease; %Nif-axotomy
JMC_WD_HalfTreatplots

%Cell containing the species
species =
{'Cytosolic_Calcium','AR_Calcium','Mitochndrial_Calcium','Cytosolic_Sodium',...

'Active_IP3R','Mitochondrial_Sodium','Active_RR2','H_mito_matrix','Rate_SERCA','Rate_PMCA','ATP','IP3','PLC_Ca_bound',...

'Rate_PIP2_IP3','Rate_Active_RR3','Intact_Structural','Rate_Cv1_2','Active_Calpain',...

'Degraded_Structures','Rate_Degradation_CAPN','Rate_mPTP','Rate_NCLX_Na','Rate_NCX_Na',...

'Rate_LETM1_Ca','Rate_NCLX_Ca','Rate_MCU','Rate_NCX_Ca','PMCA_CaM','Rate_LETM1_H','Rate_active_IP3R',...

'Active_RR2_bycADPR','Rate_NaK_Pump','Hcyt','NCXmt','Rate_ATPsyn_ADP','Rate_ATPsyn_H','Hims',...

'FADH2','FADH','NADHcyt','NADcyt','NMNAT2_axon','NAMcyt','NMNcyt','SARM_active',...

'cADPR','ADPR','TRPM2_Active','TRPM2_inactive','PKC_active','RR2_inactive','CaM_active',...

'NADmt','NMNmt','NADHmt','TRPM2_activeby_Ca_ADPR','IP3R_inactive','CaM_inactive','rateSerca_CaM',...

'rate_NAMPT','rateADPR_activTRPM2','rate_NMNAT2','rate_NMNAT_ATP','rate_CD38_cleaveNAD','rate_SARMcleaveNAD',...

'rate_CD38_NADtocADPR','rate_cADPRtoADPR_CD38','rate_TRPM2cleaveADPR','rate_TRPM2_transpCa',...

'rate_PHR1','rate_SARM_ADPR','rate_SARM_cADPR','rate_NAMinhibitSARM','rate_mPTP_NADmt','RR2_active_cADPR','SARM_NAM',...
```

```
'rate_CI_Hmt','rate_CIII_Hmt','rate_CIV_Hmt','PMCA_inactive','rate_activPMCAp
hos','rate_phosPKCPMCA',...

'PMCA_phos','PKC_inactive','Hextracell','rate_NAHpm','Naextracell','rate_NMNA
T2inhibSARM',...

'rate_maldehyd_cyt','rate_maldehyd_mt','PLC_woCa','rate_SIRT2','rate_NMNAT3',
'rate_SIRT5','inactive_SARM1'};

TcalciumDiff = cell(95,1);
TCaBLDiff = cell(95,1); %%%update! 83 X's
Tdegtest = cell(95,1);
TFKtest=cell(95,1);
TNiftest=cell(95,1);
for i = 1:95
    TCaBLDiff(i) = {TCaBL(:,i)};
    Tdegtest(i) = {TBLdiff(:,i)};
    TFKtest(i)={TFK866diff(:,i)};
    TNiftest(i)={TNifdiff(:,i)};
end
```

Example Plot Script

```
figure (1) %Plot NADcyt in control and axotomy treatment
plot(t,dataDisease(:,41),t,dataBaseline(:,41))
legend('Axotomy','Control','Location','SouthEast')
xlabel('Time', 'Fontsize', 10)
ylabel('Concentration (uM)', 'Fontsize', 10)
set(gca, 'Fontsize', 10)
title('Cytosolic NAD+','Fontsize',12)

figure (2) %Plot NADmt in control and axotomy treatment
plot(t,dataDisease(:,41),t,dataBaseline(:,41),t,dataDisease(:,54),t,dataBasel
ine(:,54))
legend('Axotomy NADcyt','Control NADcyt','Axotomy NADmt','Control
NADmt','Location','SouthEast')
xlabel('Time', 'Fontsize', 10)
ylabel('Concentration (uM)', 'Fontsize', 10)
set(gca, 'Fontsize', 10)
title('Mitochondrial and Cytosolic NAD+','Fontsize',12)
```

Reaction-Diffusion Script

```
function diffaxonCa_2 % one unit size 10um
m = 0;
x=0:0.08:10; %axon unit size (units: um)
t = [0 0.005 0.01 0.05 0.1 0.5 1 1.5 2]; %units: seconds

sol = pdepe(m,@diffaxonCa_2pde,@diffaxonCa_2ic,@diffaxonCa_2bc,x,t);
u1 = sol(:,:,1);
u2 = sol(:,:,2);
u3 = sol(:,:,3);

%%Conservation of Mass
```

```
sumInitialCa= sum(u1(1,1))
sumInitialCN= sum(u2(1,1))
sumInitialCaCN= sum(u3(1,1))
totalInitial=sumInitialCa+sumInitialCN+sumInitialCaCN

sumFinalCa=sum(u1(end,end))
sumFinalCN=sum(u2(end,end))
sumFinalCaCN=sum(u3(end,end))
totalFinal=sumFinalCa+sumFinalCN+sumFinalCaCN

figure
plot(x,sol(1,:,1),x,sol(3,:,1),x,sol(5,:,1),x,sol(7,:,1),...
    x,sol(9,:,1))
 title('Cytosolic Calcium')
 xlabel('Distance (um)')
 ylabel('Cytosolic Calcium (uM)')
 legend('t=0','t=0.01','t=0.1','t=1','t=2')

 figure
 plot(x,sol(1,:,3),x,sol(3,:,3),x,sol(5,:,3),x,sol(7,:,3),...
    x,sol(9,:,3))
 title ('Active Calpain')
 xlabel('Distance (um)')
 ylabel('Active Calpain (uM)')
 legend('t=0','t=0.01','t=0.1','t=1','t=2')

figure
surf(x,t,u1)
title('Calcium (uM)')
xlabel('Distance x (um)')
ylabel('Time t (seconds)')

figure
surf(x,t,u3)
title('Active Calpain (uM)')
xlabel('Distance x (um)')
ylabel('Time t (seconds)')


% --------------------------------------------------------------
function [c,f,s] = diffaxonCa_2pde(x,t,u,DuDx)
%Diffusion Coefficients. units: um2/s
D1 = 5.30; %Calcium
D2 = 0.7;  %Inactive calpain
D3 = 0.5;  %Active calpain

if u(1)>100 %Calpain only bind Ca high concentrations
a=0.01*u(1)*u(2); %Generation of active calpain
else
    a=0;
end
b=0.25*u(3); %Dissociation of calpain and calcium
F1=-a+b;
F2=-a+b;
F3=a-b;
```

```
c = [1; 1; 1];
f = [D1; D2; D3] .* DuDx;
s = [F1; F2; F3];
% -------------------------------------------------------------

function u0 = diffaxonCa_2ic(x) %Initial conditions for each species
%(units:uM)
u01=2000*exp(-(x-5)^2/0.1); %Calcium
u02=1.816; %homogenous distribution of inactive calpain
u03=0; %Active calpain
u0= [u01; u02; u03];

% -------------------------------------------------------------
function [pl,ql,pr,qr] = diffaxonCa_2bc(xl,ul,xr,ur,t)
pl = [0; 0; 0]; %No flux/reflecting BC's
ql = [1; 1; 1];
pr = [0; 0; 0];
qr = [1; 1; 1];
```